Spring 5-31-1968

Measurement of Deformations an a Large Displacement Gradient Field

Lowell P. Martin

This dissertation, directed and approved by the candidate's committee, has been accepted by the Graduate Committee of The University of New Mexico in partial fulfillment of the requirements for the degree of

Doctor of Philosophy

Measurement of Deformations in a Large Displacement Gradient Field

Title

Lowell P. Martin

Candidate

Mechanical Engineering

Department

A. L. Sheyer

Dean

5-31-68

Date

Committee

Frederick R. Steinhagen

Chairman

W. E. Baker

H. L. Schreyer

R. C. Dove

MEASUREMENT OF DEFORMATIONS IN A LARGE DISPLACEMENT GRADIENT FIELD

BY

LOWELL P. MARTIN

B.S.M.E., Purdue University, 1954
M.S., University of New Mexico, 1958

DISSERTATION

Submitted in Partial Fulfillment of the
Requirements for the Degree of
Doctor of Philosophy in Mechanical Engineering
in the Graduate School of
The University of New Mexico
Albuquerque, New Mexico
June, 1968

ACKNOWLEDGMENTS

I would like to thank Dr. Frederick D. Ju for his support, guidance and advice; not only during the course of this research, which was suggested by him, but also during the preceding years of the author's graduate studies. Additional thanks are due to Dr. Ju and Dr. Richard C. Dove for their assistance in obtaining film, photoengraving materials and test fixtures through the cooperation of the United States Air Force Office of Scientific Research.

Further thanks are due to Dr. John C. Rowley and Mr. Joe W. Neudecker of N-Division at Los Alamos Scientific Laboratory, for their cooperation in the use of laboratory facilities and equipment.

I am deeply indebted to Messrs. William F. Lindsay and Richard F. Merian of the Albuquerque Division of EG&G whose encouragement and arrangements for financial assistance are gratefully acknowledged.

The rather staggering job of typing this dissertation fell on the willing shoulders of my wife, Diane Martin. However, her contribution in this respect is overshadowed by her continuing and understanding support throughout my program of graduate studies.

MEASUREMENT OF DEFORMATIONS IN A LARGE DISPLACEMENT GRADIENT FIELD

BY

Lowell P. Martin

ABSTRACT OF DISSERTATION

Submitted in Partial Fulfillment of the
Requirements for the Degree of
Doctor of Philosophy in Mechanical Engineering
in the Graduate School of
The University of New Mexico
Albuquerque, New Mexico
June, 1968

ABSTRACT

A summary of the general kinematical theory of finite deformations is presented together with analyses of the specific deformations of simple shear, bending of a block and bending of an initially curved cuboid.

The moiré fringe equations for large homogeneous deformation are developed. The extension to the nonhomogeneous case is presented and specific analyses are given for the deformations noted above. The moiré theory is combined with the results of the large deformation analyses.

Theoretical results are verified by the study of geometrically produced moiré patterns, and by actual experiments conducted on synthetic rubber specimens. The experiments included the deformations due to simple shear, bending of a block, bending of an initially curved cuboid, and extension of a plane tapered tensile specimen.

It is concluded that the moiré fringe method is a convenient, versatile and precise method to determine the components of Green's and Cauchy's deformation tensors for large two-dimensional deformations.

CONTENTS

LIST OF FIGURES

LIST OF TABLES

NOMENCLATURE

Symbol	Description	Page First Used
A, A_δ	Constant related to the magnitude of bending of a cuboid	20
A_m	Constant related to the size of a Fresnel figure master grid	71
a	Integer accounting for moiré pattern replications	26
B, B_δ	Constant related to the magnitude of bending of a cuboid	20
b	Integer accounting for moiré pattern replications	26
$\underline{\underline{C}}$, C_{JK}	Green's deformation tensor	6
C, C_δ	Constant related to the magnitude of bending of a cuboid	21
$\underline{\underline{c}}$, c_{jk}	Cauchy's deformation tensor	6
c	Displacement of master grid from origin	71
D	Constant related to the magnitude of bending of a cuboid	21
$\|\|D\|\|$	Deformation gradient matrix	5
d	b/a	33
dS	Length of undeformed line segment	5
ds	Length of deformed line segment	5
$\underline{\underline{E}}$, E_{JK}	Lagrangian strain tensor	6
E	Extension	7
e	Extension	7
$\underline{\underline{e}}$, e_{jk}	Eulerian strain tensor	6
F	Initial fringe pitch	34
f	Final fringe pitch	42
G_{JK}	Metric tensor of material coordinates	5
g_{jk}	Metric tensor of spatial coordinates	5

Symbol	Description	Page First Used
H	Initial fringe pitch	32
h	Final fringe pitch	46
$\underline{I}_K$	Rectangular base vector in Z^K	5
$\underline{i}_k$	Rectangular base vector in z^k	5
J	Specific master grid parameter value	67
j	Master grid parameter	26
K	Specific specimen grid parameter value	67
k	Specimen grid parameter	26
L	Constant related to the magnitude of bending of a cuboid	18
M	Initial master grating pitch	28
m	Final master grating pitch	29
N	Initial master grating pitch	28
n	Final master grating pitch	29
P, $\underline{P}$	Point or position vector in the undeformed body	3
p, $\underline{p}$	Point or position vector in the deformed body	3
P	Specific moiré fringe parameter value	67
p	Moiré fringe parameter	26
Q	Constant related to magnitude of simple shear	15
q	Moiré fringe parameter	66
R_i	Radii of undeformed specimen	18
r_i	Radii of deformed specimen	18
R_p	Radii of moiré fringe	64
S	Initial specimen grid pitch	29
s	Final specimen grid pitch	42

Symbol	Description	Page First Used
T	Initial specimen grid pitch	29
t	Final specimen grid pitch	46
t	Time	4
X^K	General material coordinates	3
x^k	General spatial coordinates	3
x_d	Center of moiré fringe replication	64
Z^K	Rectangular material coordinates	4
z^k	Rectangular spatial coordinates	4
α	Angle of simple shear deformation or angle of cuboid bending	16
$\mathcal{B}_i$	Principal angles	12
β_i	Principal angles	15
Γ	Initial specimen grid angle	29
γ	Final specimen grid angle	29
δ_{MN}	Kronecker delta	5
Θ	Initial master grid angle	28
θ	Final master grid angle	29
Λ	Stretch	7
λ	Stretch	7
Ξ	Initial angle between line segments	9
ξ	Final angle between line segments	9
Σ	Shear	9
σ	Shear	9
Υ	Initial master grid angle	28
υ	Final master grid angle	29

Symbol	Description	Page First Used
Φ	Initial moiré fringe angle	34
ϕ	Final moiré fringe angle	42
Ψ	Initial moiré fringe angle	32
ψ	Final moiré fringe angle	46
Ω	Initial specimen grid angle	29
ω	Final specimen grid angle	29

1. INTRODUCTION

1.1 General Background

In the past two decades the theory of finite deformations of continuous media has received a great deal of attention, culminating in a refined and sophisticated body of literature. Much of this work is critically summarized and presented by Truesdell and Toupin(18)[1] as part of their presentation of "The Classical Field Theories." Experimental methods for measuring finite or large strains have not achieved the same level of refinement. This can be attributed to two general circumstances. First, the common methods of biaxial strain measurement such as photoelasticity, electrical resistance strain gages and brittle coatings encountered nonlinearities or suffered from lack of adequate precision. Grid methods, described in detail by Durelli, Phillips and Tsao(5), provided perhaps the most reliable method, but at great cost in labor and time. Secondly, the experimentalists of the period often misinterpreted the theory or their measurements, or both, to such an extent that needless complications and discrepancies were encountered. This resulted in a great deal of confusion which lingers to the present time, even though an adequate experimental technique, the moiré fringe method, has been recognized for some time as a logical and versatile measurement tool for large two-dimensional deformations. Some specific problem areas are discussed in the summary of large deformation theory presented as Chapter 2.

Moiré patterns or fringes result from the superposition of two or more geometric figures which consist of fairly orderly, relatively closely spaced systems of curves, dots or other elementary geometric

[1]Numbers in parentheses refer to the List of References.

quantities. The fringes are the loci of points of intersection of the overlapping figures. Under certain circumstances the moiré patterns become quite obvious and easy to see. Furthermore, if after superposition one or both of the geometric figures are subsequently distorted, the pattern may change, often to a dramatic extent. It is this response of the moiré fringes to the distortion of an initial geometric figure which makes it a useful method for the measurement of surface strain in solid media.

In 1962, Theocaris(17) presented an exhaustive review of the literature on the moiré fringe method. In a recent article, Duffey and Mesmer(2) described a method of measuring finite rotation and strain using moiré. The technique, in which moiré fringes are used to find required displacement gradients, is limited to the case involving initially identical rectangular specimen and master grids aligned with the initial coordinate axes. Other recent publications such as those by Sciammarella(15), and Ross, Sciammarella and Sturgeon(14) discuss refinements in experimental technique to improve the precision of the measurements. Additional references are cited in the text as they become pertinent to the discussion.

1.2 Purpose of the Investigation

The purpose of this investigation is to extend and generalize the moiré fringe method for measuring large two-dimensional deformations; and to unambiguously relate the moiré results to fundamental measures and quantities encountered in the modern theory of large deformations.

2. LARGE DEFORMATION THEORY

2.1 General

The theory of large or finite deformations of continuous media is well established and has been presented in numerous reports, journals and textbooks. A convenient reference, which includes an extensive bibliography, is the text, Nonlinear Theory of Continuous Media, by Eringen(7). A more comprehensive treatment is given in the previously cited article, "The Classical Field Theories," by Truesdell and Toupin(18). Except for minor changes in nomenclature, the summary of the theory of large deformations presented in the sequel is taken from these sources. While it is possible to develop the governing equations for moiré fringes without reference to large deformation theory, the usefulness of the moiré theory is considerably diminished if not directly related to fundamental deformation measures.

The last three sections of this chapter present the governing equations for the deformations of simple shear, bending of a block, and bending of an initially curved cuboid. These equations are used later in the report to develop and/or verify the moiré fringe theory as applied to the specific deformations.

2.1.1 Coordinates

At a given reference time, the material points of a continuous medium occupy a region B, as shown in Figure 2.1. The position of a material point P in the region is denoted by a curvilinear coordinate system X^K, (K = 1,2,3). At a later time after deformation takes place, the material points of region B go into a region b. A point p in the deformed state is represented by a new set of curvilinear coordinates x^k, (k = 1,2,3). When points of B are referred to a rectangular coor-

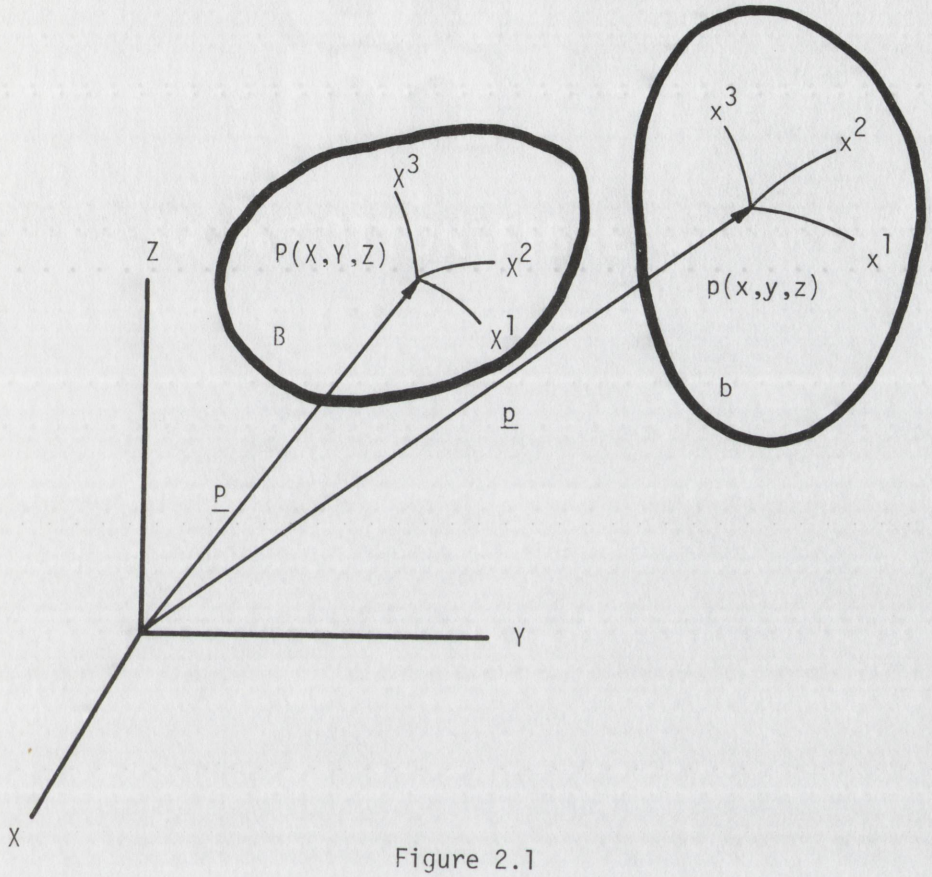

Figure 2.1

Coordinate System

dinate system, Z^K are used in place of X^K where $Z^1 = X$, $Z^2 = Y$, $Z^3 = Z$. Similarly, $z^1 = x$, $z^2 = y$, and $z^3 = z$. By current usage, X^K and Z^K are called "material" or "lagrangian" coordinates, while x^k and z^k are called "spatial" or "eulerian" coordinates.

The motion of the body during deformation carries various material points through various spatial positions. This is expressed by

$$x^k = x^k(X^K,t) \quad \text{or} \quad X^K = X^K(x^k,t) \tag{2.1}$$

where t is time. When the functional relationship is known, the par-

tial derivatives form a double-vector field called the deformation gradient. The matrix is

$$\|D\| = \left[\frac{\partial x^k}{\partial X^K}\right] \quad . \tag{2.2}$$

Except where noted, dimensional quantities before deformation will be represented by capital letters, while after deformation, they will be represented by small letters.

2.1.2 Base Vectors and Metric Tensors

The position vector $\underline{P}$ of a point P in B and $\underline{p}$ of a point p in b are given by

$$\underline{P} = Z^K \underline{I}_K$$

and

$$\underline{p} = z^k \underline{i}_k$$

where $\underline{I}_K$ and $\underline{i}_k$ are the rectangular base vectors in Z^K and z^k. The covariant metric tensors in B and b are defined as

$$G_{JK} = \delta_{MN} \frac{\partial Z^M}{\partial X^J} \frac{\partial Z^N}{\partial X^K} \tag{2.3}$$

and

$$g_{jk} = \delta_{mn} \frac{\partial z^m}{\partial x^j} \frac{\partial z^n}{\partial x^k} \tag{2.4}$$

respectively, where δ_{MN} and δ_{mn} are the Kronecker deltas.

2.1.3 Deformation and Strain Tensors

The squares of the lengths of line elements in B and in b are given respectively by the equations

$$dS^2 = G_{JK}\, dX^J\, dX^K$$

and

$$ds^2 = g_{jk}\, dx^j\, dx^k$$

where G_{JK} and g_{jk} are the appropriate covariant metric tensors. These equations can also be expressed as

$$dS^2 = c_{jk}\, dx^j\, dx^k$$

and

$$ds^2 = C_{JK}\, dX^J\, dX^K$$

where c_{jk}, called Cauchy's deformation tensor, is defined by

$$c_{jk} = G_{JK} \frac{\partial X^J}{\partial x^j} \frac{\partial X^K}{\partial x^k} \tag{2.5}$$

and C_{JK}, called Green's deformation tensor, is defined by

$$C_{JK} = g_{jk} \frac{\partial x^j}{\partial X^J} \frac{\partial x^k}{\partial X^K} \quad . \tag{2.6}$$

Both of the deformation tensors are symmetrical and positive-definite.

The difference of the squares of the line elements containing the same material points in B and b implies a length change due to deformation. This can be expressed as

$$ds^2 - dS^2 = 2E_{JK}\, dX^J\, dX^K$$

or

$$ds^2 - dS^2 = 2e_{jk}\, dx^j\, dx^k$$

where

$$E_{JK} = \frac{1}{2}(C_{JK} - G_{JK}) \tag{2.7}$$

is called the lagrangian strain tensor and

$$e_{jk} = \frac{1}{2}(g_{jk} - c_{jk}) \tag{2.8}$$

is called the eulerian strain tensor.

It can be shown that

$$E_{JK} = e_{jk} \frac{\partial x^j}{\partial X^J} \frac{\partial x^k}{\partial X^K}$$

and

$$e_{jk} = E_{JK} \frac{\partial X^J}{\partial x^j} \frac{\partial X^K}{\partial x^k}$$

The strain tensors are related to the displacement field. However, as pointed out by Truesdell and Toupin(18), "While the displacement vector figures largely in many of the older treatments and in approximate theories...in general its introduction serves only to lengthen and complicate the formulae in which it appears." Since the strain tensor can be conveniently related to the deformation through Equations (2.7) and (2.8), no consideration will be given to the displacement vector. Eringen(7) presents a fairly complete discussion of the displacement vector.

2.1.4 Length and Angle Changes

The ratio of the length of a deformed line element to the length of an undeformed line element, ds/dS, is called the "stretch." The stretch, $\Lambda = \lambda$, is defined by

$$\Lambda = \frac{ds}{dS} = \left(C_{JK} \frac{dX^J}{dS} \frac{dX^K}{dS} \right)^{\frac{1}{2}}$$

and

$$\lambda = \frac{ds}{dS} = \frac{1}{\left(c_{jk} \frac{dx^j}{ds} \frac{dx^k}{ds} \right)^{\frac{1}{2}}} \quad . \tag{2.9}$$

where $\frac{dX^K}{dS}$ is the component set of the orientation of dS and $\frac{dx^k}{ds}$ is the component set of the orientation of ds. The "extension" E and e is defined by

$$E = e = \Lambda - 1 = \frac{ds - dS}{dS} \quad .$$

Truesdell and Toupin(18), page 268, point out that all sorts of strain measures and definitions have been proposed through the years. While some of these definitions simplify selected problems, the advantage is usually lost in the general case. The main trouble appears to be a reluctance on the part of investigators to use the strain tensors $\underline{\underline{E}}$ and $\underline{\underline{e}}$ as strain measures since they are rather complicated quadratic functions of the displacement gradients. Consequently numerous definitions of "linear strains" or natural strains are proposed. This tendency seems to be particularly strong among the experimentalists. For example, Durelli, Parks and Feng(4) use the extension as their definition of "Lagrangian strain," and the ratio of the extension to the stretch as the definition of "Eulerian strain." In a prior paper Parks and Durelli(12) justify the use of various strain definitions and conclude that the experimentalist should use his own definitions of strain and "apply tensor analysis as an adjunct whenever it suits his purpose." Here Parks and Durelli make use of the equivalence of many of the strain measures. Meyer(9) defines an "elongation" which is the square of the stretch. He also defines an "actual finite strain" which is the same as the extension; and a "finite homogeneous strain" which is equivalent to the normal component of the lagrangian strain tensor $\underline{\underline{E}}$.

A brief survey of the references cited verifies Truesdell's observation that the use of strain measures or tensors rather than the deformation tensors $\underline{\underline{C}}$ or $\underline{\underline{c}}$ succeeds in making many simple problems appear complicated.

To demonstrate the relationship between the extensions and the normal components of the lagrangian strain tensor, consider the uni-

axial case in a cartesian coordinate system. Then

$$E_{JJ} = \frac{1}{2}\left(\Lambda^2_{(J)} - 1\right)$$

$$= \frac{1}{2}\left\{ \left(1 + E_{(J)}\right)^2 - 1 \right\}$$

$$= E_{(J)} + \frac{1}{2} E^2_{(J)} \quad .$$

In the case of small strains the extension is approximately equal to the lagrangian strain tensor component since the second order term may then be ignored.

As will be seen, much of the confusion concerning strain definitions may be avoided by first determining the deformation tensor components and then calculating the strains, extensions, or other quantities as desired.

To investigate angle changes, let two line elements $\underline{dS}$ and $\underline{dT}$ be deformed into the elements $\underline{ds}$ and $\underline{dt}$ as shown in Figure 2.2. It can be shown that the angles between the line elements can be calculated from

$$\cos\Xi_{S,T} = G_{JK} \frac{dX^J_{(S)}}{dS} \frac{dX^K_{(T)}}{dT}$$

$$= c_{jk}\, \lambda_{(s)}\, \lambda_{(t)} \frac{dx^j_{(s)}}{ds} \frac{dx^k_{(t)}}{dt} \qquad (2.10)$$

and

$$\cos\xi_{s,t} = \frac{C_{JK}}{\Lambda_{(S)}\Lambda_{(T)}} \frac{dX^J_{(S)}}{dS} \frac{dX^K_{(T)}}{dT} \quad . \qquad (2.11)$$

The shear in the plane determined by the line elements is defined as the decrease in angle

$$\Sigma_{S,T} = \sigma_{s,t} = \Xi_{S,T} - \xi_{s,t} \quad . \qquad (2.12)$$

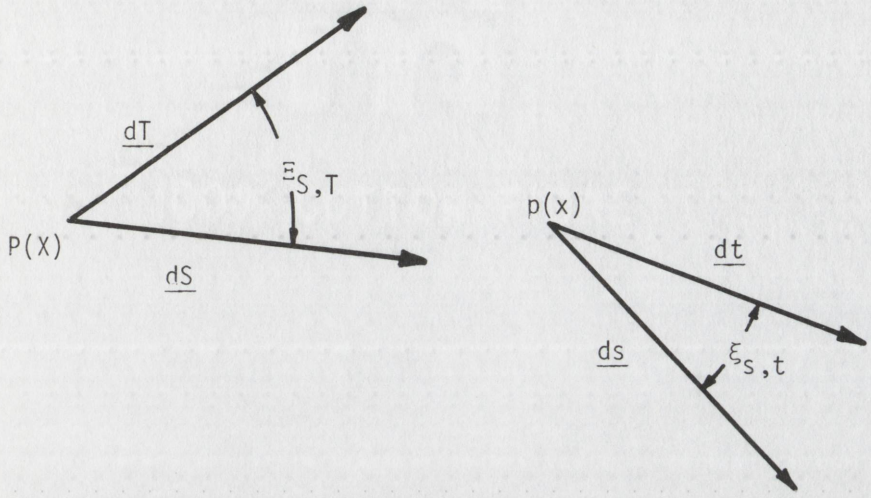

Figure 2.2

Angle Change

If the line elements $\underline{dS}$ and $\underline{dT}$ are initially orthogonal

$$\Sigma_{S,T} = \frac{\pi}{2} - \xi_{s,t}$$

then

$$\sin\Sigma_{S,T} = \cos\xi_{s,t} \quad .$$

If the line elements $\underline{dS}$ and $\underline{dT}$ are in the direction of the axes of a rectangular coordinate system

$$\sin\Sigma_{J,K} = \frac{C_{JK}}{\Lambda_{(J)}\Lambda_{(K)}} \quad , J \neq K \quad .$$

In terms of the strain components

$$\sin\Sigma_{J,K} = \frac{\delta_{JK} + 2E_{JK}}{\sqrt{(1 + 2E_{\underline{JJ}})(1 + 2E_{\underline{KK}})}} \quad , J \neq K$$

where the underline suspends the summation convention.

This may also be written

$$2E_{JK} = (1 + E_{(J)})(1 + E_{(K)}) \sin\Sigma_{J,K} \quad .$$

For small extensions

$$2E_{JK} \simeq \sin\Sigma_{J,K} \quad .$$

If the shear is also small,

$$2E_{JK} = \Sigma_{J,K}$$

which is the classical result in the theory of small deformations.

Equations (2.9) and (2.11) can be used to find the components of Green's deformation tensor. As an example, for two-dimensional deformation where $X^J = Z^J$, the referenced equations may be expanded as shown below:

$$C_{XX}\left(\frac{dX_S}{dS}\right)^2 + C_{XY}\left(2\,\frac{dX_S}{dS}\,\frac{dY_S}{dS}\right)^2 + C_{YY}\left(\frac{dY_S}{dS}\right)^2 = \Lambda_S^2$$

$$C_{XX}\left(\frac{dX_T}{dT}\right)^2 + C_{XY}\left(2\,\frac{dX_T}{dT}\,\frac{dY_T}{dT}\right) + C_{YY}\left(\frac{dY_T}{dT}\right)^2 = \Lambda_T^2$$

$$C_{XX}\left(\frac{dX_S}{dS}\,\frac{dX_T}{dT}\right) + C_{XY}\left(\frac{dX_S}{dS}\,\frac{dY_T}{dT} + \frac{dY_S}{dS}\,\frac{dX_T}{dT}\right) + C_{YY}\left(\frac{dY_S}{dS}\,\frac{dY_T}{dT}\right) =$$

$$= \Lambda_S\,\Lambda_T \cos\xi_{s,t} \qquad (2.13)$$

where the parentheses are omitted from the subscripted terms for convenience. If the orientations of the material line segments, the stretches, and the angle $\xi_{s,t}$ can be measured, the solution of Equations (2.13) gives the components of Green's deformation tensor in two dimensions

$$\underline{\underline{C}} = \begin{bmatrix} C_{XX} & C_{XY} \\ C_{XY} & C_{YY} \end{bmatrix} \quad . \qquad (2.14)$$

Using Equation (2.7) the lagrangian strain tensor is then found to be

$$\underline{\underline{E}} = \begin{bmatrix} E_{XX} & E_{XY} \\ E_{XY} & E_{YY} \end{bmatrix} = \frac{1}{2} \begin{bmatrix} C_{XX}-1 & C_{XY} \\ C_{XY} & C_{YY}-1 \end{bmatrix} \quad . \tag{2.15}$$

The principal values of the deformation tensor are found by reducing $\underline{\underline{C}}$ to a diagonal form. That is, for the two-dimensional case

$$\underline{\underline{C}} = \begin{bmatrix} C_{XX} & C_{XY} \\ C_{XY} & C_{YY} \end{bmatrix} \leftrightarrow \begin{bmatrix} C_1 & 0 \\ 0 & C_2 \end{bmatrix} \quad . \tag{2.16}$$

Explicitly, the principal values are

$$C_1 = \frac{C_{XX} + C_{YY}}{2} + \left\{ \left(\frac{C_{XX} - C_{YY}}{2} \right)^2 + C_{XY}^2 \right\}^{\frac{1}{2}} \tag{2.17}$$

$$C_2 = \frac{C_{XX} + C_{YY}}{2} - \left\{ \left(\frac{C_{XX} - C_{YY}}{2} \right)^2 + C_{XY}^2 \right\}^{\frac{1}{2}} \quad . \tag{2.18}$$

The maximum value of the shear component of $\underline{\underline{C}}$ in the X-Y plane is

$$C_{12} = \pm \frac{C_1 - C_2}{2} \tag{2.19}$$

The principal directions are found from the relations

$$\tan\beta_1 = \frac{C_{YY} - C_{XX}}{2C_{XY}} + \left\{ \left(\frac{C_{YY} - C_{XX}}{2C_{XY}} \right)^2 + 1 \right\}^{\frac{1}{2}} \tag{2.20}$$

$$\tan\beta_2 = \frac{C_{YY} - C_{XX}}{2C_{XY}} - \left\{ \left(\frac{C_{YY} - C_{XX}}{2C_{XY}} \right)^2 + 1 \right\}^{\frac{1}{2}} \quad . \tag{2.21}$$

where the angles β_i are measured counterclockwise from the x-axis. It is well known that the principal values C_1 and C_2 are associated with orthogonal directions. In addition, the directions of the planes of

the maximum shear components bisect the angles between the principal directions.

From Equation (2.9) the stretches of elements initially lying in the X and Y directions are respectively

$$\Lambda_X = C_{XX}^{\frac{1}{2}}$$

$$\Lambda_Y = C_{YY}^{\frac{1}{2}} \quad .$$

The corresponding extensions are

$$E_X = \Lambda_X - 1 = C_{XX}^{\frac{1}{2}} - 1$$

$$E_Y = \Lambda_Y - 1 = C_{YY}^{\frac{1}{2}} - 1 \quad .$$

The principal stretches corresponding to C_1 and C_2 are

$$\Lambda_1 = C_1^{\frac{1}{2}}$$

$$\Lambda_2 = C_2^{\frac{1}{2}} \quad .$$

The principal values of the extensions are

$$E_1 = \Lambda_1 - 1 = C_1^{\frac{1}{2}} - 1$$

$$E_2 = \Lambda_2 - 1 = C_2^{\frac{1}{2}} - 1 \quad .$$

The principal values of the lagrangian strain tensor are

$$E_1 = \frac{1}{2}(C_1 - 1)$$

$$E_2 = \frac{1}{2}(C_2 - 1) \quad .$$

Similar equations can be developed for the spatial coordinates, z^k.

From Equations (2.9) and (2.10)

$$c_{xx}\left(\frac{dx_s}{ds}\right)^2 + c_{xy}\left(2\,\frac{dx_s}{ds}\,\frac{dy_s}{ds}\right) + c_{yy}\left(\frac{dy_s}{ds}\right)^2 = \frac{1}{\lambda_s^2}$$

$$c_{xx}\left(\frac{dx_t}{dt}\right)^2 + c_{xy}\left(2\,\frac{dx_t}{dt}\,\frac{dy_t}{dt}\right) + c_{yy}\left(\frac{dy_t}{dt}\right)^2 = \frac{1}{\lambda_t^2}$$

$$c_{xx}\left(\frac{dx_s}{ds}\,\frac{dx_t}{dt}\right) + c_{xy}\left(\frac{dx_s}{ds}\,\frac{dy_t}{dt} + \frac{dy_s}{ds}\,\frac{dx_t}{dt}\right) + c_{yy}\left(\frac{dy_s}{ds}\,\frac{dy_t}{dt}\right) = \frac{\cos\Xi_{S,T}}{\lambda_s\,\lambda_t} \quad . \qquad (2.22)$$

The solution of Equations (2.22) gives the components of Cauchy's deformation tensor in two dimensions

$$\underline{\underline{c}} = \begin{bmatrix} c_{xx} & c_{xy} \\ c_{xy} & c_{yy} \end{bmatrix} \quad .$$

The eulerian strain tensor is, from Equation (2.8),

$$\underline{\underline{e}} = \frac{1}{2}\begin{bmatrix} 1-c_{xx} & -c_{xy} \\ -c_{xy} & 1-c_{yy} \end{bmatrix} \quad .$$

The principal values of $\underline{\underline{c}}$ are found using equations similar to Equations (2.17) through (2.21). That is

$$c_1 = \frac{c_{xx} + c_{yy}}{2} - \left\{\left(\frac{c_{xx} - c_{yy}}{2}\right)^2 + c_{xy}^2\right\}^{\frac{1}{2}}$$

$$c_2 = \frac{c_{xx} + c_{yy}}{2} + \left\{\left(\frac{c_{xx} - c_{yy}}{2}\right)^2 + c_{xy}^2\right\}^{\frac{1}{2}}$$

$$c_{12} = \pm\frac{c_1 - c_2}{2}$$

The principal direction is

$$\tan\beta_1 = \frac{c_{yy} - c_{xx}}{2c_{xy}} - \left\{\left(\frac{c_{yy} - c_{xx}}{2c_{xy}}\right)^2 + 1\right\}^{\frac{1}{2}} \quad .$$

2.2 Simple Shear Deformation

As mentioned at the beginning of this chapter, certain specific deformations will be investigated later in this report to verify the moiré analyses. The homogeneous deformation to be studied is simple shear. For this purpose the following discussion is presented, as outlined by Eringen(7). It is noted that simple shear is included in the class of deformations given by a homogeneous affine transformation relating the positions of Z^K and z^k of a material point before and after deformation as

$$z^k = D^k{}_K \, Z^K \tag{2.23}$$

$$Z^K = {}^{-1}D^K{}_k \, z^k \tag{2.24}$$

$$D^k{}_K \, {}^{-1}D^K{}_j = \delta^k{}_j \tag{2.25}$$

where $D^k{}_K$ and the inverse ${}^{-1}D^K{}_k$ are constant matrices. $\|D\|$ is the deformation gradient matrix defined by Equation (2.2). Strains described by Equations (2.23) through (2.25) are called homogeneous strains. Simple shear is defined specifically by the matrix

$$\|D\| = \begin{bmatrix} 1 & Q & 0 \\ 0 & 1 & 0 \\ 0 & 0 & 1 \end{bmatrix}$$

where Q is a constant. From Equation (2.23)

$$\begin{aligned} x &= X + QY \\ y &= Y \\ z &= Z \end{aligned} \tag{2.26}$$

where the coordinates are shown in Figure 2.3.

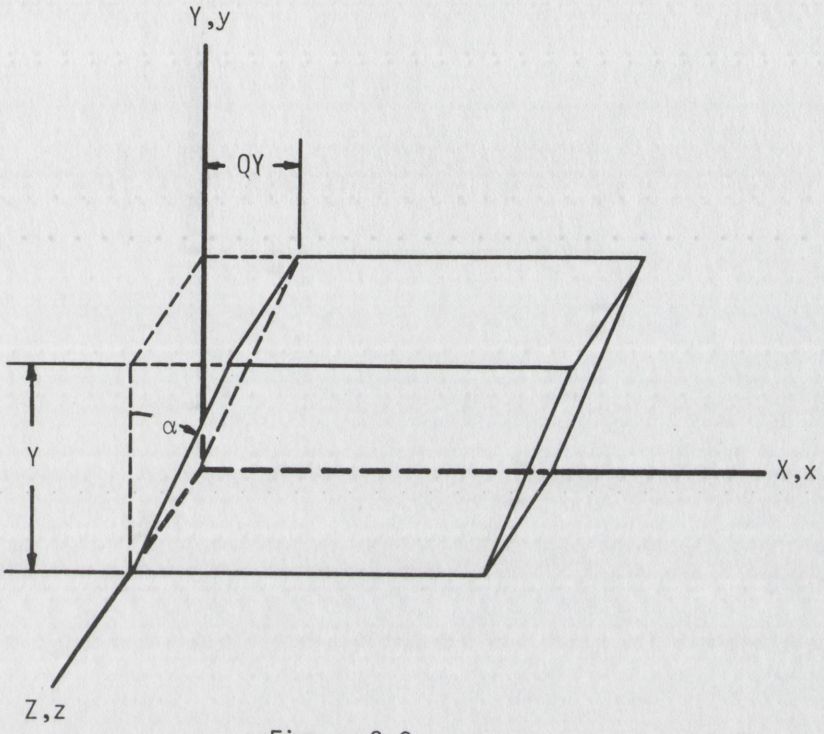

Figure 2.3

Simple Shear

From Figure 2.3

$$\alpha = \arctan Q \quad . \tag{2.27}$$

Equations (2.26) and (2.27) indicate that the X = constant planes are rotated rigidly through an angle α about elements lying parallel to the Z-axis in the Y = 0 plane. The Y = constant and Z = constant planes do not rotate as a result of the deformation.

From Equations (2.5) and (2.6), Cauchy's and Green's deformation

tensors in rectangular cartesian coordinates are given respectively by

$$c_{jk} = \delta_{JK} \frac{\partial Z^J}{\partial z^j} \frac{\partial Z^K}{\partial z^k}$$

and

$$C_{JK} = \delta_{jk} \frac{\partial z^j}{\partial Z^J} \frac{\partial z^k}{\partial Z^K} \quad .$$

Consequently the components of Green's deformation tensor can be obtained from Equations (2.26). Thus

$$\underline{\underline{C}} = \begin{bmatrix} 1 & Q & 0 \\ Q & 1+Q^2 & 0 \\ 0 & 0 & 1 \end{bmatrix} \quad . \tag{2.28}$$

Similarly Cauchy's deformation tensor is

$$\underline{\underline{c}} = \begin{bmatrix} 1 & -Q & 0 \\ -Q & 1+Q^2 & 0 \\ 0 & 0 & 1 \end{bmatrix} \quad . \tag{2.29}$$

From Equations (2.7) and (2.28) the lagrangian strain tensor is

$$\underline{\underline{E}} = \begin{bmatrix} 0 & Q/2 & 0 \\ Q/2 & Q^2/2 & 0 \\ 0 & 0 & 0 \end{bmatrix} \quad .$$

Similarly the eulerian strain tensor is

$$\underline{\underline{e}} = \begin{bmatrix} 0 & Q/2 & 0 \\ Q/2 & -Q^2/2 & 0 \\ 0 & 0 & 0 \end{bmatrix} \quad .$$

From Equations (2.17) and (2.18) the proper numbers C_1 and C_2 are found to be

$$C_1 = \frac{1}{c_1} = 1 + Q^2/2 + Q(1 + Q^2/4)^{\frac{1}{2}} = \Lambda_1^2 \tag{2.30}$$

$$C_2 = \frac{1}{c_2} = 1 + Q^2/2 - Q(1 + Q^2/4)^{\frac{1}{2}} = \Lambda_2^2 \quad . \tag{2.31}$$

Note also that for the three-dimensional case

$$C_3 = \frac{1}{c_3} = 1 = \lambda_3^2 \quad .$$

The principal directions for C_1 and c_1 are found from Equations (2.20), (2.28) and (2.29)

$$\tan\beta_1 = Q/2 + (1 + Q^2/4)^{\frac{1}{2}}$$

$$\tan\beta_1 = Q/2 - (1 + Q^2/4)^{\frac{1}{2}} \quad . \tag{2.32}$$

where the angles are measured counterclockwise from the X-axis.

2.3 Pure Bending of a Block

Pure bending of a block or cuboid belongs to the class of deformations that result from an appropriate deformation of an object having a special geometry. The block is initially a rectangular parallelepiped in which the X = constant planes become circular sections, the Y = constant planes become radial planes and the Z = constant planes are preserved. The deformation is illustrated in Figure 2.4 which also presents the coordinate systems used. If cylindrical coordinates are chosen to represent the strained body, the origin of coordinates can be chosen to coincide with the origin of the rectangular material coordinate system so that

$$\begin{aligned} x^1 &= r = f(X) \\ x^2 &= \alpha = g(Y) \\ x^3 &= z = h(Z) \quad , \end{aligned} \tag{2.33}$$

and

$$\begin{aligned} X &= r\cos\alpha \\ Y &= r\sin\alpha \\ Z &= Lz \quad . \end{aligned} \tag{2.34}$$

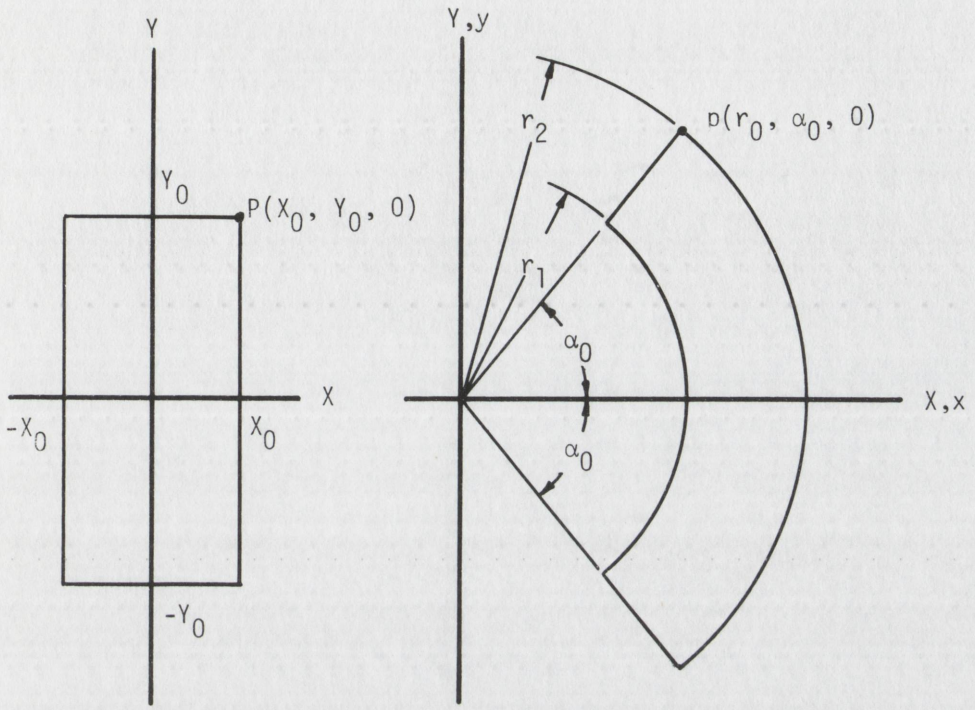

Figure 2.4

Bending of a Block

From Equations (2.3) and (2.4) the metric tensors are

$$G_{JK} = \begin{bmatrix} 1 & 0 & 0 \\ 0 & 1 & 0 \\ 0 & 0 & 1 \end{bmatrix}$$

and

$$g_{jk} = \begin{bmatrix} 1 & 0 & 0 \\ 0 & r^2 & 0 \\ 0 & 0 & 1 \end{bmatrix} .$$

From Equation (2.6), Green's deformation tensor is found to be

$$C = \begin{bmatrix} \left(\frac{\partial f}{\partial X}\right)^2 & 0 & 0 \\ 0 & \left(r\frac{\partial g}{\partial Y}\right)^2 & 0 \\ 0 & 0 & \left(\frac{\partial h}{\partial Z}\right)^2 \end{bmatrix} .$$

Since the tensor $\underline{\underline{C}}$ is already in diagonal form, the coordinates Z^K in the undeformed or material state are in the principal directions. The proper numbers of $\underline{\underline{C}}$ are then by definition

$$C_1 = \left(\frac{\partial f}{\partial X}\right)^2$$

$$C_2 = \left(r\frac{\partial g}{\partial Y}\right)^2$$

$$C_3 = \left(\frac{\partial h}{\partial Z}\right)^2 \quad .$$

Thus the principal stretches are

$$\Lambda_1 = C_1^{\frac{1}{2}} = \frac{\partial f}{\partial X}$$

$$\Lambda_2 = C_2^{\frac{1}{2}} = r\frac{\partial g}{\partial Y}$$

$$\Lambda_3 = C_3^{\frac{1}{2}} = \frac{\partial h}{\partial Z}$$

If the deformation is isochoric, it can be shown that the trace of Green's deformation tensor must satisfy the relation

$$f \frac{\partial f}{\partial X} \frac{\partial g}{\partial Y} \frac{\partial h}{\partial Z} = 1 \quad .$$

Then

$$\frac{\partial}{\partial X}\left(\frac{1}{f\frac{\partial f}{\partial X}}\right) = \frac{\partial}{\partial X}\left(\frac{\partial g}{\partial Y}\frac{\partial h}{\partial Z}\right) = 0 \quad .$$

Integrating

$$\frac{1}{f\frac{\partial f}{\partial X}} = A_1 \quad .$$

Integrating again

$$f^2 = \frac{2}{A_1}(X - A_2) \quad .$$

Let

$$A = \frac{1}{A_1}$$

and

$$B = \frac{-2\,A_2}{A_1} \quad .$$

Then the expression for f may be written

$$f = r = (2AX + B)^{\frac{1}{2}} \quad .$$

Now

$$f' = A(2AX + B)^{-\frac{1}{2}} \quad .$$

Thus,

$$A \frac{\partial g}{\partial Y} \frac{\partial h}{\partial Z} = 1 \quad .$$

Then

$$\frac{\partial}{\partial Y} \left(\frac{\partial g}{\partial Y} \right) = \frac{\partial}{\partial Y} \left(\frac{1}{A \frac{\partial h}{\partial Z}} \right) = 0 \quad .$$

Integrating

$$\frac{\partial g}{\partial Y} = C$$

$$g = CY + A_3 \quad .$$

Similarly

$$h = DZ + A_4 \quad .$$

If the body is bent symmetrically with respect to the X-axis and if it is cut exactly in half by the X-Y plane, then without loss of generality

$$A_3 = A_4 = 0 \quad .$$

Thus in summary

$$r = (2AX + B)^{\frac{1}{2}}$$

$$\alpha = CY$$

$$z = DZ \quad . \qquad (2.35)$$

From Equations (2.34) and (2.35)

$$L = \frac{1}{D}$$

From Figure 2.4 and Equations (2.35)

$$r_2^2 = 2AX_0 + B$$

$$r_1^2 = -2AX_0 + B \quad .$$

Thus

$$r_2^2 - r_1^2 = 4AX_0 \tag{2.36}$$

$$r_2^2 + r_1^2 = 2B \quad . \tag{2.37}$$

Also

$$\alpha_0 = CY_0$$

and

$$\alpha_0 D(r_2^2 - r_1^2) = 4X_0Y_0 \quad .$$

Finally, the radius to any point in the deformed block is found to be

$$r = \frac{\sqrt{2}}{2}\left[\frac{X}{X_0}(r_2^2 - r_1^2) + (r_1^2 + r_2^2)\right]^{\frac{1}{2}}$$

$$= \frac{\sqrt{2}}{2}\left[r_2^2(1 + \frac{X}{X_0}) + r_1^2(1 - \frac{X}{X_0})\right]^{\frac{1}{2}} \quad . \tag{2.38}$$

The angle α to any point is

$$\alpha = \frac{\alpha_0}{Y_0} Y \tag{2.39}$$

and the dimension z is

$$z = \frac{4X_0Y_0Z}{\alpha_0(r_2^2 - r_1^2)} \quad . \tag{2.40}$$

Equations (2.38) through (2.40) define the motion between corresponding material and spatial points of the block due to pure bending.

The proper numbers of Green's deformation tensor are

$$C_1 = \frac{A^2}{r^2} = \frac{(r_2^2 - r_1^2)^2}{16X_0^2r^2} = \Lambda_1^2$$

$$C_2 = C^2r^2 = \frac{\alpha_0^2}{Y_0^2} r^2 = \Lambda_2^2$$

$$C_3 = D^2 = \frac{16X_0^2Y_0^2}{\alpha_0^2(r_2^2 - r_1^2)^2} = \Lambda_3^2 \tag{2.41}$$

2.4 Flexure of an Initially Curved Cuboid

The undeformed body is a sector of a circular ring, which is deformed into another circular ring sector. The cylindrical coordinate systems (R,Θ,Z) and (r,θ,z) are selected for X^K and x^k. The origin of coordinates is chosen such that the undeformed body is bounded by the curved surfaces $R=R_1$, $R=R_2$, $(R_2>R_1)$; the planes $\Theta=\pm\Theta_0$; and the planes $Z=\pm Z_0$. After deformation, the corresponding bounding surfaces are $r=r_1$, $r=r_2$; $\theta=\pm\theta_0$ and $z=\pm z_0$. The ring surfaces are shown in Figure 2.5.

From Equations (2.3) and (2.4) the metric tensors are

$$G_{JK} = \begin{bmatrix} 1 & 0 & 0 \\ 0 & R^2 & 0 \\ 0 & 0 & 1 \end{bmatrix}$$

and

$$g_{jk} = \begin{bmatrix} 1 & 0 & 0 \\ 0 & r^2 & 0 \\ 0 & 0 & 1 \end{bmatrix} .$$

The deformation may be represented by the equations

$$r = f(R)$$

$$\theta = g(\Theta)$$

$$z = h(Z)$$

where attention is restricted to the case where f, g and h are continuously differentiable functions.

It can be shown that

$$\underline{\underline{c}}^{-1} = \begin{bmatrix} \left(\frac{\partial f}{\partial R}\right)^2 & 0 & 0 \\ 0 & \frac{1}{R^2}\left(\frac{\partial g}{\partial \Theta}\right)^2 & 0 \\ 0 & 0 & \left(\frac{\partial h}{\partial Z}\right)^2 \end{bmatrix} \qquad (2.42)$$

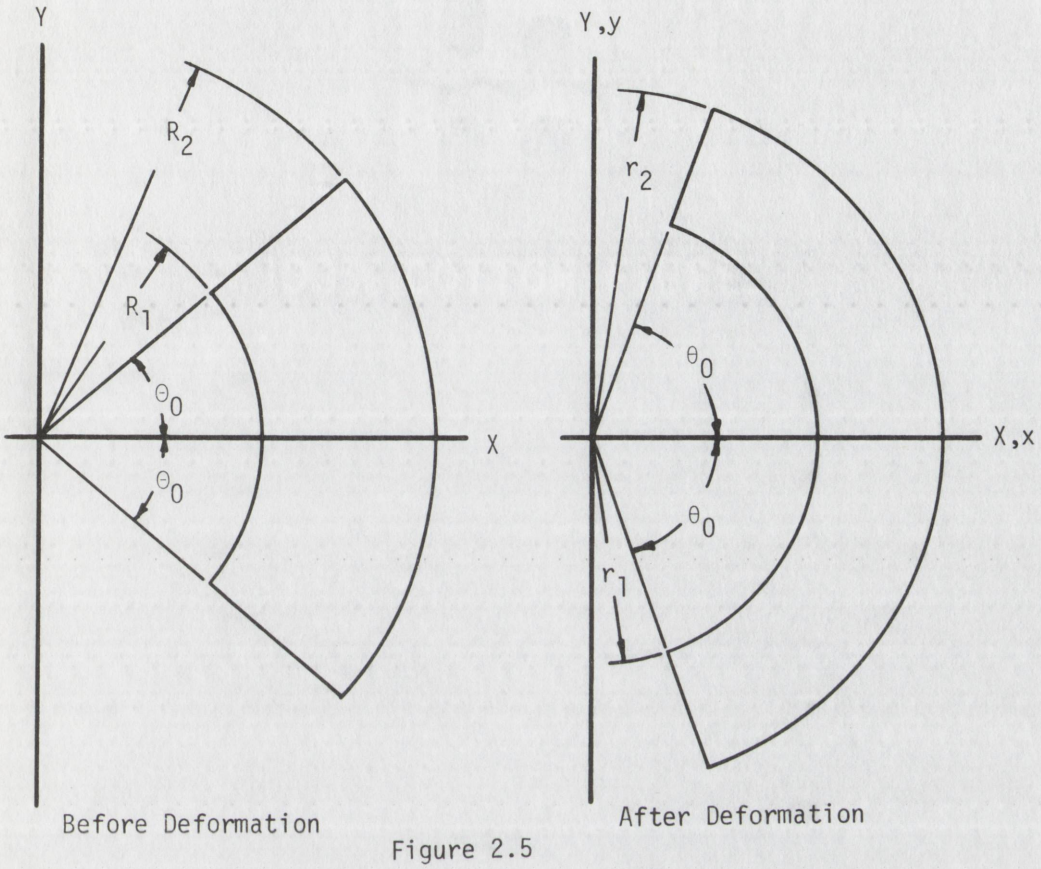

Figure 2.5

Bending of an Initially Curved Cuboid

and that the condition of incompressibility requires that

$$\frac{f}{R}\frac{\partial f}{\partial R}\frac{\partial g}{\partial \Theta}\frac{\partial h}{\partial Z} = 1 \quad .$$

Then

$$\frac{\partial}{\partial R}\left(\frac{1}{\frac{f}{R}\frac{\partial f}{\partial R}}\right) = \frac{\partial}{\partial R}\left(\frac{\partial g}{\partial \Theta}\frac{\partial h}{\partial Z}\right) = 0 \quad .$$

Integrating

$$\frac{1}{\frac{f}{R}\frac{\partial f}{\partial R}} = A_1 \quad .$$

Integrating again

$$f^2 = \frac{R^2}{A_1} + A_2 \quad .$$

Let

$$A = \frac{1}{A_1}$$

and

$$B = A_2 \quad .$$

Then

$$f = r = (AR^2 + B)^{\frac{1}{2}} \quad . \tag{2.43}$$

By similar methods it is found that

$$\Theta = C\theta \tag{2.44}$$

and

$$z = DZ \quad . \tag{2.45}$$

Equations (2.43), (2.44) and (2.45) can be used to show that

$$A = \frac{r_2^2 - r_1^2}{R_2^2 - R_1^2}$$

$$B = \frac{R_2^2 r_1^2 - R_1^2 r_2^2}{R_2^2 - R_1^2}$$

$$C = \frac{\theta_0}{\Theta_0}$$

$$D = \frac{z_0}{Z_0} \quad . \tag{2.46}$$

Substituting into Equation (2.42) and inverting the matrix, the proper numbers of $\underline{\underline{c}}$ are found to be

$$c_1 = \frac{r^2}{A(r^2 - B)} = \frac{(R_2^2 - R_1^2)^2 r^2}{(r_2^2 - r_1^2)\left[r^2(R_2^2 - R_1^2) - (R_2^2 r_1^2 - R_1^2 r_2^2)\right]} = \frac{1}{\lambda_1^2}$$

$$c_2 = \frac{r^2 - B}{AC\, r^2} = \frac{\Theta_0^2 \left[r^2(R_2^2 - R_1^2) - (R_2^2 r_1^2 - R_1^2 r_2^2)\right]}{\theta_0^2\, r^2 (r_2^2 - r_1^2)} = \frac{1}{\lambda_2^2}$$

$$c_3 = A^2 C^2 = \frac{\theta_0^2 (r_2^2 - r_1^2)}{\Theta_0^2 (R_2^2 - R_1^2)} = \frac{1}{\lambda_3^2} \quad . \tag{2.47}$$

3. MOIRÉ THEORY

3.1 General

As previously mentioned, moiré patterns or fringes result from the superposition of two or more geometric figures consisting of fairly orderly systems of curves or dots. The equations for the simpler moiré patterns can be derived by a number of methods including elementary geometry (10), (16), (6) and tensor analysis (1). However, a more versatile and descriptive method is that using indicial representation of the figures and patterns (11), (3). Due to the complexity of moiré patterns caused by large nonhomogeneous deformations, the indicial method will be used exclusively in the sequel, even though it is not absolutely necessary for the moiré analysis of homogeneous deformations.

Consider two geometric figures as shown in Figure 3.1, each consisting of a family of curves indexed by a numerical parameter ranging over some subset of the integers. The two geometric figures may be characterized by the equations

$$L(X^K) = L(j)$$

$$G(X^K) = G(k) \quad .$$

A family of moiré fringes is formed by the sets of intersections of the geometric figures. The fringes, in turn, may be characterized by the equation

$$Q(X^K) = q(j,k) = Q(p)$$

where j, k, and p are numerical parameters. Although there may be many functional relationships between the parameters which give rise to moiré patterns, the most obvious and visible patterns correspond to the simple relation

$$aj - bk = p - p_0 = \Delta p$$

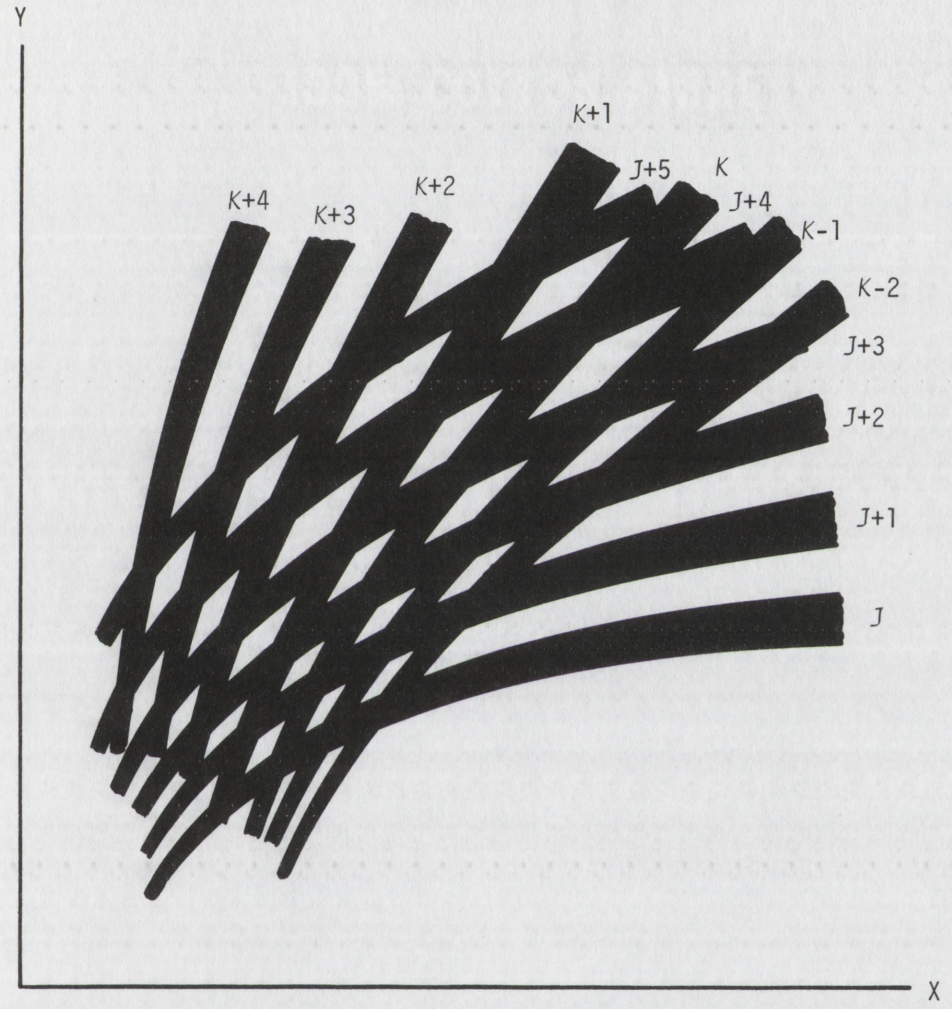

Figure 3.1

Formation of Moiré Fringes

where a and b are integers accounting for multiple moiré patterns or replications. For many practical cases, a = b = 1 or a = b = -1 as will be seen in the following sections. In addition there are many instances where $p_0 = 0$ so that

$$a\vec{j} - b\vec{k} = \vec{p} \quad . \tag{3.1}$$

3.2 Moiré Analysis of Two-Dimensional Homogeneous Deformations

In a homogeneous deformation, an initially straight line remains straight after deformation, even though it may experience a change in length and angle. It will be shown in this chapter that the change in length and angle of a line element may be determined from the response of moiré fringes to a deformation of a specimen grid. The angular orientation and spacing, or pitch, between line elements completely defines the geometry of a grid of equispaced parallel lines. The objective of the immediately following portion of this report is to find the pitch and orientation of a grid imprinted on a specimen in terms of the response or geometry of moiré fringes produced by the interaction of the specimen grid with a master grid or grating. Later in this section the specimen grid parameters will be related in a completely general fashion to the components of the deformation tensors discussed in Chapter 2.

The master gratings[1] are initially two families of equispaced straight lines with pitches M and N and angular orientations Θ and T.

---

[1]This analysis considers gratings no finer than approximately 1000 lines/inch, thus avoiding phenomena, such as diffraction of light, which may occur for gratings with finer pitch. Consequently all derivations are satisfactorily based on the approximate theory of rectilinear propagation of light. See Theocaris(17), p. 333.

The master gratings may experience subsequent uniform changes in pitch and rotation such that the final values are m and n and θ and υ respectively. The specimen grid is a rectangular array formed by two sets of parallel straight lines intersecting at some angle. The initial pitches of each set, S and T, are not necessarily equal. Furthermore, each set of lines on the specimen grid may have an initial angular orientation Γ and Ω, and a final orientation γ and ω, respectively.

When a master grating and specimen grid are superimposed, moiré fringes are formed as indicated in Figures 3.2, 3.3 and 3.4. For clarity, only one set of lines from the specimen grid is shown in each of the figures. This does not result in any loss of generality so long as the master grating consists of only one set of parallel lines. Although there is a set of moiré fringes formed by the intersections of the master grating lines with the specimen grid lines omitted in the figures, these fringes are not visible. This phenomenon is discussed in detail by Durelli and Parks(3).[2]

It can be seen from Figures 3.2 and 3.3 that moiré fringes with identical spacing and angular orientation may be formed by two completely different specimen grid geometries superimposed on identical master gratings. This characteristic will be explored in some detail later in the analysis.

By means of indicial Equation (3.1) it is possible to obtain relations describing the geometry of the moiré fringes in terms of the specimen and master grid parameters as shown on page 33.

---

[2]There is no fundamental reason preventing the use of both specimen and master grids simultaneously providing the resulting families of moiré fringes can be distinguished from each other. This can be accomplished by the proper selection of master grid pitches and orientations as discussed by Post(13).

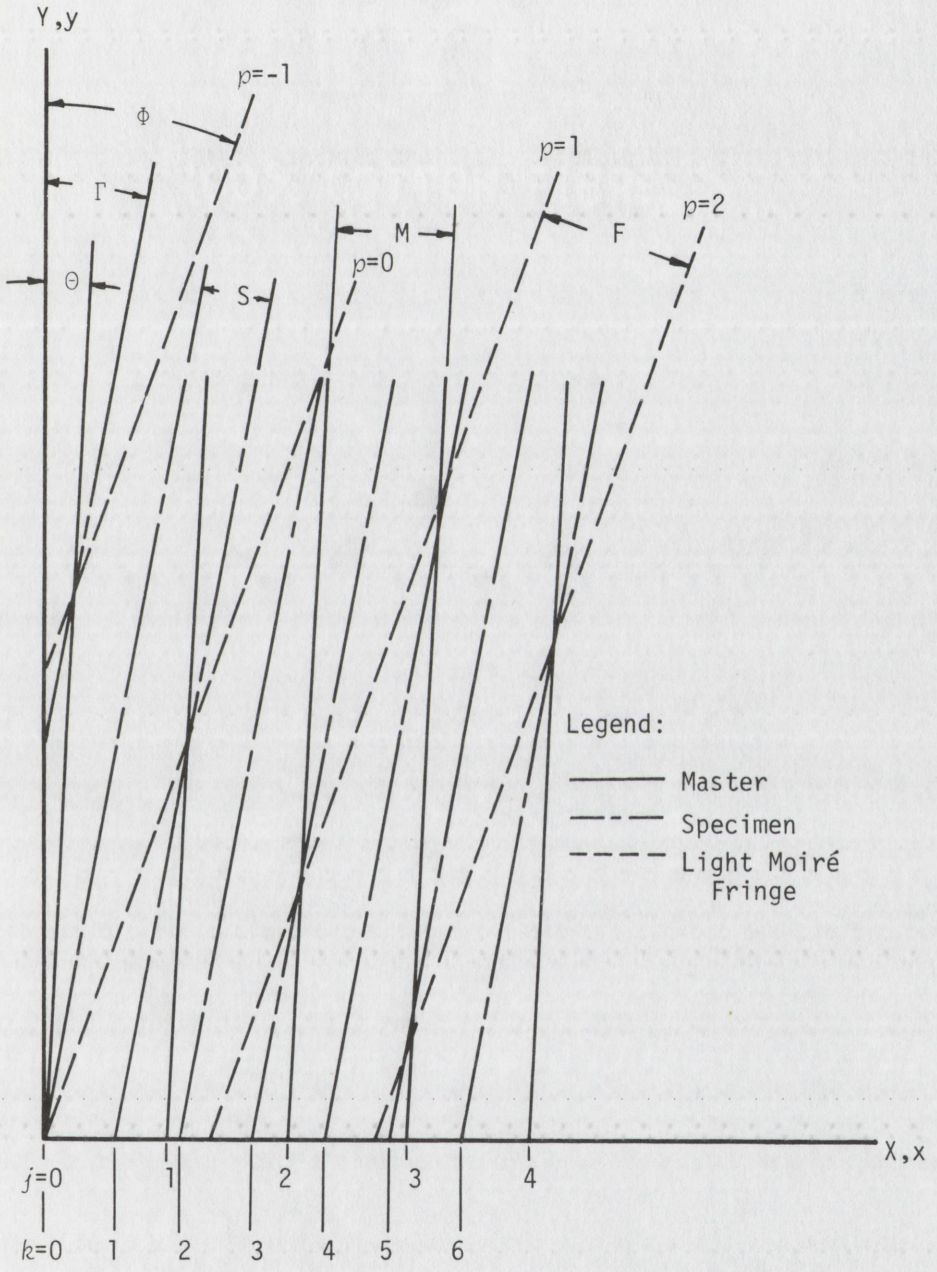

Figure 3.2

Moiré Pattern due to Grid System Referenced to Y-axis, S < M

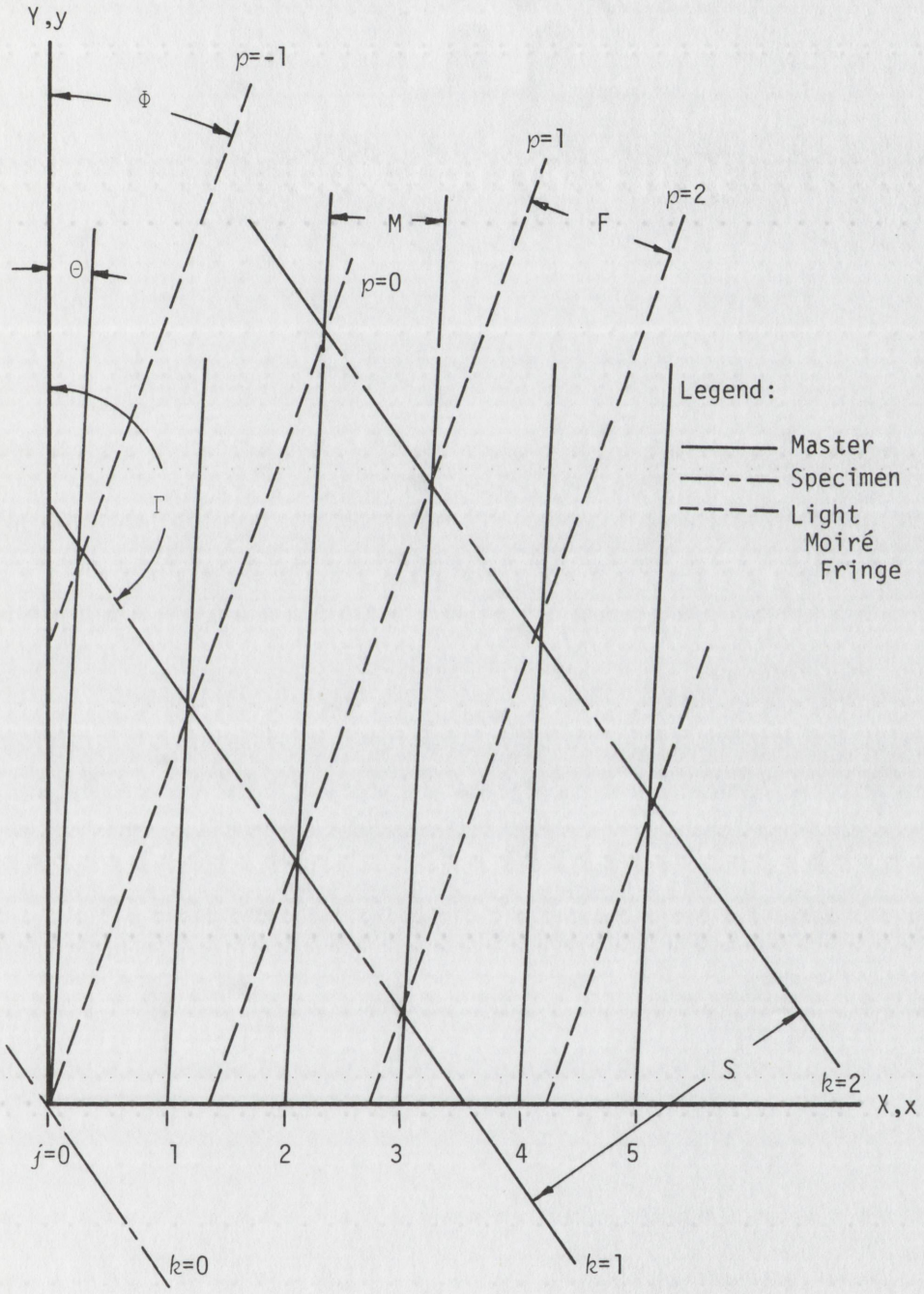

Figure 3.3

Moiré Pattern due to Grid System Referenced to Y-axis, S > M

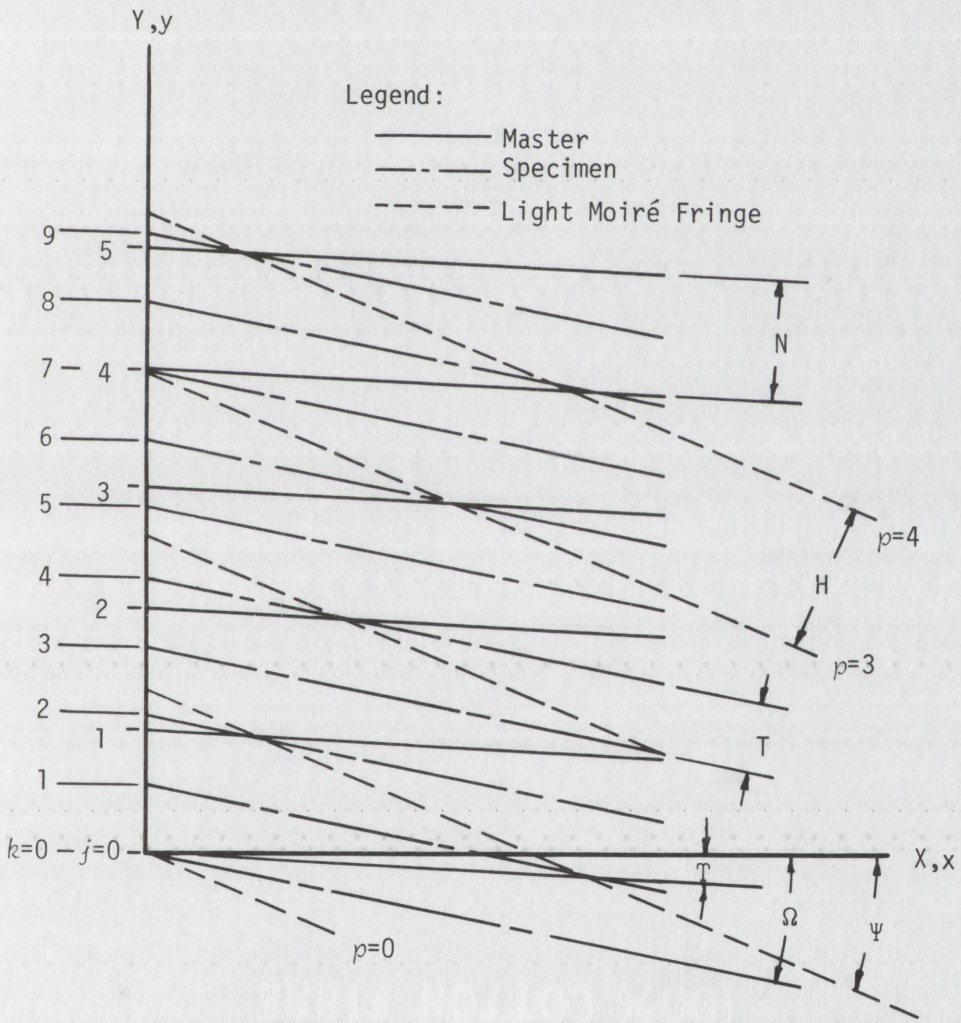

Figure 3.4

Moiré Pattern due to Grid System Referenced to X-axis, T < N

The family of lines comprising the initial master grating may be characterized by the equation

$$X = \frac{jM}{\cos\Theta} + Y \tan\Theta \tag{3.2}$$

where j is any integer. The portions of the initial specimen grids shown in Figures 3.2 or 3.3 may be characterized by the equation

$$X = \frac{kS}{\cos\Gamma} + Y \tan\Gamma \tag{3.3}$$

and the portion shown in Figure 3.4 may be characterized by the equation

$$Y = \frac{kT}{\cos\Omega} - X \tan\Omega \quad . \tag{3.4}$$

Using the line indexing system shown in Figure 3.2 where S<M, the indicial equation is obtained from Equation (3.1) by setting a = b = -1. Conversely from Figure 3.3 where S>M, the indicial equation is obtained by setting a = b = 1. The fringe pattern arising when S=M is discussed later in this analysis. As previously mentioned, Figures 3.2 and 3.3 show that two entirely different specimen grids can give rise to identical fringe patterns. This apparent ambiguity is directly related to the relative sizes of the specimen grid and master grating pitches. As the analysis is developed it will be seen that to overcome this uncertainty it is necessary to obtain qualitative information pertaining to the relative sizes of the grid pitches.[3] An experimental method for

[3]Figures 3.2 and 3.3 illustrate the fringes obtained when specimen grid lines and master grating lines interfere on a one-to-one basis to form the fringes. If there is a rather large mismatch in pitches, it is possible for multiple specimen grid lines to interfere with one (or more) master grating lines to form visible fringes. In this case the parameter d = b/a would be the ratio of the number of master grating lines interfering with the number of specimen grid lines to form fringes. The signs of a and b would be determined by the relative magnitudes of "b" master grating line pitches compared to "a" specimen grid line pitches.

obtaining this information is described later in this report.

The two indicial equations can be conveniently combined in the form

$$j - k = \pm p \quad . \tag{3.5}$$

Expressions for j and k are obtained by rearranging Equations (3.2) and (3.3). Thus

$$j = \frac{X \cos\Theta - Y \sin\Theta}{M}$$

and

$$k = \frac{X \cos\Gamma - Y \sin\Gamma}{S} \quad .$$

An equation for the moiré fringes is obtained by substituting the expressions for j and k into the indicial equation. This can be conveniently expressed as

$$Y = \frac{X\left(\frac{\cos\Theta}{M} - \frac{\cos\Gamma}{S}\right)}{\left(\frac{\sin\Theta}{M} - \frac{\sin\Gamma}{S}\right)} - \frac{(\pm p)}{\left(\frac{\sin\Theta}{M} - \frac{\sin\Gamma}{S}\right)} \quad . \tag{3.6}$$

The uncertainty in the sign of the last term in Equation (3.6) is due to the previously noted ambiguity of the specimen grid geometry. In Equation (3.6), if the specimen grid pitch is greater than the master grating pitch, the plus sign (+) applies. If the specimen grid pitch is smaller than the master grating pitch, the minus sign (-) applies. Thus the geometry of the moiré fringes is now given in terms of the specimen and master grid parameters. It is desirable to carry the analysis one step further to obtain specific expressions for the moiré fringe pitch and angle in terms of these same parameters. From Figures 3.2 and 3.3 another equation for the moiré pattern is

$$Y = X \cot\Phi - \frac{p}{\left(\frac{\sin\Phi}{F}\right)} \quad . \tag{3.7}$$

Equations (3.6) and (3.7) are for identical moiré patterns, thus corresponding coefficients may be equated. Consequently

$$\cot\Phi = \frac{\frac{\cos\Theta}{M} - \frac{\cos\Gamma}{S}}{\frac{\sin\Theta}{M} - \frac{\sin\Gamma}{S}} = \frac{S\cos\Theta - M\cos\Gamma}{S\sin\Theta - M\sin\Gamma} \tag{3.8}$$

or

$$\tan\Phi = \frac{S\sin\Theta - M\sin\Gamma}{S\cos\Theta - M\cos\Gamma} \tag{3.9}$$

and

$$\frac{F}{\sin\Phi} = \frac{\pm SM}{S\sin\Theta - M\sin\Gamma} \quad . \tag{3.10}$$

From trigonometry,

$$\sin^2\Phi = \frac{1}{1 + \cot^2\Phi}$$

$$= \frac{1}{1 + \frac{(S\cos\Theta - M\cos\Gamma)^2}{(S\sin\Theta - M\sin\Gamma)^2}} \quad . \tag{3.11}$$

Thus

$$\sin\Phi = \frac{\pm(S\sin\Theta - M\sin\Gamma)}{[S^2 + M^2 - 2SM\cos(\Theta-\Gamma)]^{\frac{1}{2}}} \quad . \tag{3.12}$$

From Equations (3.10) and (3.12)

$$F = \frac{SM}{[S^2 + M^2 - 2SM\cos(\Theta-\Gamma)]^{\frac{1}{2}}} \quad . \tag{3.13}$$

In Equations (3.10) and (3.12), if S>M, the plus sign (+) applies; if S<M, the minus sign (-) applies.

Equations (3.8) through (3.13) give a variety of expressions for the relationships between the moiré fringe pitch and orientation, and the specimen and master grid parameters. Equations (3.9) and (3.13), in particular, are in the most useful form for subsequent work.

Before continuing with the main course of the analysis, it is instructive to deviate temporarily to consider some of the implications and features of moiré fringes. The main analysis resumes at Equation (3.17).

Equations (3.9) and (3.13) reveal certain basic characteristics associated with the behavior of moire fringes. For instance, if the master grating and specimen grid are exactly aligned, $\Theta = \Gamma$ and

$$\tan\Phi = \tan\Theta = \tan\Gamma$$

or

$$\Phi = \Theta = \Gamma \quad . \tag{3.14}$$

Thus the angle of the fringes is equal to the angles associated with the specimen and master grids. Also the fringe pitch is simply

$$F = \frac{SM}{|S - M|} \quad , (\Theta = \Gamma) \quad .$$

Alternatively, if the master grating and specimen grid pitches are the same, S = M and

$$\tan\Phi = \frac{\sin\Theta - \sin\Gamma}{\cos\Theta - \cos\Gamma}$$

$$= -\cot\left(\frac{\Theta + \Gamma}{2}\right)$$

$$= \tan\left(90° + \frac{\Theta + \Gamma}{2}\right) \quad , (S = M) \quad .$$

Thus

$$\Phi = 90° + \frac{\Theta + \Gamma}{2} \quad , (S = M) \quad .$$

A moiré pattern of this type is illustrated in Figure 3.5. The equation above indicates that when S = M the fringe angle is a function only of the specimen grid and master grating angles. Under the same circumstances the fringe pitch is

$$F = \frac{M}{[2 - 2\cos(\Theta - \Gamma)]^{\frac{1}{2}}}$$

$$= \frac{\pm M}{2\sin\left(\frac{\Theta - \Gamma}{2}\right)} \quad , (S = M) \quad .$$

Since F is always positive, the plus sign (+) is used when $(\Theta - \Gamma)$ is

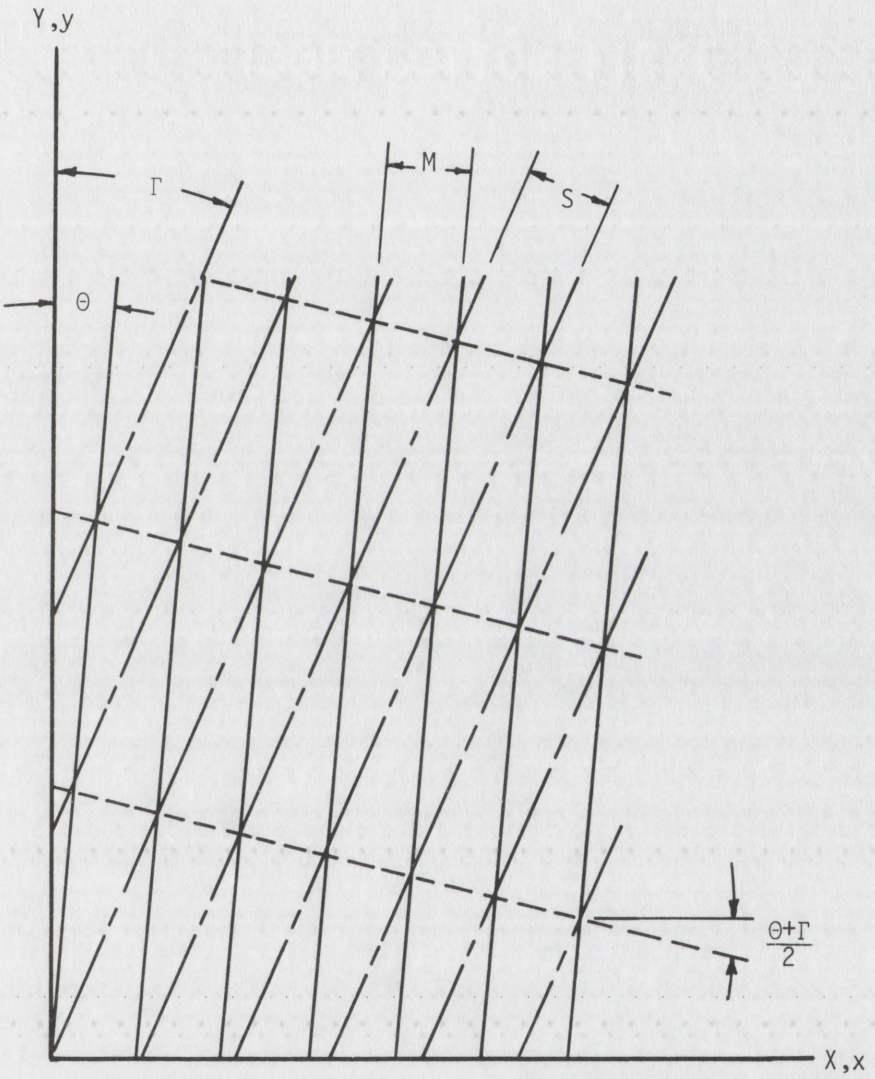

Figure 3.5

Moiré Pattern for S = M

positive and the minus sign (-) is used when $(\Theta - \Gamma)$ is negative. If $S = M$ and $\Theta + \Gamma = 0$, the fringe angle is

$$\Phi = 90^\circ \quad , (S = M, \Theta + \Gamma = 0)$$

and the fringe pitch is

$$F = \frac{\pm M}{2 \sin\Theta} \quad , (S = M, \Theta + \Gamma = 0) \quad .$$

If $\Theta = \Gamma = 0$, the fringe pitch becomes unbounded and the fringe is not visible, even though the fringe angle is still nominally 90 degrees.

Further investigation of Equation (3.9) reveals a method of qualitatively determining the size of the specimen grid pitch, S, relative to the master grating pitch, M. By definition

$$\Phi = \arctan(\tan\Phi)$$

$$\frac{d\Phi}{d\Theta} = \frac{d}{d\Theta}[\arctan(\tan\Phi)]$$

$$= \frac{\frac{d}{d\Theta}(\tan\Phi)}{1 + \tan^2\Phi} \quad .$$

Thus

$$\frac{d\Phi}{d\Theta} = \frac{S[S - M\cos(\Theta - \Gamma)]}{S^2 + M^2 - 2SM\cos(\Theta - \Gamma)} \quad . \qquad (3.15)$$

Since S and M are positive real numbers, and since the maximum value of $\cos(\Theta - \Gamma)$ is +1, the denominator of Equation (3.15) is always positive. Consequently the sign of $d\Phi/d\Theta$ is determined by the quantity $[S - M\cos(\Theta - \Gamma)]$. If $S > M\cos(\Theta - \Gamma)$, $d\Phi/d\Theta$ is positive; if $S < M\cos(\Theta - \Gamma)$, $d\Phi/d\Theta$ is negative. This feature can be used to experimentally find the sign of the quantity $(S - M)$. From Equation (3.14), if $\Theta = \Phi$, then $\Theta = \Gamma$. Thus if the master grating lines are aligned with the fringe lines,

$$\frac{d\Phi}{d\Theta} = \frac{S}{S - M} \quad , (\Theta = \Gamma) \quad . \qquad (3.16)$$

Therefore it is possible to determine if the pitch of the specimen grid is greater than the pitch of the master grating by merely rotating the master grating through the angular position $\Theta = \Gamma = \Phi$. If the moiré fringes rotate in the same direction, the specimen grid pitch is greater than the master grating pitch. If the moiré fringes rotate in the opposite direction, the converse is true.

It is interesting to note from Equation (3.15) if S = M and $\Theta \neq \Gamma$,

$$\frac{d\Phi}{d\Theta} = \frac{1}{2} \quad , (S = M) \quad .$$

Thus for any angle $\Theta \neq \Gamma$, if S = M the fringes rotate in the same direction as the master grating and at one-half the rate. If $\Theta = \Gamma$ and S = M, $d\Phi/d\Theta$ is undefined.

If $S = M \cos(\Theta - \Gamma)$, then from Equation (3.15)

$$\frac{d\Phi}{d\Theta} = 0$$

and from Equation (3.9)

$$\tan\Phi = -\cot\Theta$$

$$= \tan(90° + \Theta) \quad .$$

Thus, as illustrated in Figure 3.6

$$\Phi = 90° + \Theta \quad .$$

This equation indicates that if $S = M \cos(\Theta - \Gamma)$, the fringe angle is perpendicular to the master grating angle. This suggests a rather direct method of experimentally finding the specimen pitch if Γ is known and if $S/M \leq 1$. The master grating can be rotated until Φ is perpendicular to Θ. The angles Θ, Γ and the master grating pitch, M, can then be used to calculate specimen grid pitch as

$$S = M \cos(\Theta - \Gamma) \quad , (\Phi = 90° + \Theta) \quad .$$

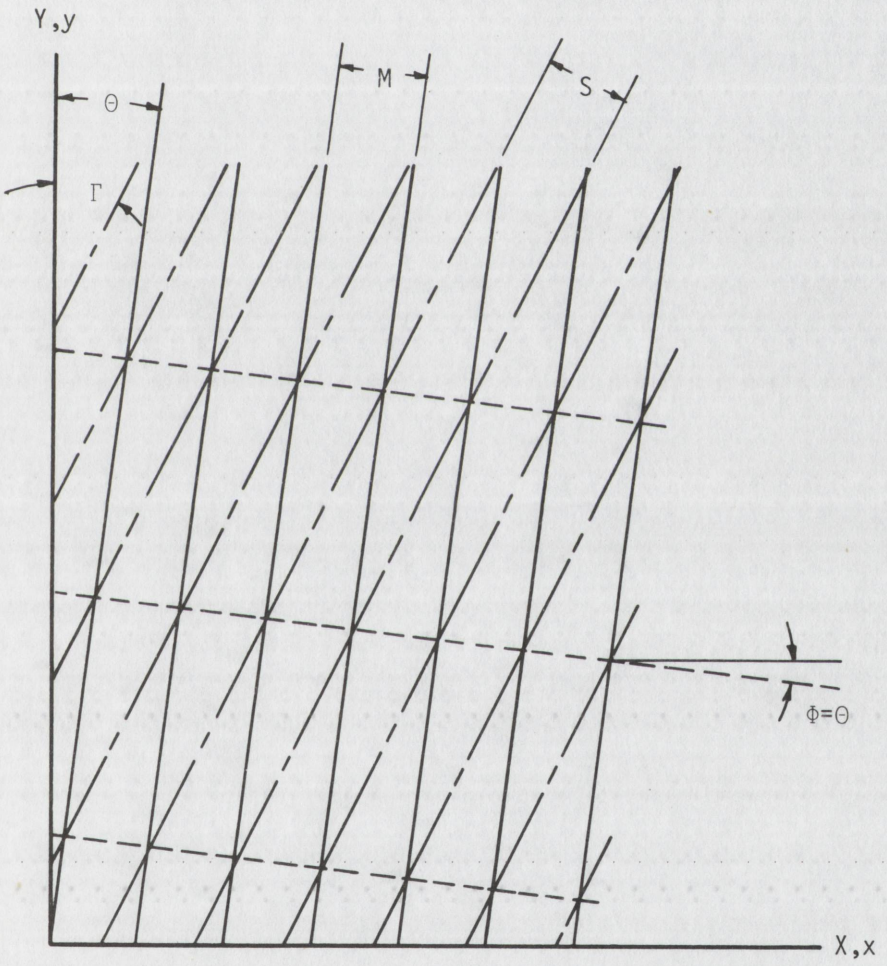

Figure 3.6

Moiré Pattern for S = M cos(Θ - Γ)

However, this equation is restricted to values of $S \leq M$ since the value of S/M is limited by the relation

$$\frac{S}{M} = \cos(\Theta - \Gamma) \quad , (\Phi = 90° + \Theta) \quad .$$

If $S > M$ it is impossible to find a value of $(\Theta - \Gamma)$ such that $\Phi = 90° + \Theta$.

Equation (3.16) also implies an extremely sensitive method of determining the angle Γ. If the specimen grid pitch is almost equal to the master grating pitch the value of $d\Phi/d\Theta$ is large at $\Theta = \Gamma$. Hence, a small rotation of the master grating results in a large rotational response of the moiré fringe. In practice the precision of determining the angle Γ is limited primarily by the experimenter's ability to measure the angle Θ.

Returning to the general analysis it is noted that since the pitch and angle of the specimen grid are usually unknown in an experiment, it is more useful to have expressions for S and Γ in terms of M, F, Θ and Φ. Using Equations (3.8) and (3.10),

$$\frac{S}{\sin\Gamma} = \frac{FM}{F\sin\Theta \pm M\sin\Phi} \tag{3.17}$$

and

$$\frac{\cos\Gamma}{S} = \frac{F\cos\Theta \pm M\cos\Phi}{FM} \quad .$$

Thus

$$\cot\Gamma = \frac{F\cos\Theta \pm M\cos\Phi}{F\sin\Theta \pm M\sin\Phi} \tag{3.18}$$

or

$$\tan\Gamma = \frac{F\sin\Theta \pm M\sin\Phi}{F\cos\Theta \pm M\cos\Phi} \quad . \tag{3.19}$$

From Equations (3.11) and (3.18)

$$\sin\Gamma = \frac{\pm(\pm F\sin\Theta - M\sin\Phi)}{[F^2 + M^2 \pm 2FM\cos(\Theta - \Phi)]^{\frac{1}{2}}}$$

$$= \frac{F\sin\Theta \pm M\sin\Phi}{[F^2 + M^2 \pm 2FM\cos(\Theta - \Phi)]^{\frac{1}{2}}} \quad . \tag{3.20}$$

Multiplying Equations (3.17) and (3.20),

$$S = \frac{FM}{[F^2 + M^2 \pm 2FM \cos(\Theta - \Phi)]^{\frac{1}{2}}} \quad . \tag{3.21}$$

In Equations (3.18) through (3.21), if $S > M$, the minus sign (-) must be used; if $S < M$, the plus sign (+) must be used. Equations (3.18), (3.19) and (3.21) are in the most useful forms for subsequent work and will be used repeatedly in the sequel. They give the initial specimen grid parameters in terms of the initial master grating and moiré fringe parameters. By a simple substitution of variables, corresponding relations for the deformed specimen grid may be obtained as follows.

After deformation, the specimen grid pitch and angle are s and γ respectively. If the master grating pitch and angle are also changed to m and θ respectively, the relations corresponding to those given in Equations (3.9), (3.12), (3.13), (3.19), (3.20) and (3.21) are

$$\tan\phi = \frac{s \sin\theta - m \sin\gamma}{s \cos\theta - m \cos\gamma} \tag{3.22}$$

$$\sin\phi = \frac{\pm(s \sin\theta - m \sin\gamma)}{[s^2 + m^2 - 2sm \cos(\theta - \gamma)]^{\frac{1}{2}}} \tag{3.23}$$

$$f = \frac{sm}{[s^2 + m^2 - 2sm \cos(\theta - \gamma)]^{\frac{1}{2}}} \tag{3.24}$$

$$\tan\gamma = \frac{f \sin\theta \pm m \sin\phi}{f \cos\theta \pm m \cos\phi} \tag{3.25}$$

$$\sin\gamma = \frac{f \sin\theta \pm m \sin\phi}{[f^2 + m^2 \pm 2fm \cos(\theta - \phi)]^{\frac{1}{2}}} \tag{3.26}$$

$$s = \frac{fm}{[f^2 + m^2 \pm 2fm \cos(\theta - \phi)]^{\frac{1}{2}}} \quad . \tag{3.27}$$

In Equation (3.23), if $s > m$, the plus sign (+) applies; if $s < m$, the minus sign (-) applies. Conversely in Equations (3.25) through (3.27),

if $s > m$, the minus sign (-) must be used; if $s < m$, the plus sign (+) must be used.

The equations for initial and final values of pitch and angular orientation can be combined to yield expressions for relative changes in pitch and angle; that is, before and after deformation. This is the final step required to attain the objective of the moiré analysis: to find the change in specimen grid pitch and angle in terms of moiré fringe parameters. From trigonometry

$$\tan(A - B) = \frac{\tan A - \tan B}{1 + \tan A \tan B} \quad . \tag{3.28}$$

Thus the change in fringe angle can be found from

$$\tan(\phi-\Phi) = \frac{sS \sin(\theta-\Theta) - sM \sin(\theta-\Gamma) - mS \sin(\gamma-\Theta) + mM \sin(\gamma-\Gamma)}{sS \cos(\theta-\Theta) - sM \cos(\theta-\Gamma) - mS \cos(\gamma-\Theta) + mM \cos(\gamma-\Gamma)} \quad . \tag{3.29}$$

The ratio of final to initial fringe pitch is simply

$$\frac{f}{F} = \frac{sm[S^2 + M^2 - 2SM \cos(\Theta - \Gamma)]^{\frac{1}{2}}}{SM[s^2 + m^2 - 2sm \cos(\theta - \gamma)]^{\frac{1}{2}}} \quad . \tag{3.30}$$

Similar expressions for the relative changes in specimen grid pitch and angle require careful consideration of the proper signs to be used, depending upon the relative magnitudes of the specimen grid and master grating pitches. For clarity, four cases are defined:

Case I: $S > M$, $s > m$.

$$\tan(\gamma-\Gamma) = \frac{fF \sin(\theta-\Theta) - fM \sin(\theta-\Phi) - mF \sin(\phi-\Theta) + mM \sin(\phi-\Phi)}{fF \cos(\theta-\Theta) - fM \cos(\theta-\Phi) - mF \cos(\phi-\Theta) + mM \cos(\phi-\Phi)} \tag{3.31}$$

$$\frac{s}{S} = \frac{fm[F^2 + M^2 - 2FM \cos(\Theta - \Phi)]^{\frac{1}{2}}}{FM[f^2 + m^2 - 2fm \cos(\theta - \phi)]^{\frac{1}{2}}} \quad . \tag{3.32}$$

Case II: $S > M$, $s < m$.

$$\tan(\gamma-\Gamma) = \frac{fF \sin(\theta-\Theta) - fM \sin(\theta-\Phi) + mF \sin(\phi-\Theta) - mM \sin(\phi-\Phi)}{fF \cos(\theta-\Theta) - fM \cos(\theta-\Phi) + mF \cos(\phi-\Theta) - mM \cos(\phi-\Phi)} \tag{3.33}$$

$$\frac{s}{S} = \frac{fm[F^2 + M^2 - 2FM \cos(\Theta - \Phi)]^{\frac{1}{2}}}{FM[f^2 + m^2 + 2fm \cos(\theta - \phi)]^{\frac{1}{2}}} \quad . \tag{3.34}$$

Case III: $S < M$, $s > m$.

$$\tan(\gamma-\Gamma) = \frac{fF \sin(\theta-\Theta) + fM \sin(\theta-\Phi) - mF \sin(\phi-\Theta) - mM \sin(\phi-\Phi)}{fF \cos(\theta-\Theta) + fM \cos(\theta-\Phi) - mF \cos(\phi-\Theta) - mM \cos(\phi-\Phi)} \tag{3.35}$$

$$\frac{s}{S} = \frac{fm[F^2 + M^2 + 2FM \cos(\Theta - \Phi)]^{\frac{1}{2}}}{FM[f^2 + m^2 - 2fm \cos(\Theta - \Phi)]^{\frac{1}{2}}} \quad . \tag{3.36}$$

Case IV: $S < M$, $s < m$.

$$\tan(\gamma-\Gamma) = \frac{fF \sin(\theta-\Theta) + fM \sin(\theta-\Phi) + mF \sin(\phi-\Theta) + mM \sin(\phi-\Phi)}{fF \cos(\theta-\Theta) + fM \cos(\theta-\Phi) + mF \cos(\phi-\Theta) + mM \cos(\phi-\Phi)} \tag{3.37}$$

$$\frac{s}{S} = \frac{fm[F^2 + M^2 + 2FM \cos(\Theta - \Phi)]^{\frac{1}{2}}}{FM[f^2 + m^2 + 2fm \cos(\theta - \phi)]^{\frac{1}{2}}} \quad . \tag{3.38}$$

Equations (3.29) through (3.38) are quite general. Although they may be rather cumbersome to use for computations it will be seen that they represent fundamental quantities in the theory of large deformations. Furthermore, they are useful for evaluating techniques to reduce the number of experimental measurements required for any given experiment. For instance for homogeneous deformations, it would be quite simple to set $\Theta = \theta = \Phi$. Then the tangent of the change in specimen grid angle given for Case I by Equation (3.31) becomes simply

$$\tan(\gamma-\Gamma) = \frac{-m \sin(\phi - \Phi)}{f - m \cos(\phi-\Phi)} \quad .$$

Similarly, the pitch ratio is

$$\frac{s}{S} = \frac{fm(F - M)}{FM[f^2 + m^2 - 2fm\cos(\phi - \Phi)]^{\frac{1}{2}}} \quad .$$

If in any experiment, certain types of measurements can be made more conveniently or accurately than others, Equations (3.29) through (3.38) can be used as guides in designing the experiment to depend as heavily as possible on the more desirable methods.

A similar general analysis can be conducted for the portion of the specimen grid shown in Figure 3.4. Repeating Equation (3.4)

$$Y = \frac{kT}{\cos\Omega} - X\tan\Omega \quad . \tag{3.4}$$

The master grating in Figure 3.4 may be characterized by the equation

$$Y = \frac{jN}{\cos\Upsilon} - X\tan\Upsilon \quad .$$

Using the line indexing system shown in Figure 3.4, the indicial equation for the moiré pattern is the same as that previously used, that is

$$j - k = \pm p \quad . \tag{3.5}$$

Proceeding as before,

$$j = \frac{Y\cos\Upsilon + X\sin\Upsilon}{N}$$

$$k = \frac{Y\cos\Omega + X\sin\Omega}{T} \quad .$$

Then the equation for the moiré fringes is

$$X = \frac{-Y\left(\frac{\cos\Upsilon}{N} - \frac{\cos\Omega}{T}\right)}{\left(\frac{\sin\Upsilon}{N} - \frac{\sin\Omega}{T}\right)} + \frac{(\pm p)}{\left(\frac{\sin\Upsilon}{N} - \frac{\sin\Omega}{T}\right)} \quad . \tag{3.39}$$

This may also be expressed as

$$X = -Y\cot\Psi + \frac{p}{\frac{\sin\Psi}{H}} \tag{3.40}$$

where H is the moiré fringe pitch. As before, Equations (3.39) and (3.40) are for identical moiré patterns, thus corresponding coefficients may be equated. Consequently

$$\cot\Psi = \frac{T\cos\Upsilon - N\cos\Omega}{T\sin\Upsilon - N\sin\Omega} \tag{3.41}$$

and

$$\frac{H}{\sin\Psi} = \frac{\pm TN}{T\sin\Upsilon - N\sin\Omega} \quad . \tag{3.42}$$

Equations (3.41) and (3.42) are exactly analogous in form to Equations (3.8) and (3.10). Consequently the relationships between the moiré fringes, specimen grid and master grating geometries may be obtained from the previously derived equations by making the following substitutions:

$$\begin{aligned} &N, n \rightarrow M, m \\ &\Upsilon, \upsilon \rightarrow \Theta, \theta \\ &T, t \rightarrow S, s \\ &\Omega, \omega \rightarrow \Gamma, \gamma \\ &H, h \rightarrow F, f \\ &\Psi, \psi \rightarrow \Phi, \phi \quad . \end{aligned} \tag{3.43}$$

In addition, the same sign conventions are valid with respect to the relative magnitudes of the specimen grid and master grating pitches.

It should be emphasized that up to this point the moiré analysis is independent of the deformation theory presented in the previous chapter. A basic objective of this research is to unambiguously relate the results of the moiré fringe analysis to fundamental measures and quantities encountered in the modern theory of large deformations. From Section 2.1 the stretch is defined as

$$\Lambda = \lambda = \frac{ds}{dS} \quad . \tag{2.9}$$

From Figure 3.7 for a two-dimensional homogeneous deformation, the stretch of a line element of initial length G and orientation Ω is

$$\Lambda_G = \frac{g}{G} = \frac{s}{S} \frac{\cos(\Omega - \Gamma)}{\cos(\omega - \gamma)} \quad .$$

Similarly, the stretch of a line element with initial length W and orientation Γ is

$$\Lambda_W = \frac{w}{W} = \frac{t}{T} \frac{\cos(\Omega - \Gamma)}{\cos(\omega - \gamma)} \quad .$$

Furthermore, the corresponding extensions then become

$$E_G = \frac{g}{G} - 1 = \frac{s}{S} \frac{\cos(\Omega - \Gamma)}{\cos(\omega - \gamma)} - 1$$

$$E_W = \frac{w}{W} - 1 = \frac{t}{T} \frac{\cos(\Omega - \Gamma)}{\cos(\omega - \gamma)} - 1 \quad .$$

All of the quantities entering into the terms on the right hand side of the equations above can be found directly from moiré measurements.

The shear is defined by Equation (2.12) as the decrease in angle

$$\Sigma_{G,W} = \sigma_{g,w} = \Xi_{G,W} - \xi_{g,w} \quad .$$

From an examination of Figures 2.2 and 3.7 it can be seen that for a two-dimensional homogeneous deformation the shear can be expressed as

$$\begin{aligned} \Sigma_{G,W} &= (90° + \Omega - \Gamma) - (90° + \omega - \gamma) \\ &= (\gamma - \Gamma) - (\omega - \Omega) \end{aligned} \tag{3.44}$$

where

$$\Xi_{G,W} = 90° + \Omega - \Gamma$$

$$\xi_{g,w} = 90° + \omega - \gamma \; .$$

From Equations (3.28), (3.31), (3.33), (3.35), (3.37) and (3.43) the shear is calculated from

$$\tan\Sigma_{G,W} = \frac{\tan(\gamma - \Gamma) - \tan(\omega - \Omega)}{1 + \tan(\gamma - \Gamma)\tan(\omega - \Omega)} \quad . \tag{3.45}$$

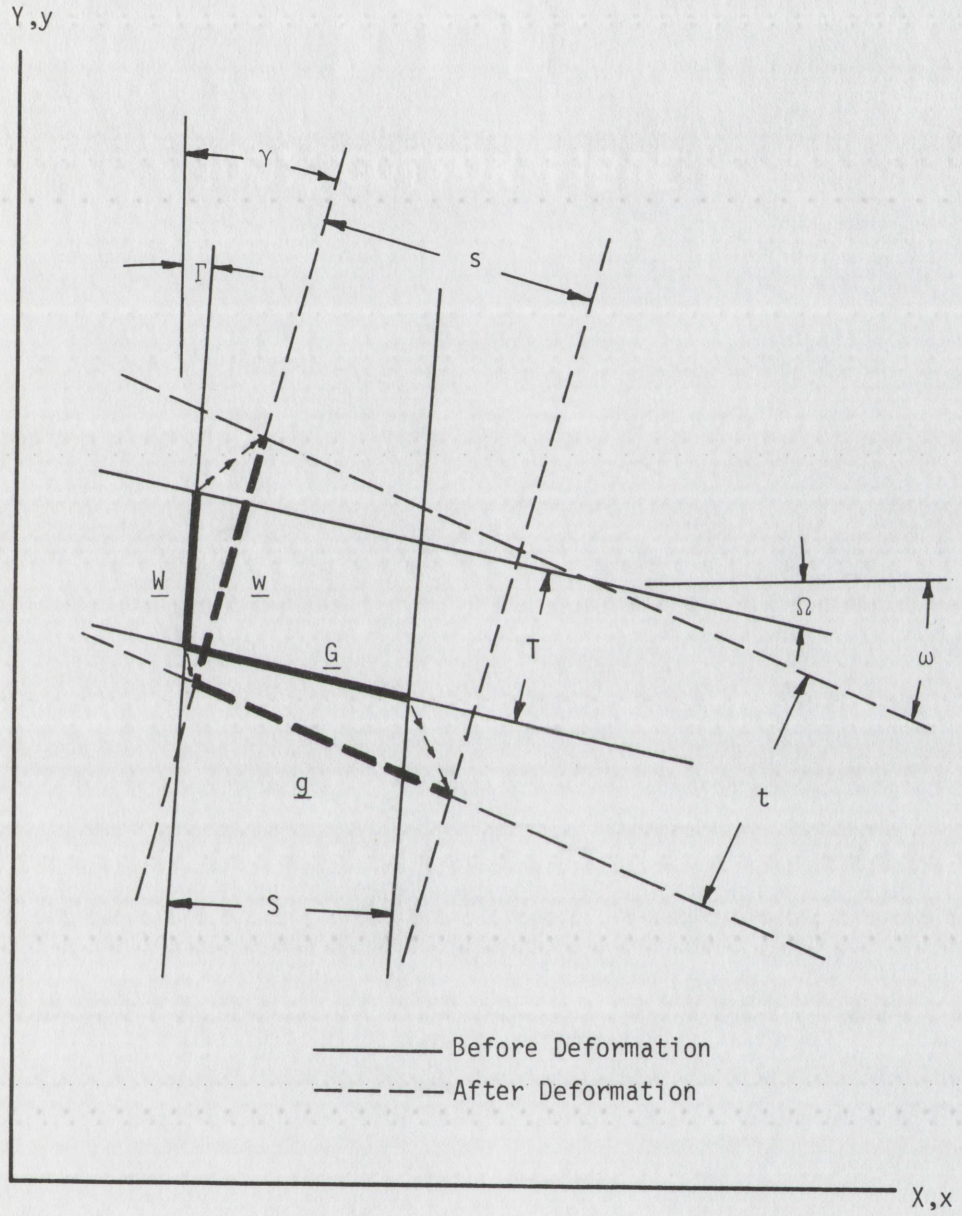

Figure 3.7

Specimen Grid Before and After Deformation

A crucial point in the analysis is to relate the specimen grid parameters to the components of the deformation and strain tensors. This is accomplished by introducing the expressions for stretch, just derived, into Equations (2.13); and by identifying specimen grid angles with the direction cosines encountered in Equations (2.13). Referring to Figure 3.7, Equations (2.13) may thus be rewritten in terms of the specimen grid parameters as:

$$C_{XX}\cos^2\Omega - C_{XY}\,2\cos\Omega\sin\Omega + C_{YY}\sin^2\Omega = \Lambda_G^2 = \left(\frac{s}{S}\right)^2 \frac{\cos^2(\Omega - \Gamma)}{\cos^2(\omega - \gamma)}$$

$$C_{XX}\sin^2\Gamma + C_{XY}\,2\cos\Gamma\sin\Gamma + C_{YY}\cos^2\Gamma = \Lambda_W^2 = \left(\frac{t}{T}\right)^2 \frac{\cos^2(\Omega - \Gamma)}{\cos^2(\omega - \gamma)}$$

$$C_{XX}\cos\Omega\sin\Gamma + C_{XY}\cos(\Omega + \Gamma) - C_{YY}\sin\Omega\cos\Gamma = \Lambda_G\Lambda_W\cos\xi_{g,w}$$

$$= -\left(\frac{s}{S}\right)\left(\frac{t}{T}\right)\frac{\cos^2(\Omega-\Gamma)}{\cos^2(\omega-\gamma)}\sin(\omega-\gamma) \quad .$$

These equations may be rearranged so that the coefficients of the tensor components C_{JK} are functions of the trigonometric tangents and cotangents of the angles Ω and Γ, respectively. The revised equations, which are more convenient for computation, are:

$$C_{XX} - 2C_{XY}\tan\Omega + C_{YY}\tan^2\Omega = (1 + \tan^2\Omega)\left(\frac{s}{S}\right)^2 \frac{\cos^2(\Omega - \Gamma)}{\cos^2(\omega - \gamma)}$$

$$C_{XX} + 2C_{XY}\cot\Gamma + C_{YY}\cot^2\Gamma = (1 + \cot^2\Gamma)\left(\frac{t}{T}\right)^2 \frac{\cos^2(\Omega - \Gamma)}{\cos^2(\omega - \gamma)}$$

$$C_{XX} + C_{XY}(\cot\Gamma - \tan\Omega) - C_{YY}\cot\Gamma\tan\Omega =$$

$$= -(\cot\Gamma + \tan\Omega)\left(\frac{s}{S}\right)\left(\frac{t}{T}\right)\frac{\cos(\Omega-\Gamma)}{\cos(\omega-\gamma)}\tan(\omega-\gamma) \quad . \tag{3.46}$$

Note that if the specimen grids are initially aligned with the X and

Y axes, the tensor components are simply

$$C_{XX} = \frac{\left(\frac{s}{S}\right)^2}{\cos^2(\omega - \gamma)}$$

$$C_{YY} = \frac{\left(\frac{t}{T}\right)^2}{\cos^2(\omega - \gamma)}$$

$$C_{XY} = \frac{-\left(\frac{s}{S}\right)\left(\frac{t}{T}\right)\sin(\omega - \gamma)}{\cos^2(\omega - \gamma)} \quad . \tag{3.47}$$

After Equations (3.46) or (3.47) are solved for the components of $\underline{\underline{C}}$, the strain tensors, extensions, principal values and principal directions may be computed by the equations developed in Section 2.1. It is immediately apparent from Equations (3.46) that a complete moiré analysis of a two-dimensional deformation requires consideration of the fringe patterns generated by at least two independent sets of specimen grid lines. The only restriction on the initial pitch and orientation of the lines is that they be suited to produce a reasonable moiré response for the deformation being investigated. The two sets of specimen grid lines need not have any particular relationship between their pitches and angular orientations. Furthermore, the master grating pitches and angular orientations are essentially arbitrary and may be adjusted at will during an experiment to produce the most advantageous moiré patterns.

In certain instances it may be desirable to obtain the components of the lagrangian strain tensor directly from the moiré measurements. If so, equations comparable to those for the deformation tensor components may be derived using Equations (2.7) and (3.46).

Thus

$$E_{XX} - 2E_{XY}\tan\Omega + E_{YY}\tan^2\Omega = \frac{1}{2}(1 + \tan^2\Omega)\left[\left(\frac{s}{S}\right)^2 \frac{\cos^2(\Omega - \Gamma)}{\cos^2(\omega - \gamma)} - 1\right]$$

$$E_{XX} + 2E_{XY}\cot\Gamma + E_{YY}\cot^2\Gamma = \frac{1}{2}(1 + \cot^2\Gamma)\left[\left(\frac{t}{T}\right)^2 \frac{\cos^2(\Omega - \Gamma)}{\cos^2(\omega - \gamma)} - 1\right]$$

$$E_{XX} + E_{XY}(\cot\Gamma - \tan\Omega) - E_{YY}\cot\Gamma\tan\Omega =$$

$$= -\frac{1}{2}\left[(\cot\Gamma + \tan\Omega)\left(\frac{s}{S}\right)\left(\frac{t}{T}\right) \frac{\cos(\Omega-\Gamma)}{\cos(\omega-\gamma)} \tan(\omega-\gamma) + (1 - \cot\Gamma\tan\Omega)\right] .$$

In a manner similar to the foregoing, Equations (2.22) for Cauchy's deformation tensor components may be obtained in terms of the quantities measured in the moiré analysis. That is

$$c_{xx}\cos^2\omega - c_{xy}\,2\cos\omega\sin\omega + c_{yy}\sin^2\omega = \frac{1}{\lambda_g^2} = \left(\frac{S}{s}\right)^2 \frac{\cos^2(\omega - \gamma)}{\cos^2(\Omega - \Gamma)}$$

$$c_{xx}\sin^2\gamma + c_{xy}\,2\cos\gamma\sin\gamma + c_{yy}\cos^2\gamma = \frac{1}{\lambda_w^2} = \left(\frac{T}{t}\right)^2 \frac{\cos^2(\omega - \gamma)}{\cos^2(\Omega - \Gamma)}$$

$$c_{xx}\cos\omega\sin\gamma + c_{xy}\cos(\omega + \gamma) - c_{yy}\sin\omega\cos\gamma = \frac{\cos\Xi_{G,W}}{\lambda_g\,\lambda_w} =$$

$$= -\left(\frac{S}{s}\right)\left(\frac{T}{t}\right) \frac{\cos^2(\omega-\gamma)}{\cos^2(\Omega-\Gamma)} \sin(\Omega-\Gamma) .$$

Then

$$c_{xx} - 2c_{xy}\tan\omega + c_{yy}\tan^2\omega = (1 + \tan^2\omega)\left(\frac{S}{s}\right)^2 \frac{\cos^2(\omega - \gamma)}{\cos^2(\Omega - \Gamma)}$$

$$c_{xx} + 2c_{xy}\cot\gamma + c_{yy}\cot^2\gamma = (1 + \cot^2\gamma)\left(\frac{T}{t}\right)^2 \frac{\cos^2(\omega - \gamma)}{\cos^2(\Omega - \Gamma)}$$

$$c_{xx} + c_{xy}(\cot\gamma - \tan\omega) - c_{yy}\cot\gamma\tan\omega =$$

$$= -(\cot\gamma + \tan\omega)\left(\frac{S}{s}\right)\left(\frac{T}{t}\right) \frac{\cos(\omega-\gamma)}{\cos(\Omega-\Gamma)} \tan(\Omega-\Gamma) . \qquad (3.48)$$

Thus, from the same set of moiré measurements, Cauchy's deformation tensor may be obtained. Note that if the specimen grids are aligned with the x and y axes after deformation, the tensor components become simply

$$C_{xx} = \frac{1}{\left(\frac{S}{\bar{S}}\right)^2 \cos^2(\Omega - \Gamma)}$$

$$C_{yy} = \frac{1}{\left(\frac{t}{\bar{T}}\right)^2 \cos^2(\Omega - \Gamma)}$$

$$C_{xy} = \frac{-\sin(\Omega - \Gamma)}{\left(\frac{S}{\bar{S}}\right)\left(\frac{t}{\bar{T}}\right) \cos^2(\Omega - \Gamma)} \quad . \tag{3.49}$$

The corresponding equations for the eulerian strain tensor components are found with the aid of Equation (2.8). Thus

$$e_{xx} - 2e_{xy} \tan\omega + e_{yy} \tan^2\omega = -\frac{1}{2}(1 + \tan^2\omega)\left[\left(\frac{S}{s}\right)^2 \frac{\cos^2(\omega - \gamma)}{\cos^2(\Omega - \Gamma)} - 1\right]$$

$$e_{xx} + 2e_{xy} \cot\gamma + e_{yy} \cot^2\gamma = -\frac{1}{2}(1 + \cot^2\gamma)\left[\left(\frac{T}{t}\right)^2 \frac{\cos^2(\omega - \gamma)}{\cos^2(\Omega - \Gamma)} - 1\right]$$

$$e_{xx} + e_{xy}(\cot\gamma - \tan\omega) - e_{yy} \cot\gamma\tan\omega =$$

$$= \frac{1}{2}\left[(\cot\gamma + \tan\omega)\left(\frac{S}{s}\right)\left(\frac{T}{t}\right) \frac{\cos(\omega-\gamma)}{\cos(\Omega-\Gamma)} \tan(\Omega-\Gamma) + (1 - \cot\gamma\tan\omega)\right] \quad .$$

3.3 Moiré Analysis of Simple Shear Deformation

Although any two-dimensional homogeneous deformation may be analyzed using the general equations developed in Section 3.2, it is instructive to consider the response of the moiré fringes due to a specific well-defined deformation such as simple shear.

From Section 2.2 the equations for simple shear deformation re-

ferred to a rectangular coordinate system are

$$x = X + QY = X + Y \tan\alpha$$

$$y = Y$$

$$z = Z \qquad (3.50)$$

where x, y, and z are the positions of the material points X, Y, and Z after deformation. As can be seen, a complete description of the classical simple shear deformation requires explicitly that there is no extension parallel to the Z-axis. Since the moiré method is essentially a two-dimensional technique, attention will be restricted to the deformations occurring in the X-Y plane. No attempt will be made to show, using the moiré method, that there is actually no extension in the Z direction. If a kinematic straining frame which controls deformations in the X-Y plane is used in an experiment, uniform extension parallel to the Z-axis will not affect the moiré pattern.

From Section 3.2, the equation for the specimen grid oriented as shown in Figure 3.2 is

$$X = \frac{kS}{\cos\Gamma} + Y \tan\Gamma \qquad (3.3)$$

where Γ is the angle between the grid lines and the Y-axis, and S is the initial specimen grid pitch. After deformation, the equation for the specimen grid is

$$x = \frac{kS}{\cos\gamma} + y \tan\gamma \quad . \qquad (3.51)$$

The change in the X coordinate can be found by subtracting Equation (3.3) from (3.51). Thus

$$x - X = k\left(\frac{S}{\cos\gamma} - \frac{S}{\cos\Gamma}\right) + y \tan\gamma - Y \tan\Gamma \quad . \qquad (3.52)$$

Introducing Equations (3.50) into (3.52),

$$x - X = k\left(\frac{s}{\cos\gamma} - \frac{S}{\cos\Gamma}\right) + Y(\tan\gamma - \tan\Gamma)$$

$$= Y \tan\alpha \quad . \tag{3.53}$$

Equating corresponding coefficients in Equation (3.53)

$$\frac{s}{\cos\gamma} = \frac{S}{\cos\Gamma} \tag{3.54}$$

$$\tan\alpha = \tan\gamma - \tan\Gamma \quad . \tag{3.55}$$

Equations (3.54) and (3.55) give relationships between specimen grid parameters for a test sample subjected to simple shear.

A complete analysis of the deformation in the X-Y plane requires similar consideration of another set of specimen grid lines. Again referring to Section 3.2, the equation for the initial specimen grid oriented as shown in Figure 3.4 is

$$X = \frac{kT}{\sin\Omega} - Y \cot\Omega \tag{3.56}$$

where Ω is the angle between the grid lines and the X-axis, and T is the initial specimen grid pitch. After deformation, the equation for the specimen grid is

$$x = \frac{kt}{\sin\omega} - y \cot\omega \quad . \tag{3.57}$$

Subtracting Equation (3.56) from (3.57)

$$x - X = k\left(\frac{t}{\sin\omega} - \frac{T}{\sin\Omega}\right) - y \cot\omega + Y \cot\Omega \quad . \tag{3.58}$$

Introducing Equations (3.50) into (3.55)

$$x - X = k\left(\frac{t}{\sin\omega} - \frac{T}{\sin\Omega}\right) - Y(\cot\omega - \cot\Omega)$$

$$= Y \tan\alpha \quad . \tag{3.59}$$

Equating corresponding coefficients in Equation (3.59),

$$\frac{t}{\sin\omega} = \frac{T}{\sin\Omega}$$

$$-\tan\alpha = \cot\omega - \cot\Omega \quad . \tag{3.60}$$

If $\Gamma \geq 0$ and $\alpha > 0$, then from Equation (3.55)

$$\Gamma < \gamma \quad .$$

Under the restriction,[4] $0 \leq \Gamma < \gamma < \pi/2$, it can be seen from Equation (3.54) that

$$s < S \quad .$$

Similarly, if $\Omega \leq 0$ and $\alpha > 0$, then from Equation (3.60)

$$\omega < \Omega \quad .$$

Under the restriction $0 > \Omega > \omega > -\pi/2$, it can be seen from Equations (3.60) that

$$t < T \quad .$$

If it is assumed, without loss of generality, that $S < M$, $s < m$, $T < N$ and $t < n$, then from Equations (3.19), (3.25) and (3.43)

$$\tan\alpha = \frac{fF \sin(\theta-\Theta) + fM \sin(\theta-\Phi) + mF \sin(\phi-\Theta) + mM \sin(\phi-\Phi)}{(f \cos\theta + m \cos\phi)(F \cos\Theta + M \cos\Phi)} \quad . \tag{3.61}$$

For the case of simple shear deformation, Equation (3.61) is sufficient to completely solve the problem, since the various deformation and strain tensors can then be found in terms of $\tan\alpha$ as given in Section 2.2. Nevertheless, if it is not known for sure

---

[4]This restriction does not result in any loss of generality. It is imposed to allow unambiguous assignment of the proper signs in the appropriate moiré fringe equations.

whether a true simple shear deformation was achieved, the general moiré fringe equations from Section 3.2 may be used to obtain the required results.

To determine the anticipated behavior of the moiré patterns due to a simple shear deformation, two examples are outlined which present certain simplifying assumptions and conditions.

Example I:

Assume that the master gratings undergo neither pitch nor angular change, and that there is no angular misalignment of the initial specimen grids and master gratings with respect to the X- and Y-axes. Then, from the appropriate equations in Sections 3.2 and 3.3

$$\sin\Phi = 0$$

thus

$$\Phi = 0 \quad .$$

Then

$$\tan\alpha = \frac{M \sin\phi}{f + M \cos\phi}$$

$$= \tan\gamma \quad .$$

When $\Omega = 0$, Equations (3.56) and (3.57) assume the forms

$$Y = kT$$

and

$$y = \frac{kt}{\cos\omega} - x \tan\omega \quad .$$

From Equation (3.50)

$$y - Y = 0 = k\left(\frac{t}{\cos\omega} - T\right) - x \tan\omega \quad .$$

But since $(y - Y)$ is identically zero

$$\tan\omega = 0$$

or

$$\omega = 0$$

and

$$t = T \quad .$$

Consequently

$$\tan\psi = 0$$

or

$$\psi = 0 \quad .$$

Furthermore

$$\frac{h}{H} = 1 \quad .$$

The stretch of an element initially lying in the direction of the X-axis is

$$\Lambda_G = \frac{g}{G} = \frac{s}{S}\frac{\cos(\Omega - \Gamma)}{\cos(\omega - \gamma)}$$

$$= \frac{s}{S}\frac{1}{\cos\gamma} \quad .$$

From Equations (3.25), (3.26) and (3.38)

$$\Lambda_G = \frac{f(F + M)}{F(f + M\cos\phi)} \quad .$$

The stretch of an element initially lying in the direction of the Y-axis is

$$\Lambda_W = \frac{w}{W} = \frac{t}{T}\frac{\cos(\Omega - \Gamma)}{\cos(\omega - \gamma)}$$

$$= \frac{t}{T}\frac{1}{\cos\gamma}$$

$$= \frac{(f^2 + M^2 + 2fM\cos\phi)^{\frac{1}{2}}}{f + M\cos\phi} \quad .$$

Thus, under the assumptions of this example the expressions for $\tan\alpha$ and the stretches assume very simple forms. Also, as may be anticipated, the fringes associated with the grid lines lying parallel to the X-axis show no response due to the deformation. This last feature in itself can be a handy, easily observable control on a simple shear experiment.

Example II:

Assume the same conditions outlined in Example I, except that the master grating with initial angle $\Theta = 0$ is subsequently aligned such that $\theta = \phi$ after deformation. Then from Equations (3.61) and (3.25)

$$\tan\alpha = \tan\theta = \tan\phi = \tan\gamma \quad .$$

Thus

$$\alpha = \theta = \phi = \gamma \quad .$$

Also

$$\Lambda_G = \frac{s}{S}\frac{\cos(\Omega - \Gamma)}{\cos(\omega - \gamma)}$$

$$= \frac{f(F + M)}{F(f + M)}\frac{1}{\cos\phi}$$

$$= \frac{f(F + M)}{F(f + M)}\frac{1}{\cos\theta} \quad .$$

$$\Lambda_W = \frac{t}{T}\frac{\cos(\Omega - \Gamma)}{\cos(\omega - \gamma)}$$

$$= \frac{1}{\cos\phi}$$

$$= \frac{1}{\cos\theta} \quad .$$

Thus it is seen that the expedient of aligning the master grating angle with the moiré fringe angle after deformation results in extremely simple equations for determining the required fundamental quantities.

3.4 Moiré Analysis of Two-Dimensional Nonhomogeneous Deformations

In a homogeneous deformation, line elements which were initially straight remain straight even though their orientation and length may change. For this reason it is logical and natural to select systems

of parallel straight lines as master and specimen grids.[5] However, when nonhomogeneous deformations are allowed, other types of grids may be more convenient to use, or may produce more precise results. In all cases considered, it is assumed that the objective of the experiment is to determine either Cauchy's or Green's deformation tensor from which the various extension and strain components may be obtained as outlined in Chapter 2. As pointed out by Truesdell and Toupin(18) "...all changes of length and angle are easily calculated from the values of the components (of the deformation tensor)."

The selection of master and specimen grids for a particular experiment should be governed by the deformations expected and results desired. While many such selections may require a great deal of ingenuity and experience, others are quite obvious and only require the application of common sense.

For those deformations which are essentially arbitrary, the moiré method still has many advantages and can produce results within generally acceptable limits of approximation. In this case it is usually expedient to select parallel-lined grids for the specimen and master.

The method of indicial representation of geometric figures and patterns used for the analysis of homogeneous deformations may be generalized to include nonhomogeneous deformations. In some instances, exact solutions result. Two such examples are analyzed in the next section, using a variety of specimen and master grids.

From Section 3.1, two geometric figures consisting of families of curves indexed by numerical parameters may be characterized by

$$L(X^K) = L(j)$$
$$G(X^K) = G(k)$$

[5] This is not to imply that there are no other grid geometries which may be more suitable for a particular experiment or purpose.

where j and k are the parameters. The family of moiré fringes is formed by the sets of intersections of the geometric figures. As before, the fringes are characterized by the equation

$$Q(X^K) = q(j,k) = Q(p)$$

where p is the fringe parameter.

Often the preceding equations may be solved explicitly for j and k. Thus

$$j = L^*(X^K)$$

$$k = G^*(X^K) \quad .$$

Upon substitution into the indicial equation

$$aj - bk = p$$

$$aL^*(X^K) - bG^*(X^K) = p \quad ,$$

or upon rearranging

$$F(X^K,a,b) = F(p,a,b) \quad .$$

In many instances the functions F and F may be directly identified with Q and Q of the fringe equations. If this is the case it may be possible to relate important characteristics of the specimen grid with easily discernible and measurable characteristics of the moiré pattern. For example in the case of homogeneous deformations examined in Section 3.2 the specimen grid pitch and orientation was explicitly determined in terms of the fringe pitch and orientation. It is not always necessary to relate the characteristics of the deformation to the pitch or distance between fringes. As will be demonstrated later, at times it is more convenient to work with terms more readily identified with areas or angular measurements.

In the general case it is not feasible to determine the functional

form of the deformed specimen grid geometry. In such cases satisfactory approximate results may be obtained if the deformation in a local or restricted area of interest may be considered homogeneous. If so, the realtionships derived in Section 3.2 can be used without change. However, under such circumstances it must be understood that the values of specimen grid pitch and orientation are averaged over the distance between fringes. Furthermore, the actual measurement of fringe pitch and angle may become more difficult for nonhomogeneous patterns. In many cases more precise measurements of the fringe geometry in a particular area of interest may be obtained by actually changing the fringe pattern by rotating the master grid or replacing it with one having a more suitable pitch.

3.5 Moiré Analyses for Specific Nonhomogeneous Deformations

3.5.1 Moiré Analysis of Pure Bending of a Block Using Rectangular Master Gratings

From Section 2.3 the equations for pure bending of a block or cuboid are

$$r = (2A_{\delta}X + B_{\delta})^{\frac{1}{2}}$$

$$\alpha = C_{\delta}Y$$

$$z = D_{\delta}Z \quad . \tag{2.35}$$

where the cylindrical and rectangular coordinate systems have a common origin. Here the subscript δ represents a value associated with the specimen. The deformation is schematically illustrated in Figures 2.4 and 3.8. As in the previous cases only deformation in the X-Y plane will be considered.

It is assumed that before deformation the specimen grid is repre-

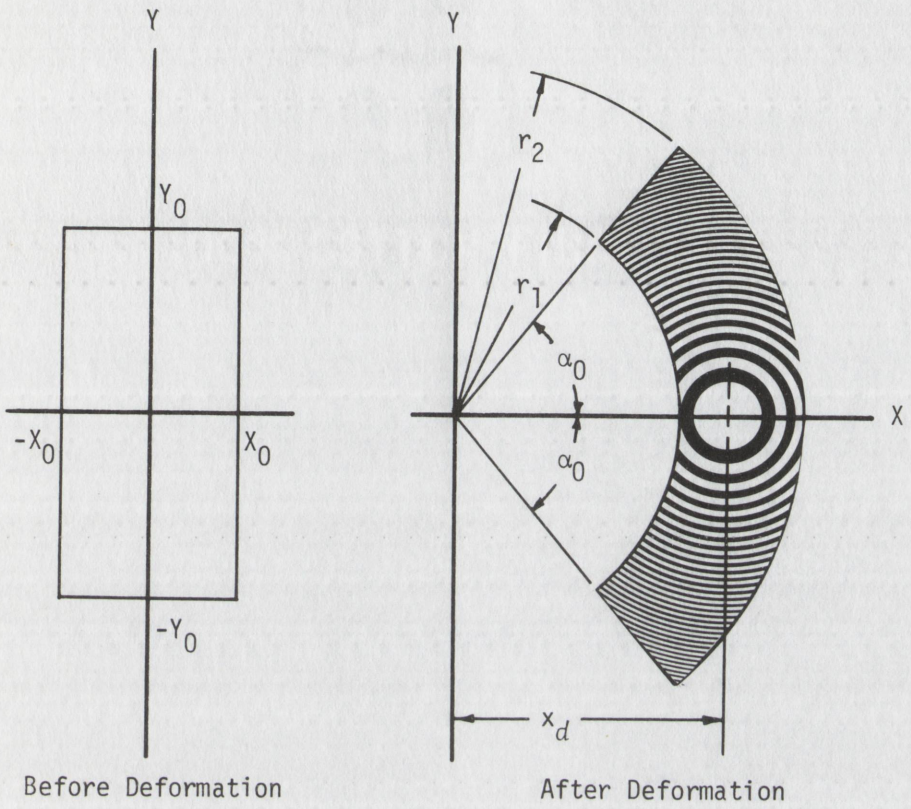

Figure 3.8
Bending of a Block

sented by two mutually orthogonal sets of equispaced parallel lines. It is further assumed that one set of lines, with pitch S, is aligned with the longitudinal or Y-axis of the cuboid, while the other set, with pitch T, is aligned with the transverse or X-axis. The master gratings are also assumed to be two mutually orthogonal sets of equispaced parallel lines of pitches M and N respectively.

If the master grating with pitch M is exactly aligned with the specimen grating with pitch S, then the equations for the sets of lines are

$$X = jM \tag{3.62}$$

and

$$X = kS \tag{3.63}$$

respectively, where j and k are numerical parameters ranging over some subset of the integers. From Equations (3.9) and (3.13), the moiré fringe angle is

$$\Phi = 0$$

and the initial fringe pitch is

$$F = \frac{SM}{S - M} \quad .$$

From Equation (3.21)

$$S = \frac{FM}{F \pm M}$$

where the plus sign (+) is used if $S < M$ and the minus sign (-) is used if $S > M$. An experimental method to determine which sign to use is described in Section 3.2.

After deformation, the lines of the specimen grid described by Equation (3.63) are characterized by the first of Equations (2.35) as

$$r^2 = x^2 + y^2 = 2A_\delta X + B_\delta$$

$$= 2kA_\delta S + B_\delta \quad . \tag{3.64}$$

The equation of the master grating is

$$x = jm \tag{3.65}$$

where m is the new pitch of the grating. The relationship between the numerical parameters is given by the indicial equation

$$aj - bk = p \tag{3.1}$$

where p is the moiré fringe parameter and a and b are integers which account for replications of the moiré pattern. The primary replication, which occurs on the positive x-axis when $a = b = -1$, is generally recognizable as the most distinct and well defined pattern. From a consideration of the indicial equation it is seen that under these circumstances each line of the master grid interferes with each line of the

specimen grid to form a fringe. However, if a = -2 and b = -1, each line of the master grid interferes with two lines of the specimen grid to form a fringe. This results in a less distinct pattern. Due to a poor selection of a master grid it may happen that there is no primary replication occurring on the part. If so, the values of a and b may easily be determined by examining a fringe with an optical magnifier and noting the number of master grid lines which interfere with each specimen grid line. Figure 3.9 illustrates primary, secondary and tertiary moiré replications.

Solving Equations (3.64) and (3.65) for k and j, and substituting in Equation (3.1)

$$\frac{ax}{m} - \frac{b(x^2 + y^2 - B_\delta)}{2A_\delta S} = p$$

or

$$x^2 - \frac{2A_\delta Sax}{mb} + y^2 = \frac{-2A_\delta Sp}{b} + B_\delta \quad .$$

Completing the square,

$$\left(x - \frac{A_\delta S}{md}\right)^2 + y^2 = \frac{-2A_\delta Sp}{b} + B_\delta + \left(\frac{A_\delta S}{md}\right)^2 \qquad (3.66)$$

where

$$d = \frac{b}{a} \quad .$$

Equation (3.66), describing the moiré fringe pattern, represents a series of concentric circles[6] with centers at $(\frac{A_\delta S}{md}, 0)$. The moiré fringes may also be represented by the relation

$$R_p^2 = (x - x_d)^2 + y^2 = A_\delta p + B_\delta \qquad (3.67)$$

---

[6]More exactly, the pattern is a Fresnel figure. See Section 3.5.2.

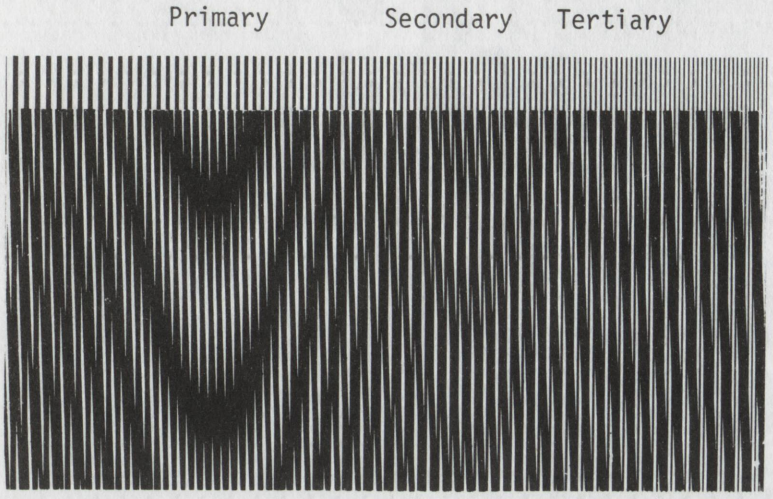

Figure 3.9

Primary, Secondary and Tertiary Replications

where the subscript δ represents a quantity or value associated with the moiré fringes. Since Equations (3.66) and (3.67) are for identical figures, corresponding coefficients may be equated. Thus

$$x_d = \frac{A_\delta S}{md} \tag{3.68}$$

$$A_\delta = \frac{-2A_\delta S}{b} \tag{3.69}$$

and

$$B_\delta = B_\delta + \left(\frac{A_\delta S}{md}\right)^2$$

$$= B_\delta + x_d^2 \quad . \tag{3.70}$$

If the location of the origin of coordinates is known in an experiment, the value of A_δ may be found directly from

$$A_\delta = \frac{x_d\, md}{S}$$

$$= \frac{x_d\, m(F \pm M)d}{FM} \tag{3.71}$$

where x_d and F are measured quantities.

If the location of the origin of coordinates is not known, the value of A_δ may be found by an alternate method. From Equation (3.67)

$$R^2_{p+q} = A_\delta(p+q) + B_\delta \tag{3.72}$$

where q is an integer. Subtracting Equation (3.67) from (3.72)

$$A_\delta = \frac{R^2_{p+q} - R^2_p}{q} \quad . \tag{3.73}$$

Consequently

$$\begin{aligned} A_\delta &= \frac{-bA_\delta}{2S} \\ &= \frac{-bA_\delta(F \pm M)}{2FM} \\ &= \frac{b(R^2_p - R^2_{p+q})(F \pm M)}{2qFM} \quad . \end{aligned} \tag{3.74}$$

To find the proper number C_1 of Green's deformation tensor, the value of the radius r to the point of interest on the specimen must be known. Referring to Figure 3.8

$$\begin{aligned} r_1 &= x_d - (x_d - r_1) \\ &= x_d - \Delta x_d \end{aligned} \tag{3.75}$$

where

$$\Delta x_d = x_d - r_1$$

is easily measured in an experiment. Then the value of r is simply

$$\begin{aligned} r &= r_1 + \Delta r \\ &= x_d - \Delta x_d + \Delta r \quad . \end{aligned} \tag{3.76}$$

From Equation (2.41) the proper number C_1 is

$$C_1 = \Lambda_1^2 = \frac{A_\delta^2}{r^2}$$

$$= \frac{x_d^2 \, m^2 (F \pm M)^2 \, d^2}{F^2 M^2 r^2}$$

or

$$= \frac{b^2 \, A_\delta^2 \, (F \pm M)^2}{4F^2 M^2 r^2} \quad . \qquad (3.77)$$

To find the value of B_δ in Equation (3.67) it is necessary to know the numerical value of the fringe parameter p. The value of p depends on the systems used to order the specimen and master grid lines.

From Equation (3.63) the value of the specimen grid parameter k at $X = -X_0$ is

$$K = \frac{-X_0}{S} = \frac{-X_0(F \pm M)}{FM} \quad .$$

After deformation the value of k at r_1 is equal to K. The value of the master grating parameter j at $x = r_1$ is

$$J = \frac{r_1}{m} \quad .$$

Finally the value of p at r_1 is

$$P = aJ - bK \quad .$$

The quantity B_δ is then

$$B_\delta = R_P^2 - A_\delta P \quad .$$

Therefore the value of B_δ in Equation (2.35) is

$$B_\delta = R_P^2 - A_\delta P - x_d^2 \quad .$$

It should be noted that it is necessary to know an initial dimension X_0

of the undeformed body to find B_δ; whereas the value of A_δ can be obtained by measurements of fringe geometry on the deformed body exclusively. However, the value of B_δ is not required to find the principal values of Green's deformation tensor.

To find the value of C_2 in Green's deformation tensor it is necessary to consider the interaction of the specimen grid with initial pitch T, oriented transverse to the axis of the beam, with the master grating with initial pitch N, oriented at the same angle. The equations for the sets of lines are

$$Y = jN \tag{3.78}$$

and

$$Y = kT \quad . \tag{3.79}$$

From Equations (3.9), (3.13) and (3.43) the moiré fringe angle is

$$\Psi = 0$$

and the fringe pitch is

$$H = \frac{TN}{|T - N|} \quad .$$

From Equations (3.21) and (3.43)

$$T = \frac{HN}{H \pm N} \tag{3.80}$$

where the plus sign (+) is used if $T < N$ and the minus sign (-) is used if $T > N$.

After deformation, the angles of the lines of the specimen grid described by Equation (3.79) are characterized by the second of Equations (2.35) as

$$\alpha = C_\delta Y$$

$$= kC_\delta T \quad .$$

But

$$\tan\alpha = \tan(kC_\delta T) = \frac{y}{x}$$

thus

$$k = \frac{\arctan(\frac{y}{x})}{C_\delta T} \quad .$$

The equation for the new master grating is

$$y = jn$$

thus

$$j = \frac{y}{n} \quad .$$

Again the indicial equation is

$$aj - bk = p$$

or

$$\frac{ay}{n} - \frac{b \arctan(\frac{y}{x})}{C_\delta T} = p \quad .$$

Solving for the constant C_δ,

$$C_\delta = \frac{b \arctan(\frac{y}{x})}{T(\frac{ay}{n} - p)}$$

$$= \frac{b(H \pm N) \arctan(\frac{y}{x})}{HN(\frac{ay}{n} - p)}$$

$$= \frac{b(H \pm N)\,\alpha}{HN(\frac{ay}{n} - p)} \quad . \qquad (3.81)$$

A moiré fringe pattern corresponding to Equation (3.81) with $a = b = 1$ is shown in Figure 3.10. With the indicial systems used for the specimen grid and master grating, the fringe corresponding to $p = 0$ appears to intersect the X-axis at the "star." The fringe index p to the right of the zero fringe is positive; and to the left, negative. Depending on the deformation, no "star" may appear on the de-

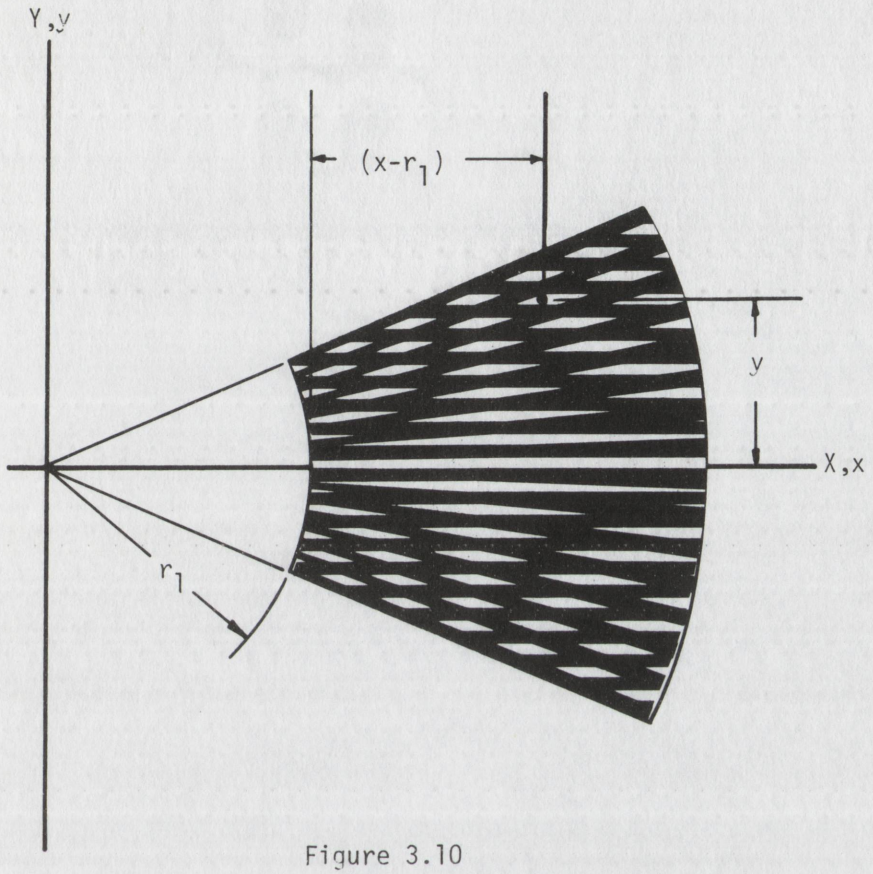

Figure 3.10

Fringe Pattern for Radial Lines Intersecting with Equispaced Lines

formed body. The fringe orders may then be assigned by noting the direction of curvature of the fringes and numbering them consecutively from the X-axis or axis of symmetry. Alternatively, the master grating pitch may be adjusted to cause a "star" to appear on the deformed body.

The constant C_δ may be determined from Equation (3.81) using two alternate methods of measurement. First, if the origin of coordinates is known, the angle α and vertical distance y to a point on a selected fringe may be measured. These values together with the proper fringe number p are then substituted into Equation (3.81) to find C_δ. If the origin of coordinates is not known, the position of the selected point

on the fringe is measured in terms of vertical distance y and horizontal distance $(x - r_1)$. The value of r_1 is given by Equation (3.75); thus the value of x may be found by

$$x = r_1 + (x - r_1) \quad .$$

These measurements are then substituted into the Equation (3.81) to find C_δ.

Finally, from Equation (2.41), the value of C_2 in Green's deformation tensor is found to be simply

$$C_2 = \Lambda_2^2 = C_\delta^2 r^2$$

$$= \frac{r^2 b^2 (H \pm N)^2 \arctan^2(\frac{y}{x})}{H^2 N^2 (\frac{ay}{n} - p)^2} \quad . \qquad (3.82)$$

For $p = 0$ on the primary replication of the pattern

$$C_2 = \frac{r^2 n^2 (H \pm N)^2 \arctan^2(\frac{y}{x})}{y^2 H^2 N^2} \quad .$$

3.5.2 Moiré Analysis of Pure Bending of a Block Using Fresnel Figure and Radial-Line Master Grids

The initial specimen grid dimensions of the undeformed body are obtained using rectangular master gratings as was done in the previous section. After the body is deformed, the initial master grating is replaced by one corresponding in geometry to a Fresnel figure[7] as shown in Figure 3.11. The equation which represents such a master grid is

$$(x - c)^2 + y^2 = jA_m + B_m \qquad (3.83)$$

[7]From Oster(11), a Fresnel figure is a standard positive Fresnel plate consisting of concentric circles alternately blacked out and constructed in such a way that the areas of the black and non-black portions are equal.

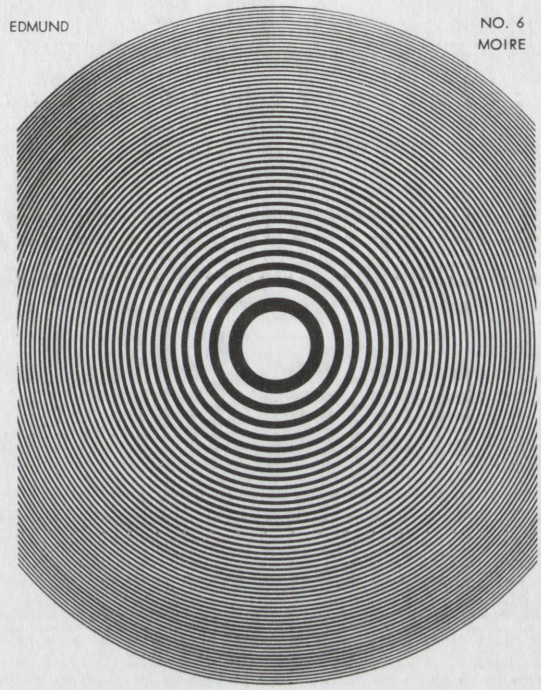

Figure 3.11

Fresnel Figure

where A_m and B_m are known constants and c is the distance the center of the grid is displaced from the origin along the x-axis. From the previous section the specimen grid is described by

$$r^2 = x^2 + y^2 = 2A_s X + B_s$$

$$= 2kA_s S + B_s \quad . \tag{3.64}$$

Substituting for j and k in the indicial equation

$$\frac{a\left[(x - c)^2 + y^2 - B_m\right]}{A_m} - \frac{b(x^2 + y^2 - B_s)}{2A_s S} = p \tag{3.84}$$

or

$$\left[x - \frac{2A_s Sac}{2A_s Sa - A_m B}\right]^2 + y^2 = \frac{2A_s A_m Sp}{2A_s Sa - A_m b} + \frac{2A_s B_m Sa - A_m B_s b}{2A_s Sa - A_m b} + \frac{2A_s A_m Sabc^2}{(2A_s Sa - A_m b)^2} \cdot \tag{3.85}$$

Equation (3.85) describes the resulting moiré pattern which is a Fresnel figure displaced from the origin along the X-axis by an amount

$$x_d = \frac{2A_\delta Sc}{2A_\delta S - A_m d} \tag{3.86}$$

where

$$d = \frac{b}{a} \quad .$$

An illustration of the pattern is shown in Figure 3.12. Another relation for the fringe pattern is

$$R_p^2 = (x - x_d)^2 + y^2 = A_\beta p + B_\beta \quad . \tag{3.87}$$

Equating corresponding coefficients

$$A_\beta = \frac{2A_\delta A_m S}{2A_\delta Sa - A_m b} \tag{3.88}$$

$$B_\beta = \frac{2A_\delta B_m Sa - A_m B_\delta b}{2A_\delta Sa - A_m b} + \frac{2A_\delta A_m abc^2}{(2A_\delta Sa - A_m b)^2} \quad . \tag{3.89}$$

To find A_β (and subsequently A_δ) subtract Equation (3.87) from

$$R_{p+q}^2 = A_\beta(p+q) + B_\beta \quad .$$

Then

$$A_\beta = \frac{R_{p+q}^2 - R_p^2}{q} \tag{3.90}$$

where q is an integer. From Equations (3.88) and (3.90)

$$A_\delta = \frac{A_m A_\beta b}{2S(A_\beta a - A_m)}$$

$$= \frac{A_m(R_{p+q}^2 - R_p^2)b}{2S(aR_{p+q}^2 - aR_p^2 - qA_m)}$$

$$= \frac{A_m(R_{p+q}^2 - R_p^2)(F \pm M)b}{2FM(aR_{p+q}^2 - aR_p^2 - qA_m)} \quad . \tag{3.91}$$

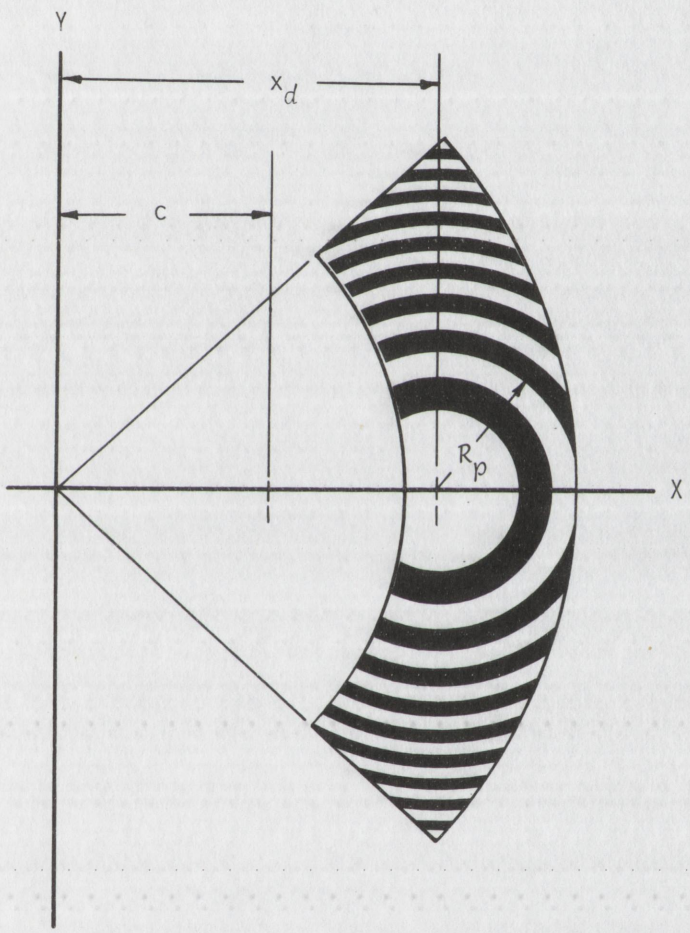

Figure 3.12

Bending of a Block

The value of A may also be found by rearranging Equation (3.86)

$$A_s = \frac{x_d A_m d}{2S(x_d - c)} \quad . \tag{3.92}$$

If j and k in Equations (3.83) and (3.64) increase as the respective radii increase, A_m and A_s are positive quantities. Thus in Equation (3.92), if $0 < x_d < c$, d is negative (or equivalently, a and b are of opposite signs); if $x_d > c$, d is positive (or a and b are of the same sign). If d is positive the moiré pattern is referred to as a positive replication. If d is negative, the pattern is a negative replication. Either type of replication may be used to determine the deformation of the specimen; however, for the sake of clarity only positive replications will be considered in this section.

Differentiating Equation (3.86) with respect to c

$$\frac{dx_d}{dc} = \frac{2A_s S}{2A_s S - A_m d}$$

$$= \frac{2A_s Sa}{2A_s Sa - A_m b} \quad .$$

If $\frac{dx_d}{dc}$ is positive, then $2A_s Sa > A_m b$; if $\frac{dx_d}{dc}$ is negative, then $2A_s Sa < A_m b$. Establishing the convention that $R_{p+1} > R_p$, from Equation (3.90) A_s is positive. Finally from Equation (3.88) and the foregoing discussion, it is apparent that if $\frac{dx_d}{dc}$ is positive, a and b are positive; if $\frac{dx_d}{dc}$ is negative, a and b are negative. Experimentally, this test may easily be applied by shifting the master grid along the x-axis and noting the direction in which x_d moves. If x_d moves in the same direction, a and b are positive. If x_d moves in the opposite direction, a and b are negative.

An interesting feature to notice is that if the specimen grid is identical to the master grid, then $2A_s Sa = A_m b$. Consequently Equa-

tion (3.84) for the moiré fringes assumes the form

$$x = \frac{-A_m p}{2ca} + \frac{1}{2c}(c^2 + B_m - B_s) \quad .$$

This equation represents a series of equispaced vertical straight lines.

For a fixed value of d in Equation (3.86) it is seen that the location of the replication or pattern is easily shifted by merely moving the master grid along the x-axis. Thus without any real restriction on experimental methods, attention could be limited to the case of primary replication. The primary pattern can generally be shifted without difficulty so that it lies on the deformed specimen. This feature is markedly different from the previous case where a rectangular master grid is used. Under those circumstances it is necessary to change the master grid pitch to shift the position of the replications.

If the location of the origin is known, A_s may be found from Equation (3.92).

If the location of the origin is unknown, the value of A_s may be determined from Equation (3.91). To find the radius to a point, the value of x_d may be found by rearranging Equation (3.92) such that

$$x_d = \frac{2A_s\, S(x_d - c)}{A_m d}$$

$$= \frac{2A_s FM(x_d - c)}{A_m(F \pm M)d}$$

where $(x_d - c)$ is measured during an experiment. The radius r may then be found as before using Equations (3.75) and (3.76). The value of the proper number C_1 in Green's deformation tensor is then

$$C_1 = \Lambda_1^2 = \frac{A^2}{r^2} \quad . \qquad (2.41)$$

In the previous section the value of C_2 in Green's deformation tensor was found from moiré patterns formed by the superposition of a radial-lined specimen grid on an equispaced parallel-lined master grid. The angular symmetry of the deformation suggests that the use of a radial-lined master grid may be advantageous after deformation.

Before deformation, Equations (3.78) through (3.80) are still applicable; however, when bending of the block occurs the rectangular master grating is replaced by a radial-lined grid whose center is at the origin and whose geometry can be represented by

$$\theta_j = \arctan \frac{y}{x} = j(\Delta\theta)$$

where $\Delta\theta$ is the angle formed by each pair of radial lines. The equation for the specimen grid is the same as before. Solving for j and k and substituting in the indicial equation

$$aj - bk = p$$

$$\frac{(a)\arctan(\frac{y}{x})}{(\Delta\theta)} - \frac{(b)\arctan(\frac{y}{x})}{C_\delta T} = p \quad .$$

Thus

$$\phi_p = \arctan(\frac{y}{x}) = \frac{(\Delta\theta)C_\delta Tp}{C_\delta Ta - (\Delta\theta)b}$$

where ϕ_p are the angles of the fringes.

This equation may also be written

$$\phi_p = \arctan(\frac{y}{x}) = (\Delta\phi)p$$

where $\Delta\phi$ is the angle between fringes. Thus

$$\Delta\phi = \frac{(\Delta\theta)C_\delta T}{C_\delta Ta - (\Delta\theta)b} \quad . \tag{3.93}$$

Equation (3.93) may be solved for the constant C_δ,

$$C_\delta = \frac{(\Delta\phi)(\Delta\theta)b}{T((\Delta\phi)a - (\Delta\theta))} \quad . \tag{3.94}$$

If the fringes are indexed such that $\phi_{p+1} > \phi_p$, then $\Delta\phi$ is positive. Furthermore, for this system of grids, a and b are always of the same sign. Consequently, if $C_\delta Ta > (\Delta\theta)b$, then a and b are positive; if $C_\delta Ta < (\Delta\theta)b$, then a and b are negative. An experimental method to determine the proper sign of a and b is easily derived. Let

$$\arctan\frac{y}{x} = j(\Delta\theta) + \delta$$

where δ is an angle by which the master grid is rotated. Let the specimen grid remain fixed. The equation for the moiré pattern is then

$$\phi_p = \arctan\frac{y}{x} = \frac{(\Delta\theta)C_\delta Tp}{C_\delta Ta - (\Delta\theta)b} + \frac{C_\delta Ta\ \delta}{C_\delta Ta - (\Delta\theta)b} \quad .$$

Now

$$\frac{d\phi_p}{d\delta} = \frac{C_\delta Ta}{C_\delta Ta - (\Delta\theta)b} \quad .$$

As the master grid is rotated, if $\frac{d\phi_p}{d\delta}$ is positive, then $C_\delta Ta > (\Delta\theta)b$, and a and b are positive. If $\frac{d\phi_p}{d\delta}$ is negative, then a and b are negative.

The proper number C_2 of Green's deformation tensor for pure bending of a block is then

$$C_2 = C_\delta^2\, r^2$$

$$= \frac{(\Delta\phi)^2(\Delta\theta)^2b^2}{T^2((\Delta\phi)a - (\Delta\theta))^2}$$

$$= \frac{(\Delta\phi)^2(\Delta\theta)^2b^2(H\pm N)^2}{H^2N^2((\Delta\phi)a - (\Delta\theta))^2} \quad . \qquad (3.95)$$

3.5.3 Moiré Analysis of Pure Bending of a Block Using a Master Grid of Equispaced Concentric Circles

As before, the initial specimen grid dimensions of the undeformed body are obtained using rectangular master gratings. In the previous section, one of the master gratings was replaced with a Fresnel figure

to obtain moiré patterns from which the tensor components could be calculated. In this section the master grating is replaced with a grid of equispaced concentric circles. Since the purpose of using this type master grid is to take advantage of the symmetry of the deformation being considered, it is assumed that the master grid center is located at the origin of coordinates.

The master grid may be characterized by the relation

$$r = jm \quad . \tag{3.96}$$

After deformation, the specimen grid is represented by

$$r^2 = 2kA_\delta S + B_\delta \quad . \tag{3.64}$$

Solving for j and k and substituting in the indicial equation

$$\frac{ar}{m} - \frac{b(r^2 - B_\delta)}{2A_\delta S} = p$$

or

$$r^2 - \frac{2A_\delta Sa}{bm} r = \frac{-2A_\delta Sp}{b} + B_\delta \quad .$$

Then

$$r = \left\{\frac{A_\delta S}{b}\left[\frac{A_\delta Sa^2}{bm^2} - 2p\right] + B_\delta\right\}^{\frac{1}{2}} + \frac{A_\delta Sa}{bm} \quad . \tag{3.97}$$

Equation (3.97) describes a series of concentric circular rings whose spacing is a function of the fringe index p.

An expression for the value of A_δ may be obtained from

$$A_\delta = \frac{bm(r^2_{p+q} - r^2_p)}{2Sa(r_{p+q} - r_p - \frac{qm}{a})} \tag{3.98}$$

where q is a positive integer.

The grid radii are indexed such that the indices increase as the radii increase. Consequently A_δ and m are positive, and a and b are of the same sign. To determine the sign of a and b it is necessary to

have a qualitative measure of the relative magnitude of the specimen and master pitches. This may be obtained experimentally. Restricting the equations of the grids to the x-axis, for the specimen

$$x = (2kA_{\delta}S + B_{\delta})^{\frac{1}{2}}$$

$$= k\left[\frac{2A_{\delta}S}{k} + \frac{B_{\delta}}{k^2}\right]^{\frac{1}{2}}$$

$$= k\,\delta_k$$

and for the master, which is shifted along the x-axis by an amount c,

$$x = jm + c \quad .$$

Substituting in the indicial equation and rearranging

$$x = \frac{m\delta_k\, p}{a\delta_k - bm} + \frac{\delta_k ac}{a\delta_k - bm}$$

$$= f_k p + \frac{\delta_k ac}{a\delta_k - bm}$$

where f_k is the fringe pitch. Since the fringe pitch is a positive quantity, if $a\delta_k > bm$, then a and b are positive; if $a\delta_k < bm$, then a and b are negative.

Differentiating the equation above with respect to c

$$\frac{dx}{dc} = \frac{\delta_k\, a}{a\delta_k - bm} \quad .$$

If $\frac{dx}{dc}$ is positive, then $a\delta_k > bm$ and a and b are positive; if $\frac{dx}{dc}$ is negative, then $a\delta_k < bm$ and a and b are negative. Thus the sign of a and b may be determined experimentally by merely shifting the master grid along the x-axis, and observing the direction in which the fringes move. It should be noted that once the sign of a and b is established for one portion of the moiré pattern, the same convention is maintained thereafter over the entire pattern.

The proper value, C_1, of Green's deformation tensor may now be calculated as in previous sections. The proper number, C_2, may be obtained by techniques already described.

3.5.4 Moiré Analysis of Flexure of an Initially Curved Cuboid Using Fresnel Figure and Radial-Line Grids

In the previously studied cases the initial moiré patterns were obtained using rectangular grids. The only reason for this was that the initial geometry suggested their use. An undeformed body may have a configuration that is more suitably analyzed using other types of grids. An example of this is the flexure of an initially curved cuboid. This case was chosen both for its different initial geometry and the fact that a theoretical solution for finite deformation exists as summarized in Section 2.4.

Due to the symmetry of the specimen and the deformation, a circular grid of some sort is the most obvious choice for the measurement of deformation in a radial direction. By the same token a radial-lined grid system appears to be a logical choice for measurements in the tangential direction.

Although grids of equispaced concentric circles appear to be the most straight-forward selection, Fresnel figure grids are selected because of the simplicity of the resulting patterns even if the centers of the specimen and master grids are not coincident. Since the technique of deriving the equations for moiré patterns has been amply illustrated in the preceding sections, some of the detailed steps will be eliminated in the sequel. Furthermore, for the sake of brevity, it is assumed that the initial specimen and master grids are identical, and the same master grid is used before and after deformation.

The equations for the initial specimen and master grids are

$$R^2 = X^2 + Y^2 = A_M j + B_M$$

$$= A_S k + B_S \qquad (3.99)$$

where

$$A_M = A_S$$

$$B_M = B_S \quad .$$

From Equations (2.43) and (3.99) the specimen grid after deformation is characterized by

$$r^2 = x^2 + y^2 = A_\delta R^2 + B_\delta$$

$$= A_\delta (A_M k + B_M) + B_\delta \quad .$$

The master grid is

$$(x - c)^2 + y^2 = A_M j + B_M$$

where now the master grid is shifted a distance c along the x-axis. After substitution in the indicial equation, the resulting moiré pattern is given by

$$R_p^2 = \left(x - \frac{aA_\delta c}{aA_\delta - b} \right)^2 + y^2 = \frac{A_\delta A_M p}{aA_\delta - b} + \frac{aA_\delta B_M - b(A_\delta B_M + B_\delta)}{aA_\delta - b}$$

$$+ \frac{aA_\delta bc^2}{(aA_\delta - b)^2} \quad . \qquad (3.100)$$

Equation (3.100) describes a Fresnel figure displaced from the origin along the x-axis by an amount

$$x_d = \frac{aA_\delta c}{aA_\delta - b}$$

$$= \frac{A_\delta c}{A_\delta - d} \qquad (3.101)$$

where

$$d = \frac{b}{a} \quad .$$

Then

$$A_{\delta} = \frac{x_d(d)}{x_d - c} \quad . \tag{3.102}$$

Let

$$A_{\beta} = \frac{A_{\delta} A_M}{aA_{\delta} - b} \tag{3.103}$$

then

$$A_{\beta} = \frac{R^2_{p+q} - R^2_p}{q} \tag{3.104}$$

where q is an integer. From Equations (3.103) and (3.104)

$$A_{\delta} = \frac{bA_{\beta}}{aA_{\beta} - A_M}$$

$$= \frac{b(R^2_{p+q} - R^2_p)}{a(R^2_{p+q} - R^2_p) - qA_M} \quad . \tag{3.105}$$

If $x_d > c$, the sign of a and b may be determined as outlined in Section 3.5.2. If $0 < x_d < c$, b and a are of opposite sign, and if $A_M > aA_{\beta}$, then a is positive and b is negative.

From Equation (3.99) the value of k at the inside radius, R_1, of the undeformed ring sector is

$$K = \frac{R_1^2 - B_M}{A_M} \quad .$$

The value of k at the inside radius after deformation remains K. The value of j at the point on the x-axis coinciding with r_1 is

$$J = \frac{(x_1 - c)^2 - B_M}{A_M} \quad .$$

Thus the value of p at the same point is

$$P = aJ - bK \quad .$$

The value for B_{δ} may now be found from Equation (3.100).

To investigate the deformations in the tangential direction, an array of equiangular radial lines is chosen for the master and initial

specimen grids. The equation for the master and initial specimen grid is

$$\Theta = j(\Delta\Theta)$$
$$= k(\Delta\Theta) \quad .$$

After deformation, the equation for the specimen grid is

$$\theta = C_{\delta}\Theta$$
$$= kC_{\delta}(\Delta\Theta) \quad .$$

Substituting in the indicial equation and rearranging, the moiré pattern is described by

$$\theta = \frac{C_{\delta}(\Delta\Theta)p}{aC_{\delta} - b}$$
$$= (\Delta\phi)p \quad .$$

Thus

$$C_{\delta} = \frac{b(\Delta\phi)}{a(\Delta\phi) - (\Delta\Theta)} \tag{3.106}$$

where the values and sign of a and b are found as described in Section 3.5.2.

The proper numbers of Cauchy's deformation tensor are given by Equation (2.47). Equations (3.100), (3.105) and (3.106) may be used to compute the constants $A = A_{\delta}$, $B = B_{\delta}$ and $C = C_{\delta}$ to find the experimental values of c_1 and c_2.

4. MOIRÉ PATTERNS FOR SPECIFIC TWO-DIMENSIONAL DEFORMATIONS

4.1 General

A convenient way to check or verify results of the theoretical moiré analyses is to create moiré patterns by superimposing appropriate master grids on "specimen" grids consisting of families of lines constructed so as to represent the results of ideal deformations. This can be easily done for the specific deformations considered in the previous chapters. From measurements of the applicable fringe pattern dimensions, the "specimen" grid parameters can be calculated and compared to the known parameters used in the construction of the "specimen" grids. This method offers advantages over a strictly experimental approach, since it is often difficult to experimentally produce a satisfactory approximation of an ideal deformation. Thus, if a predicted moiré response is not obtained from an experiment, it is open to question as to whether the theory or experiment is at fault. Since the moiré method is an experimental technique, the foregoing discussion does not eliminate the necessity of demonstrating that it can be used under actual test conditions. Consequently, results of large deformation experiments are presented in Chapter 5. Nevertheless, to complement the experimental results, moiré patterns created by idealized figures representing simple shear and bending of a block are analyzed in the following sections.

4.2 Moiré Patterns for Simple Shear

Under simple shear deformation, a family of equispaced vertical lines described by the relation

$$X = kS$$

is carried into a family of straight lines described by the equations

$$x = X + Y \tan\alpha$$

$$= kS + Y \tan\alpha \quad . \tag{4.1}$$

No change occurs to a family of horizontal lines. The moiré responses to such a deformation, corresponding to Examples I and II in Section 3.3, are illustrated in Figure 4.1.[1] Table 4.1 presents the values used in constructing the "specimen" grids, the moiré data determined from Figure 4.1, and the components and principal values of Green's deformation tensor. The analysis of simple shear summarized in Section 2.2 revealed that all deformation and strain tensors may be found from the value of the angle α. Nevertheless, for the purpose of comparison, the components of Green's deformation tensor for Figure 4.1b and 4.1c were computed from the moiré measurements using Equations (3.47). The components for Figure 4.1a were computed from the value of the angle α using the theoretical equations given in Section 2.2.

4.3 Moire Patterns for Bending of a Block

In Sections 2.3 and 3.5.1 it was shown that the proper numbers of the two-dimensional Green's deformation tensor for bending of a cuboid could be determined at any radius by finding the values of A_δ and C_δ in the equations

$$r = (2A_\delta X + B_\delta)^{\frac{1}{2}}$$

$$= (2kA_\delta S + B_\delta)^{\frac{1}{2}}$$

$$= C_\delta Y$$

$$= kC_\delta T \quad . \tag{4.2}$$

[1] Edmund Scientific Co. Moiré Pattern No. 70,719(2) was used to construct the figure.

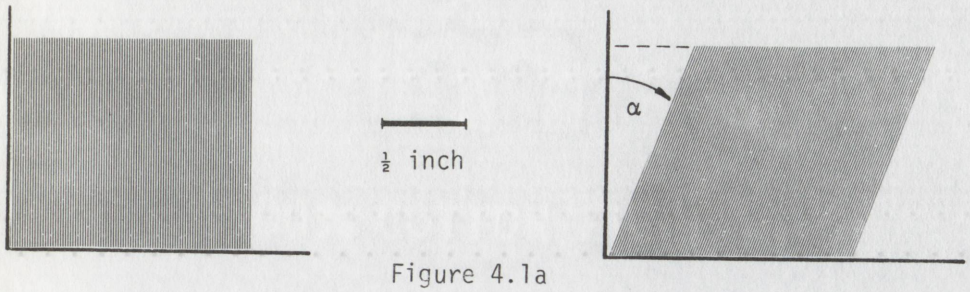

Figure 4.1a
Simple Shear "Specimen" Grid

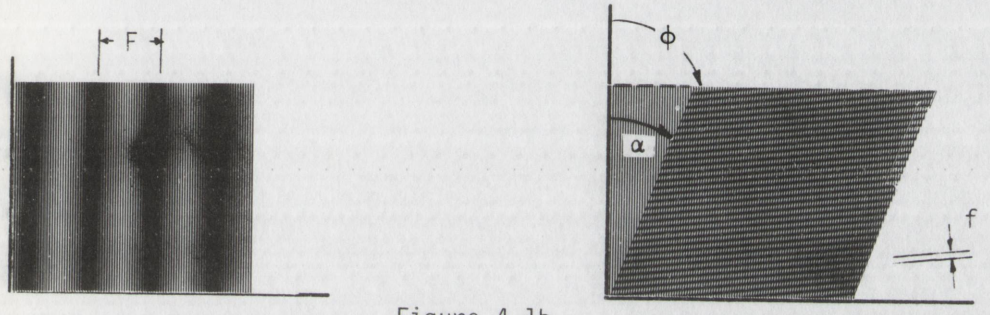

Figure 4.1b
Simple Shear, Example I

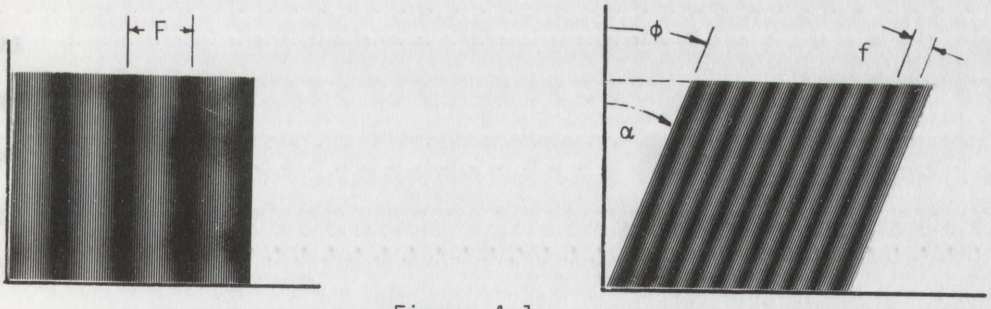

Figure 4.1c
Simple Shear, Example II

Figure 4.1

Simple Shear Deformations Corresponding
to Examples I and II, Section 3.3

Table 4.1

Specimen and Moiré Data for the Simple Shear Deformation Shown in Figure 4.1

	Values to construct "specimen" grid, Figure 4.1a	Values determined from Example I,+ Figure 4.1b	Values determined from Example II,+ Figure 4.1c
F, inch	---	0.367	0.367
f, inch	---	0.0366	0.129
ϕ, degree	---	84.9	21.2
S, inch	0.0144	0.0144	0.0144
s, inch	---	0.01347	0.01344
$\alpha=\gamma$, degree	21.2	21.4	21.2
C_{XX}	1.00000	1.00878	1.00172
C_{XY}	0.38787	0.39362	0.38821
C_{YY}	1.15044	1.15358	1.15046
C_1	1.47032	1.48140	1.47136
C_2	0.68013	0.68096	0.68082
C_{12}	0.39510	0.40023	0.39527
β_1	50.49	50.21	50.42

+The master grating pitch remained unchanged, thus M = m = 0.015 inch. It is assumed that t = T = 0.015 inch. Fringe pitches and angles were measured as described in Section 5.3.3.

Equations (4.2) describe the geometry of the deformed beam in terms of the initial specimen pitches S and T. Figure 4.2 illustrates the moiré patterns obtained for such a deformation using master gratings of equi-spaced parallel lines.[2] Table 4.2 presents the values used in constructing the "specimen" grids, and the moiré data determined from Figure 4.2. The nomenclature used in the table is defined in Section 3.5.1.

Figure 4.3 illustrates the same deformation; however, in this case a Fresnel figure master grid[3] was used in place of the parallel-lined grating. This combination is discussed in Section 3.5.2.[4] Table 4.3 presents the appropriate specimen and moiré data.

---

[2]Edmund Moiré Pattern Nos. 70,719(6) and 60,534 were used to construct the figures.

[3]Edmund Moiré Pattern No. 60,538 was used as the master grid.

[4]Radial-lined master grids are also discussed in Section 3.5.2. An example of the use of such a grid is given in Section 5.5.

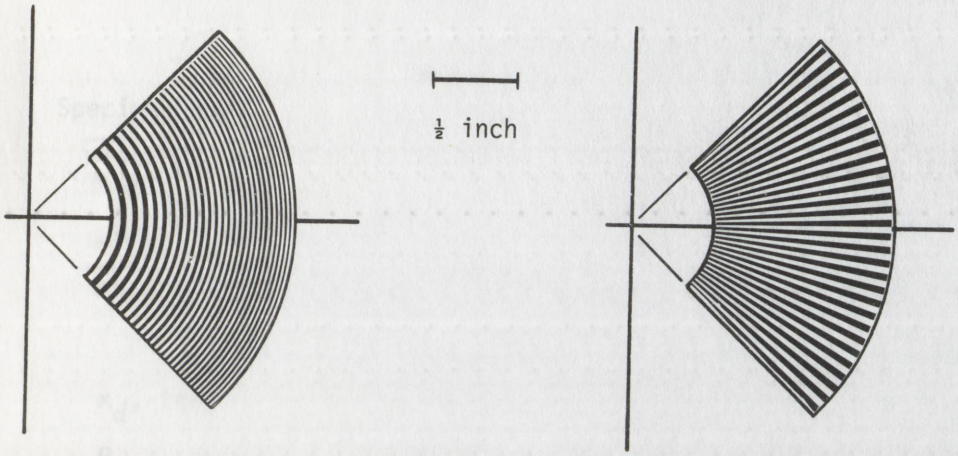

Figure 4.2a
"Specimen" Grids

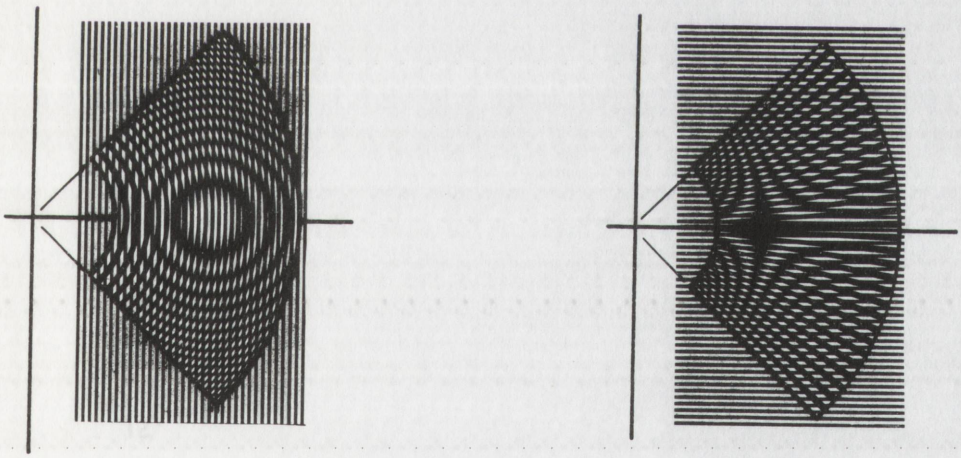

Figure 4.2b
Moiré Patterns

Figure 4.2

Moiré Patterns due to Bending of a Block
Using Equispaced Parallel-Lined Master Gratings

Table 4.2

Specimen and Moiré Data for the Block Bending Deformation Shown in Figure 4.2

	Values to construct "specimen" grid,[+] Figure 4.2a	Values determined from moiré patterns,[+] Figure 4.2b
x_d, inch	---	1.020
R_{p-1}, inch	---	0.225
R_{p-6}, inch	---	0.660
x, inch	---	0.975
y, inch	---	0.380
p	---	3
A_δ, inch	1.008	1.020[*] 1.025[†]
C_δ, radian/inch	1.395	1.390
$C_1(r=1)$	1.0161	1.0404[*] 1.0506[†]
$C_2(r=1)$	1.9460	1.9321
$C_{12}(r=1)$	0.465	0.446[*] 0.440[†]

[+]The initial specimen grid pitches were assumed to be S = T = 0.0375 inch. The master grating pitch used was m = n = 0.0375 inch.

[*]Value was found using Equation (3.71), d = 1.

[†]Value was found using Equation (3.74), b = 1.

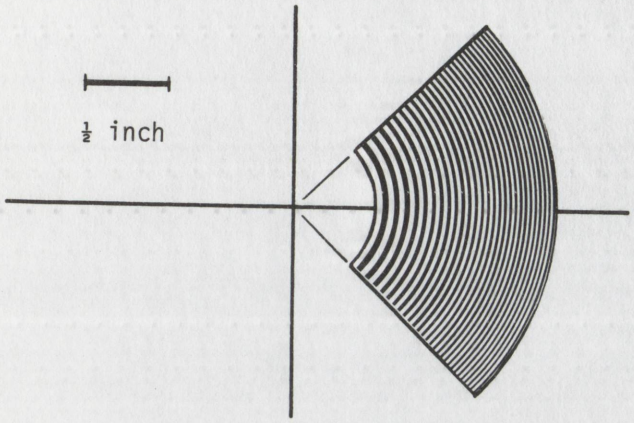

Figure 4.3a
"Specimen" Grid

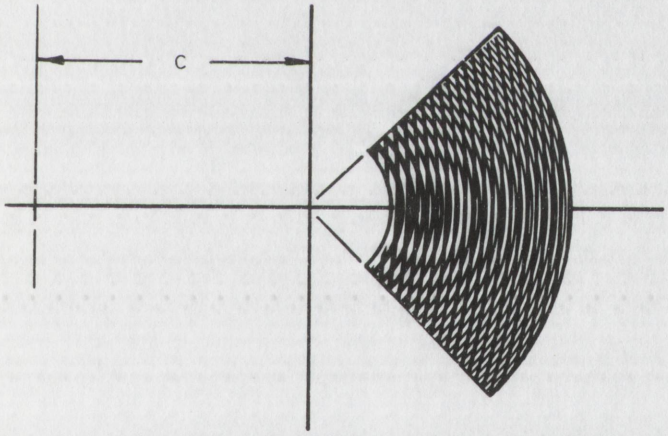

Figure 4.3b
Moiré Pattern

Figure 4.3

Moiré Pattern due to Bending of a Block
Using a Fresnel Figure Master Grid

Table 4.3

Specimen and Moiré Data for the Block Bending Deformation Shown in Figure 4.3

	Values to construct "specimen" grid,[+] Figure 4.3a	Values determined from moiré patterns,[+] Figure 4.3b
x_d, inch	---	0.68
R_{p+1}, inch	---	0.19
R_{p+6}, inch	---	0.70
c, inch	---	-3.17
A_s, inch	1.008	1.020[*]
		1.003[†]
$C_1(r=1)$	1.0161	1.0401[*]
		1.0060[†]

[+]The initial specimen grid pitch was assumed to be S = 0.0375 inch. The master grid size was characterized by A_M = 0.434 inch^2.

[*]Value was found using Equation (3.92), d = 1.

[†]Value was found using Equation (3.91), a = b = -1.

5. EXPERIMENTAL MOIRÉ INVESTIGATIONS

5.1 General

To complement the theoretical moiré analyses, patterns and results, experimental studies of actual two-dimensional deformations were conducted. The studies include the nominal deformations of simple shear, bending of a block, bending of an initially curved cuboid and extension of a plane tapered tensile specimen. Theoretical analyses have been presented in previous sections for all but the tapered specimen. Since this research is concerned only with the analysis of the deformations of a body, no attempt was made to measure the forces required to produce the deformations. In the cases of simple shear and bending of a block, kinematical straining frames were used to approximate theoretical deformations as closely as possible. Within the limitations of the materials and equipment available, specific efforts were made to assure that the deformations fell into the realm of large strain theory.

5.2 Model Materials and Preparation

In all cases the model material selected was Hysol CP-4485 produced by the Hysol Corporation, Olean, New York. This product is also commonly known as Hysol 8705. Typical mechanical properties obtained from Hysol Technical Data Sheet E-105C indicate a static modulus of elasticity of 444 psi and a Poisson's ratio of 0.465. The initial thickness of the unmachined sheet material was 3/8 inch.

Specimen grids were printed on the models using GACO Engraver's Resist, a polyvinyl-alcohol emulsion, produced by Jones Graphic Products of Ohio, Inc., Toledo, Ohio. The step-by-step procedure used

for specimen grid preparation is given below.

Specimen Grid Preparation

1) For proper printing and adhesion of the grid to the model, the surface finish of the Hysol must be dull rather than glossy. A satisfactory finish was obtained by sanding the model surface with a new 320 grit sanding belt. A coarser grit belt caused too many deep scratches resulting in discontinuities in the final printed grid.
2) The model was washed in a strong detergent solution to remove any oil, grease or dirt.
3) After rinsing, the surface to be printed was vigorously scrubbed with Grade 000 steel wool, water and ordinary household cleanser.
4) After another rinsing, the surface was again scrubbed with steel wool, water and Grade FFF fine powdered pumice. It was then rinsed in water and allowed to air-dry.
5) The model was then flow-coated with GACO Engraver's Resist which was prepared by mixing one part by volume of GACO Resist Sensitizer to 21.3 parts of GACO Engraver's Resist Base. Care was taken to assure that the proposed grid area was completely covered, and no air bubbles were entrained in the resist.
6) The model was then placed in a standard platemaker's whirler equipped with an electric heating element. The model was located on the whirler table at a radius of approximately one foot from the axis of rotation. The speed was set at 70 to 80 rpm and the heat was set at "medium." This resulted in a model temperature of approximately 120°F after the full drying time of 25 minutes.
7) After drying, the model was allowed to cool to room temperature in a dark cabinet for approximately 30 minutes.

8) The specimen was then exposed to a carbon arc light source for 6 minutes in a Model RP-21, nuArc Rapid Printer, manufactured by the nuArc Co., Inc., Chicago, Illinois. In this machine the specimen, which was held in contact with the emulsion side of the selected grid negative by a vacuum frame, was located approximately 14 inches from the arc.

9) After exposure, the model was immersed and gently agitated for one minute in a room temperature mixture of GACO Developing Solution. The solution was prepared by mixing one part by volume of GACO developer Concentrate with four parts of tap water. Development was completed by rinsing the sample under a moderate water spray for one to two minutes.

10) After fixing, the resist normally becomes relatively transparent and assumes an amber color. Therefore, to provide good color contrast, it had to be stained before the model was immersed in the fixing solution.[1] After air-drying, the developed grid was completely covered for one minute with a coating of red water-soluble dye consisting of a solution of distilled water, propylene glycol and 2.5% pure color. The model was then immersed and gently agitated in a room temperature mixture of GACO Fixing Solution for 30 seconds to one minute. The solution was prepared by mixing one part by volume of GACO Resist Fixing Concentrate with four parts of tap water. The model was then rinsed for one minute under a mild water spray and allowed to air-dry.

The procedure outlined above resulted in a fairly dense, durable spec-

[1]It was not possible to adequately stain the grid after the resist was fixed.

imen grid which was resistant to mild abrasion, water and the mineral oil used to lubricate the models or provide intimate contact with the master grids during subsequent experiments.[2]

It was found that the Hysol could be machined by a number of methods including saw cutting, turning, grinding, sanding and drilling. In all machining operations, the material had to be adequately backed up and supported to prevent flexing. Tool bits were sharp and high cutting speeds were essential. During sanding or grinding operations, the material was allowed to cool at appropriate intervals.

5.3 Simple Shear Experiment

5.3.1 Equipment and Experimental Setup

To produce a reasonable experimental approximation of a simple shear deformation, the straining frame shown in Figure 5.1 was constructed. The fixture consists of a rigid rectangular framework which supports a movable cross slide. The cross slide is equipped with leveling screws to assure that it can be aligned parallel with the base. The specimen, which measures 12 inches high by 9-1/2 inches wide by 3/8 inch thick was bolted to the framework and cross slide as shown. The 3-1/2-inch by 3-1/2-inch specimen grid was printed at the center of the test sample and consisted of a nominal 200 line-per-inch rectangular moiré grid superimposed on another 10 line-per-inch rectangular registration grid. The moiré grid was printed using a Photolastic, Inc. VPM #16-200 glass master as the negative. The registration grid

---

[2]In an attempt to obtain more opaque grid lines, the Kodak Thin Film Resist (KTFR) system was tried. The chemicals used in this system proved to be incompatible with the Hysol. The Kodak resists have proved to be highly satisfactory for metal specimens. Detailed coating and etching techniques are presented by Holister and Luxmoore(8).

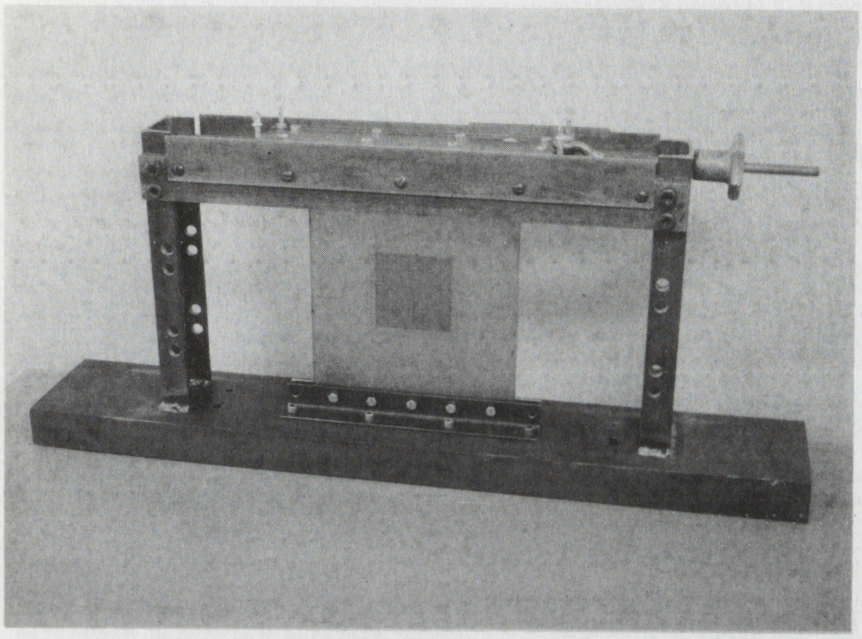

Figure 5.1

Simple Shear Straining Frame and Sample

was printed using a negative of a 6-inch by 6-inch Precision Registration Grid, No. 40,666, sold by Edmund Scientific Co., Barrington, New Jersey.

Deformation of the specimen was produced by turning the hand screw attached to the cross slide.

Moiré patterns were viewed and recorded at Los Alamos Scientific Laboratory using a Model 102 Universal Moiré Bench manufactured by Photolastic Inc., Malvern, Pa. This instrument, shown in Figure 5.2, functions by optically superimposing an image of the specimen grid on a ground glass and master grid mounted on the rear of the bench. In this respect the bench operates in much the same manner as any camera capable of being equipped with a ground-glass back. The bench has the following features:

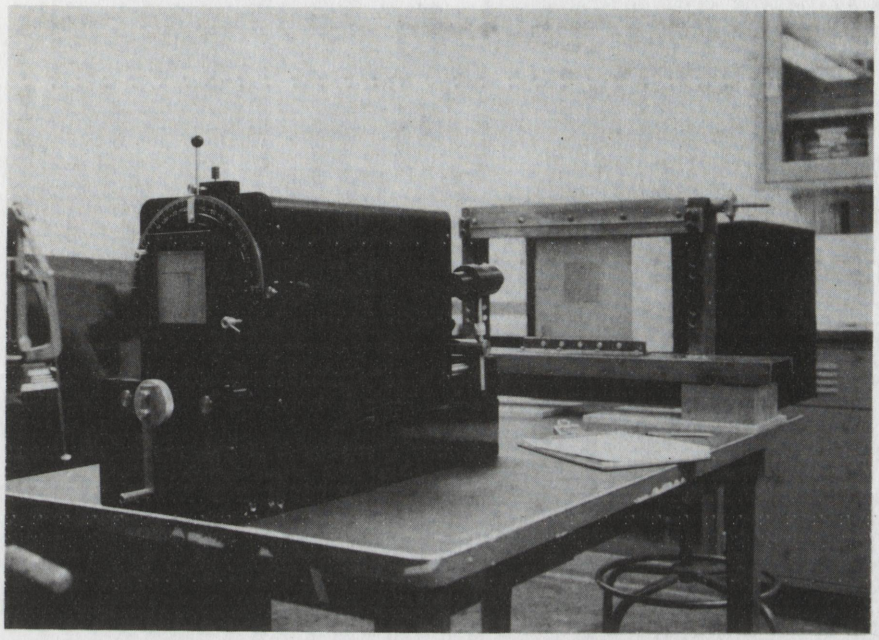

Figure 5.2

Simple Shear Test Setup

1) A Photolastic, Inc., VPM=200 parallel-lined glass master grating mounted in intimate contact with a ground-glass focusing and viewing plate. Masters can be interchanged at will, but are limited in overall size to four inches by five inches.
2) A "mismatch" selector which optically provides a variable initial grid pitch mismatch by changing the magnification of the specimen grid image.
3) A No. 5 Universal Syncro shutter manufactured by the ILEX Optical Co., Rochester, New York.
4) An Apo-Nikkor f:1.9, 300 mm lens manufactured by Nippon Kogaku, Tokyo, Japan.
5) A rotating mount for the master grating which permits

360 degree rotation of the master. The mounting mechanism is calibrated in degrees and has two adjustable stops.

Data was recorded by photographing the moiré pattern appearing on the master grating/ground glass. The camera used was a Graflex Graphic View II, equipped with an OPTAR f:4.7, 135 mm lens, manufactured by the Graflex Co., Rochester, New York. The film used was Polaroid 4X5, Type 57 with an ASA rating of 3200. The film was exposed and processed in a Polaroid No. 500, 4X5 Film Holder.

In the experiment the transmitted light technique was used. The light source consisted of a 10 inch by 10 inch opal glass illuminated by four 150 watt incandescent flood lamps. A schematic diagram of the test setup is shown in Figure 5.3.

The light intensity over the surface area of the opal glass varied less than 0.7 percent as measured by a Honeywell Pentax 1°/21° photometer with a 13/16 inch diameter aperture. The light intensity over the grid area of the test specimen also varied by less than 0.7 percent. Nevertheless, the light intensity at the master grid varied by almost 20 percent, with the peak value at the center of the grid and the lowest values at the corners. These measurements indicated that the optical system of the moiré bench caused light intensity variation similar to that in a vignette. This anomaly in light intensity proved to be beyond the latitude of the Type 57 film. The most satisfactory method found to correct the problem was to filter the light from the opal glass to balance the effect of the optical system. This was done by replacing the actual test sample with another piece of Hysol with no grid printed on it. The master grid was also replaced by a blank ground glass. The image of the

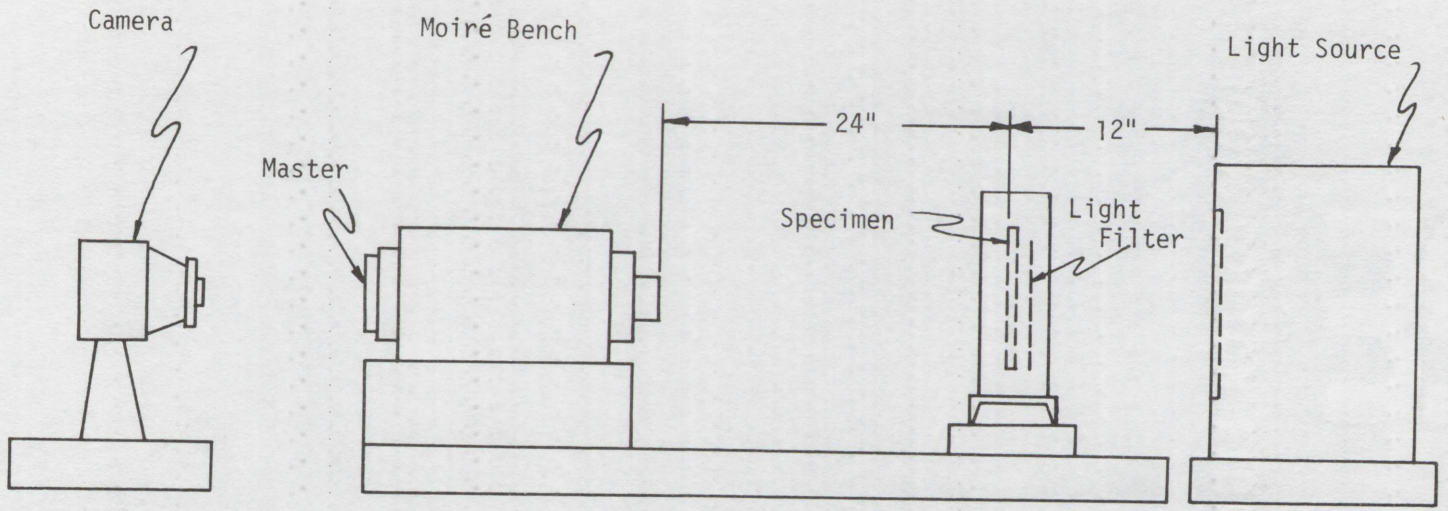

Figure 5.3

Schematic of Simple Shear Test Setup

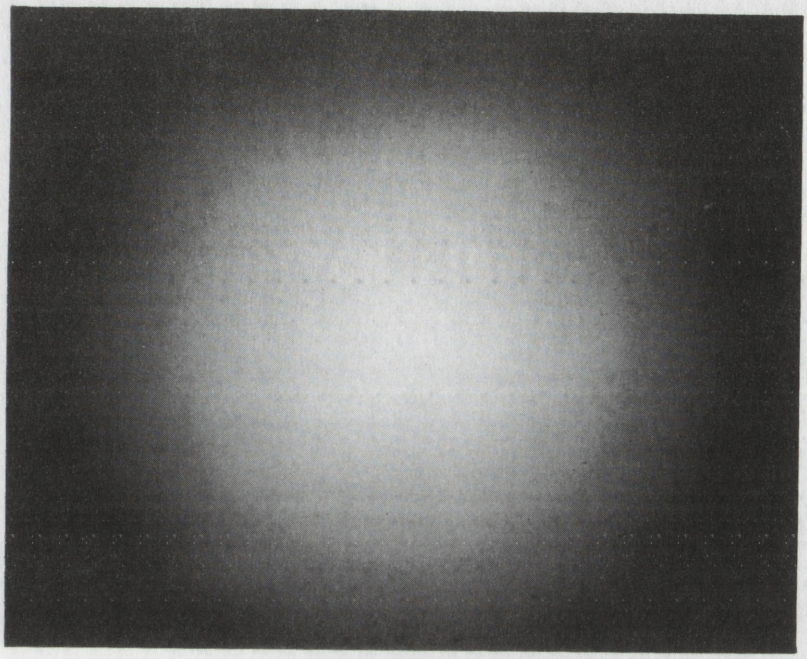

Figure 5.4

Reversed Image of Light Filter

light on the ground glass was then photographed using Polaroid Type 55 Positive/Negative film. The photographic negative obtained was then processed and used as a filter between the light source and test sample. A reversed image of the light filter is shown in Figure 5.4. The improvement obtained by this method is illustrated by comparing Figures 5.5 and 5.6.

5.3.2 Procedure

The simple shear test specimen was securely bolted into the straining frame and an initial or zero deflection was selected and recorded. After an arbitrary pitch mismatch was introduced, the moiré master grating was rotated until the fringes were parallel to the vertical master grating axis. The angular orientation of the

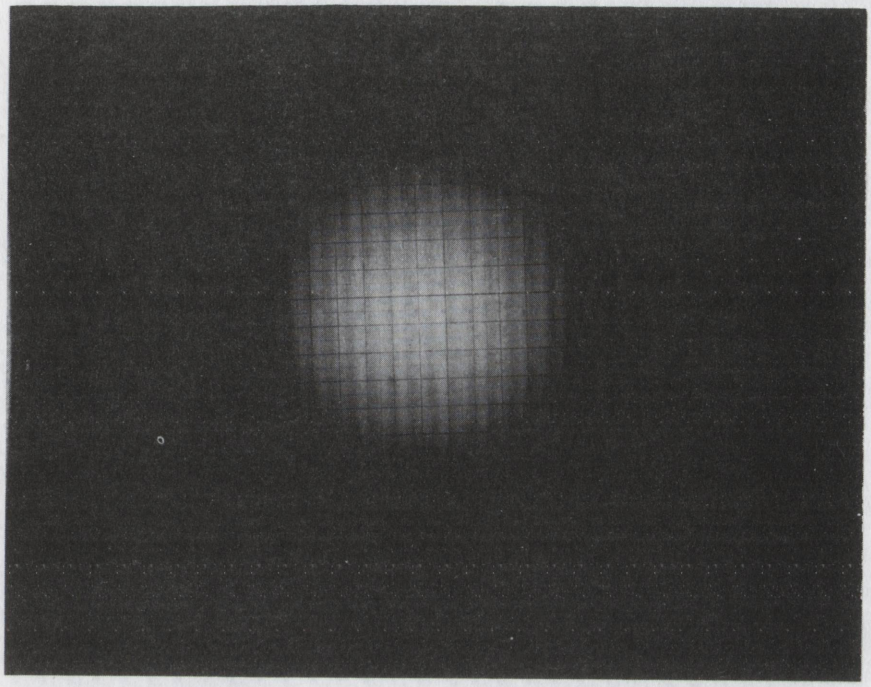

Figure 5.5

Grid Image Obtained Using Uniform Light Source

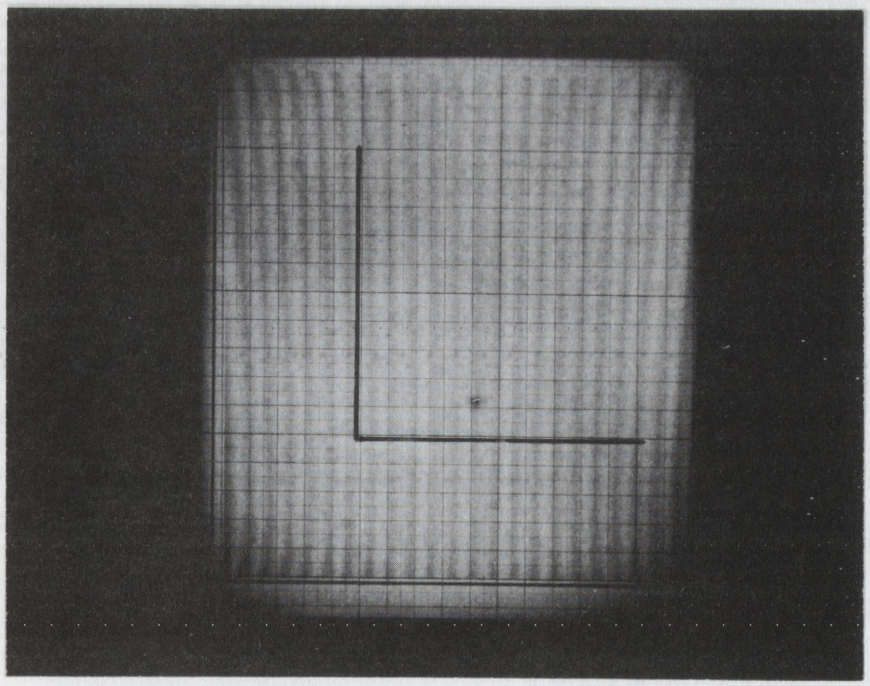

Figure 5.6

Grid Image Obtained Using Filtered Light Source

grating was recorded and the appropriate stop was set on the master mounting mechanism. After the relative sizes of the specimen and master grid pitches were determined by noting the direction of fringe rotation relative to the master rotation, the moiré pattern was photographed. The procedure was repeated after the master grating was rotated to the horizontal position. The mismatch selector was not changed throughout the experiment. The initial fringe photographs are shown in Figures 5.7 and 5.8.

The master grating was returned to the vertical orientation, and the specimen was strained by moving the cross slide 7/32 inch. The fringe rotation relative to the master grating rotation was recorded and the patterns were then photographed with the master oriented in the vertical and horizontal positions. In addition the master grating was rotated slightly from the vertical axis until the moiré fringes again were parallel to the grating axis, and the angle of rotation was recorded. The entire procedure was repeated for cross slide increments of 1/2 inch and 3/4 inch. The fringe patterns for these increments are shown in Figures 5.9 through 5.14. The 3/4-inch increment produced deformation only slightly less than that required to cause buckling and wrinkling of the specimen. The experiment was therefore terminated at the 3/4-inch increment.

5.3.3 Data and Results

Angular and linear measurements were obtained from the photographs using the equipment listed below:

1) Edmund Optical Pocket-Comparator No. 41,055 with Reticle No. 30,585. This is a 6X comparator with a variety of graduations including an angular scale

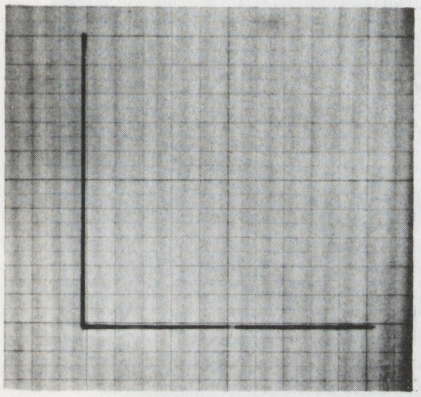

Figure 5.7

Initial Moiré Pattern
Vertical Master Grating
Run No. 71

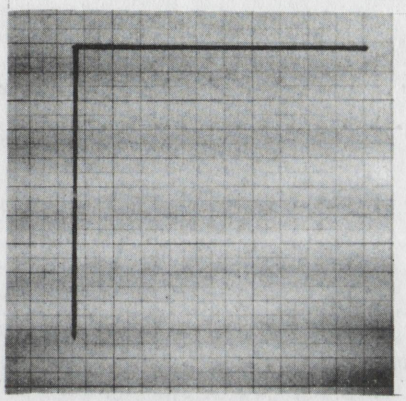

Figure 5.8

Initial Moiré Pattern
Horizontal Master Grating
Run No. 72

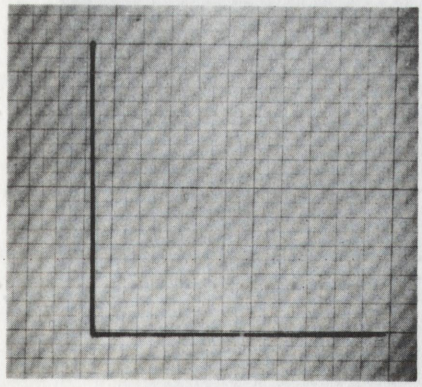

Figure 5.9

First Increment Moiré Pattern
Vertical Master Grating
Run No. 75

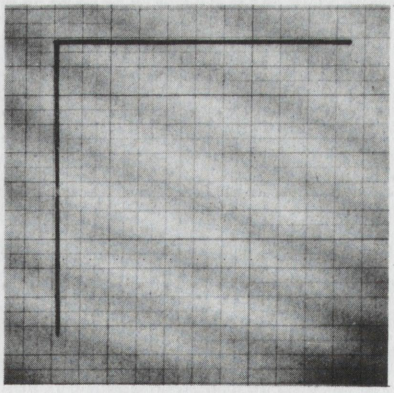

Figure 5.10

First Increment Moiré Pattern
Horizontal Master Grating
Run No. 76

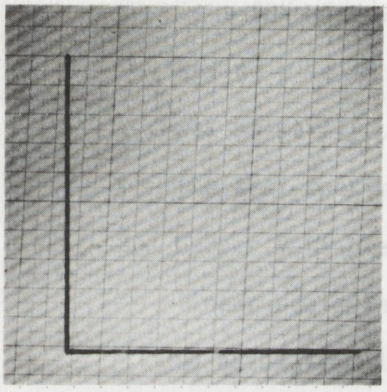

Figure 5.11

Second Increment Moiré Pattern
Vertical Master Grating
Run No. 83

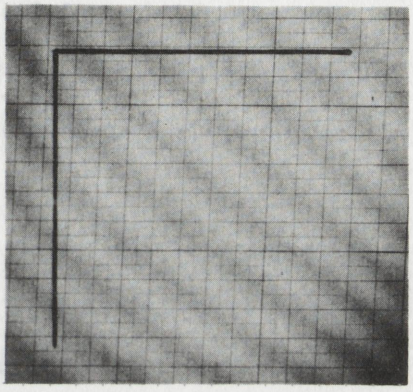

Figure 5.12

Second Increment Moiré Pattern
Horizontal Master Grating
Run No. 84

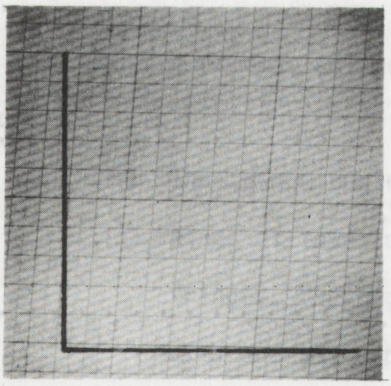

Figure 5.13

Third Increment Moiré Pattern
Vertical Master Grating
Run No. 90

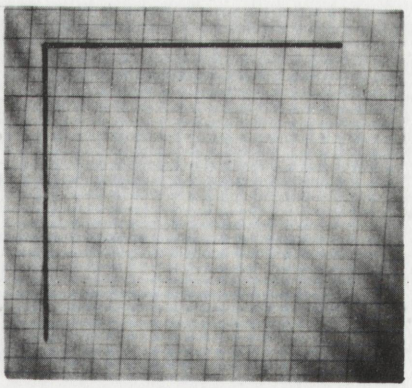

Figure 5.14

Third Increment Moiré Pattern
Horizontal Master Grating
Run No. 91

graduated in degrees and a 1/2-inch linear scale having a least count of 0.005 inch.

2) Edmund Direct Measuring Microscope No. 30,225. This is a 50X microscope with a 1/10-inch linear scale having a least count of 0.001 inch. This instrument was primarily used to determine grid alignment on the test specimen.

3) Gerber Variable Scale No. 400. This is a variable linear scale in which the increments may be adjusted to automatically match the scale of a particular drawing, sketch or photograph.

All angular measurements obtained from the photographs were referenced to the longitudinal axis of the master grating. This axis is the vertical axis in Figure 5.7 and the horizontal axis in Figure 5.8. All linear measurements were referenced to the length of the longitudinal axis.

The sequence of data collection from the photographs was as follows:

1) The fringe angle was sharply defined by applying a piece of tape to the photograph parallel to the fringe. The angle between the master longitudinal axis and the tape was then measured with the optical comparator.

2) The scale of the photograph was determined by measuring the apparent length of the master longitudinal axis and comparing it to the actual length.

3) The fringe pitch was measured by aligning the Gerber Variable Scale perpendicular to the fringes and adjust-

ing it so that each division (or constant multiple of divisions) was precisely aligned with a fringe. The Gerber scale reading, when multiplied by the photograph scale factor, then gave the value of the fringe pitch in inches. This method of measurement, which is very convenient and repeatable for homogeneous patterns, can also be used for nonhomogeneous patterns with some loss of precision since only one pair of scale divisions may then be aligned with the fringes.

A brief study of Figures 5.7 through 5.14 immediately indicates that either a theoretical simple shear deformation was not attained, or there was initial angular misalignment of the specimen grid; or both. If the specimen grids were perfectly aligned with the X- and Y-axes, and if the deformation was actually simple shear, the fringes obtained with the master grating oriented horizontally would remain unchanged as the specimen was deformed. This result was predicted in Example I of Sections 3.3 and 4.2.

Precise direct measurements of the specimen grid indicated that there was initial angular misalignment with the X- and Y-axes. Furthermore, the specimen grid lines were not perpendicular to one another. Due to the procedure used in aligning the master grating and setting the stops on the master mounting mechanism of the optical bench, this meant that the master was not rotated precisely 90 degrees between the vertical and horizontal positions. These variations in initial alignment caused no real difficulty in data reduction since the moiré equations derived in Section 3.2 easily accommodate such cases. Table 5.1 and Figure 5.15 present and illustrate the initial conditions and moiré

Table 5.1

Initial Conditions and Moiré Data
for the Simple Shear Experiment[+]

Increment	Run No.	Θ^* or θ, degrees	Φ^* or ϕ, degrees	Υ^* or υ, degrees	Ψ^* or ψ, degrees	F^* or f, inches	H^* or h, inches
0	71	-0.36*	-0.36*	--	--	0.149*	--
0	72	--	--	0.19*	0.19*	--	0.462*
1	75	-0.36	38.64	--	--	0.124	--
1	76	--	--	0.19	28.19	--	0.445
1	79	1.09	1.09	--	--	0.16	--
2	83	-0.36	60.64	--	--	0.077	--
2	84	--	--	0.19	43.19	--	0.351
2	87	2.89	2.89	--	--	0.155	--
3	90	-0.36	68.64	--	--	.054	--
3	91	--	--	0.19	52.19	--	0.256
3	94	4.39	4.39	--	--	.140	--

[+]During all runs the master pitch was constant, thus $M = N = m = n = 0.005$ inch. In addition, for all runs the specimen grid pitch was less than the master grid pitch. The length of the master grating longitudinal axis was 2.00 inches.

*Initial value.

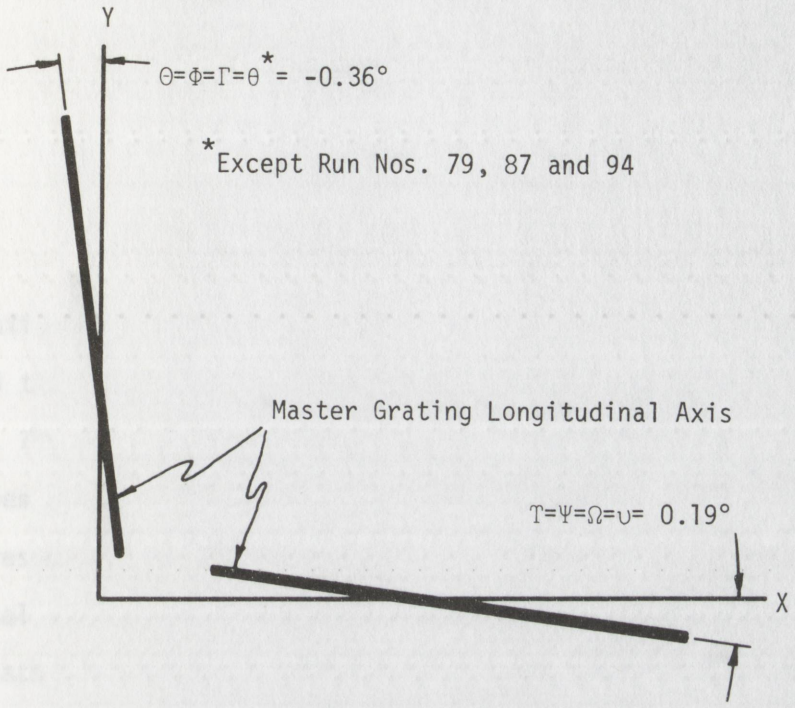

Figure 5.15

Angular Alignment Schematic
for the Simple Shear Experiment

data obtained from the photographs. Angular values for Runs 79, 87 and 94 are derived from direct readings taken from the master mounting mechanism. The nomenclature corresponds exactly to that used in the development of the moiré equations in Section 3.2.

To compute the values for the components of Green's or Cauchy's deformation tensors the quantities s/S, t/T, γ and ω had to be determined. From Section 3.2 and Table 5.1 the applicable equations are:

$$\frac{s}{S} = \frac{f[F + M]}{F[f^2 + M^2 + 2fM\cos(\theta - \phi)]^{\frac{1}{2}}}$$

$$\tan\gamma = \frac{f\sin\theta + M\sin\phi}{f\cos\theta + M\cos\phi} \quad ,$$

and

$$\frac{t}{T} = \frac{h[H + N]}{H[h^2 + N^2 + 2hN\cos(\upsilon - \psi)]^{\frac{1}{2}}}$$

$$\tan\omega = \frac{h\sin\upsilon + N\sin\psi}{h\cos\upsilon + N\cos\psi} \quad . \tag{5.1}$$

Substitution of the values from Table 5.1 into Equations (5.1) results in the values given in Table 5.2. Note that the data from Run Nos. 79, 87 and 94 were not used in these computations; however, the values of the angle γ obtained from these runs agree well with the corresponding calculated angles in Table 5.2. To obtain the experimental values of the components of the deformation tensors, the appropriate quantities from Table 5.2 were substituted into Equations (3.46) and (3.48). The equations were then arranged in matrix form and solved on a high speed digital computer by a standard matrix inversion technique. The resulting deformation tensor component values are given in Tables 5.3 and 5.4 together with principal values computed using Equations (2.17) through (2.21).

The shear experienced by line elements initially aligned with the X- and Y-axes is equal to the angle α. From the definition of shear given in Section 2.1, and from the definitions of γ and ω

$$\alpha = \gamma - \omega \quad . \tag{5.2}$$

Thus from Equation (2.27) if a simple shear deformation was achieved,

$$Q = \tan(\gamma - \omega) \quad . \tag{5.3}$$

Tables 5.5 and 5.6 present the values of the components of Green's and Cauchy's deformation tensors under the assumption that a simple shear deformation was achieved, and Equation (5.3) is valid. The computations were performed using Equations (2.28) through (2.32).

Table 5.2

Specimen Grid Parameters
for the Simple Shear Experiment

Increment	Run Nos.	Γ, degrees	γ, degrees	Ω, degrees	ω, degrees	$\frac{s}{S}$	$\frac{t}{T}$
0	71 & 72	-0.36	--	0.19	--	--	--
1	75 & 71	--	1.05	--	--	1.00185	--
1	76 & 72	--	--	--	0.49	--	1.00088
2	83 & 71	--	2.81	--	--	1.00032	--
2	84 & 72	--	--	--	0.74	--	1.00036
3	90 & 71	--	4.38	--	--	0.99721	--
3	91 & 72	--	--	--	1.06	--	0.99870

Table 5.3

Values of the Components of Green's Deformation Tensor from the Simple Shear Experiment

Increment	C_{XX}	C_{XY}	C_{YY}	C_1	C_2	C_{12}	β_1, degrees
1	1.00384	0.01976	1.00151	1.0225	0.9829	0.0198	43.31
2	1.00215	0.04579	1.00135	1.0475	0.9560	0.0458	44.75
3	0.99811	0.06740	0.99979	1.0668	0.9310	0.0678	45.35

Table 5.4

Values of the Components of Cauchy's Deformation Tensor from the Simple Shear Experiment

Increment	c_{xx}	c_{xy}	c_{yy}	c_1	c_2	c_{12}	β_1, degrees
1	0.99599	-0.01929	0.99895	0.9781	1.0168	-0.0193	-47.19
2	0.99698	-0.04558	1.00255	0.9541	1.0454	-0.0456	-46.75
3	0.99985	-0.06754	1.00969	0.9371	1.0725	-0.0677	-47.08

Table 5.5

Values of the Components of Green's Deformation Tensor from the Simple Shear Experiment, Assuming

$Q = \tan(\gamma - \omega)$

Increment	C_{XX}	C_{XY}	C_{YY}	C_1	C_2	C_{12}	B_1, degrees
1	1.0	0.00978	1.00010	1.0098	0.9902	0.0097	45.14
2	1.0	0.03615	1.00131	1.0368	0.9645	0.0361	45.56
3	1.0	0.05795	1.00336	1.0596	0.9437	0.0580	45.92

Table 5.6

Values of the Components of Cauchy's Deformation Tensor from the Simple Shear Experiment, Assuming

$Q = \tan(\gamma - \omega)$

Increment	c_{xx}	c_{xy}	c_{yy}	c_1	c_2	c_{12}	β_1, degrees
1	1.0	-0.00978	1.00100	0.9902	1.0098	0.0097	-44.86
2	1.0	-0.03615	1.00131	0.9645	1.0368	0.0361	-44.52
3	1.0	-0.05795	1.00336	0.9437	1.0596	0.0580	-44.17

5.4 Experiment on Bending of a Block

5.4.1 Equipment and Experimental Setup

Preliminary experiments on large bending of an unrestrained rectangular beam indicated that a special straining frame was required to prevent non-uniform lateral deformation. That is, the thickness or width of the beam had to be controlled to achieve a good approximation to the theoretical deformation. This was accomplished using the specimens and kinematical straining frame shown in Figures 5.16 and 5.17. The specimens are Hysol, approximately 9 inches long by 1 inch high by 3/8 inch thick. The frame was equipped with aluminum bending templates to control the inside radius of the deformed specimen to two, four or six inches. The aluminum radial arms, to which the steel end blocks of the beam specimen were attached, assured that the Y=constant end planes of the beam became radial planes after deformation. The contoured Plexiglas clamping plates were used to compress the lateral faces of the deformed beam, thus assuring uniform beam thickness.

In Figure 5.16 the upper beam specimen, Model 1, was printed with a nominal 200 line/inch rectangular grid using a Photolastic, Inc. VPM #16-200 glass master as the negative. The lower specimen, Model 2, was printed with a 26.67-line/inch grating in the longitudinal direction using Edmund Moiré Pattern No. 60,534 as the negative. The vertical lines were printed using Edmund Moiré Pattern No. 70,719(2).

5.4.2 Procedure

The beams were put into the straining frame by first screwing the radial arms to the end blocks of the specimen. The specimen and fixture were liberally coated with heavy mineral oil to provide lubrication. The beam was then formed around the aluminum bending template, and the

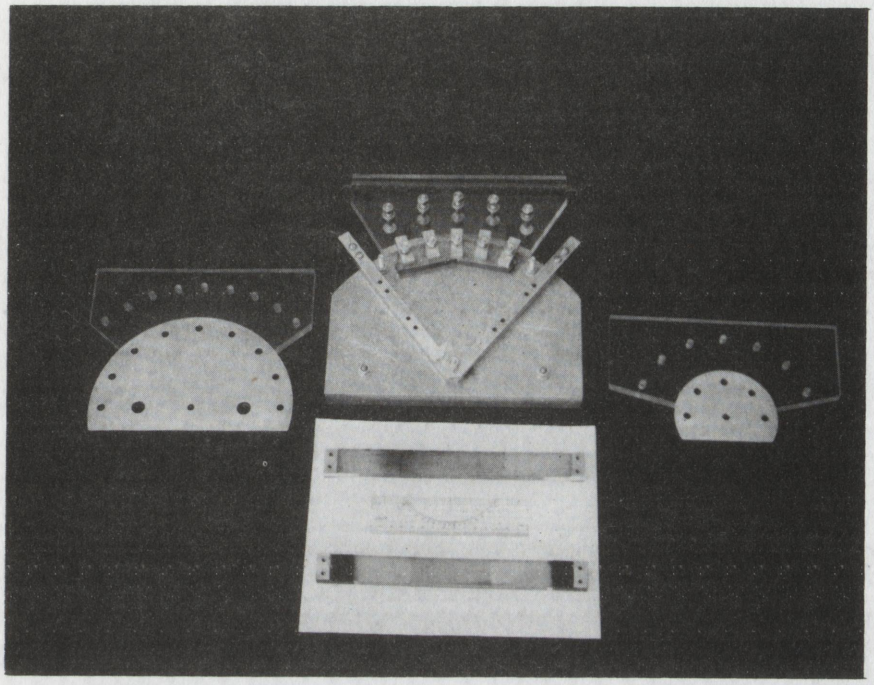

Figure 5.16

Beam Specimens and Straining Frame for Bending of a Block

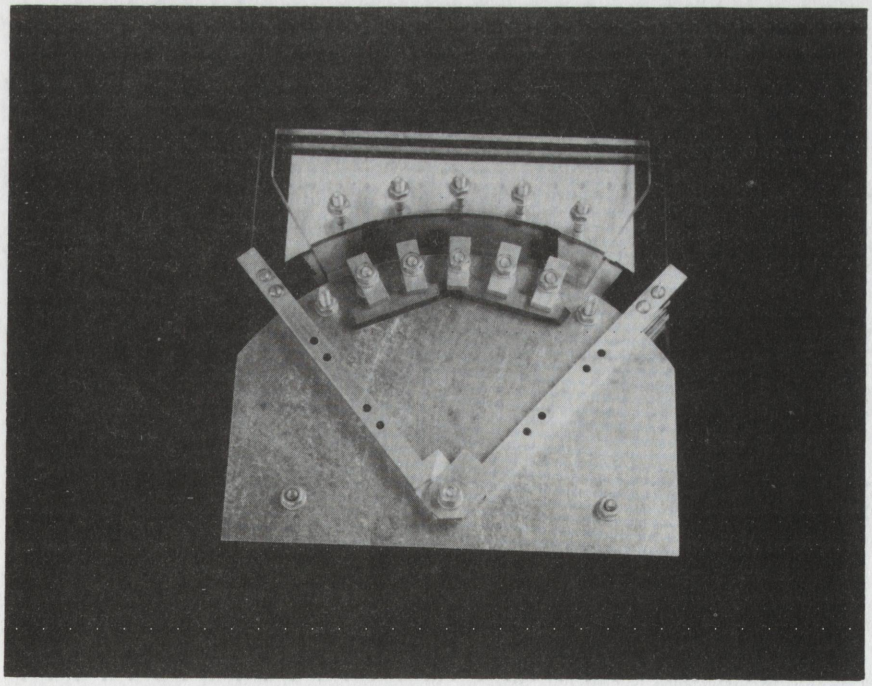

Figure 5.17

Bending Frame and Beam Using Six-Inch Radius Form

pivot bolt of the radial arms was inserted. The lubricated Plexiglas clamping plate was then installed and adjusted until the beam thickness was uniform. Figure 5.17 shows a beam specimen in the straining frame.

The moiré patterns were obtained by placing the master grid directly in contact with the beam specimen grid. Thus the master grid was inserted in the fixture along with the specimen. This was necessary to minimize the parallax effects caused by the 1/2 inch thick Plexiglas base and clamping plate. The master grid used with Model 1 was a film negative of the Photolastic, Inc. VPM #16-200 glass master. The master grid used with Model 2 was a Fresnel figure film transparency, Edmund Moiré Pattern No. 70,719(6).

As in the simple shear experiment, the transmitted light technique was used. However, since the moiré patterns were created directly at the specimen rather than by using the Photolastic, Inc. moiré bench, no lighting uniformity problems were encountered. Photographs of this experiment were obtained using a Linhof Technika camera, equipped with a Kodak Ektar f:4.5, 152 mm lens.

It should be noted that the photographs were not used to record quantitative data since they included unknown parallax effects.

Before placing the models in the straining frame, the height and thickness of the undeformed beams were measured and recorded. The initial moiré fringe spacings were also noted. The models were then strained and the appropriate data were taken. Photographs illustrating the qualitative appearance of the moiré patterns were taken and are shown in Figures 5.18 through 5.21. Note that for Model 1, both moiré patterns appear simultaneously. For Model 2 only the fringes due to the Fresnel figure are shown, since no radial-lined grid of suitable angular pitch and overall size was available to use in con-

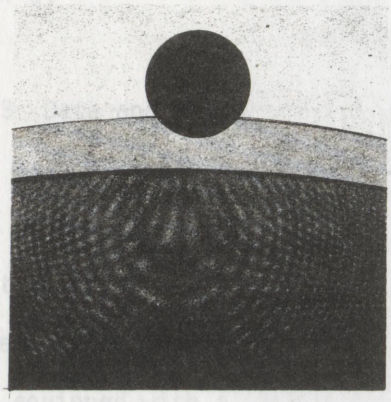

Figure 5.18

Moiré Pattern for Beam
Six-Inch Inside Radius
200 Line/inch Master Grid
Model 1, Run No. 104

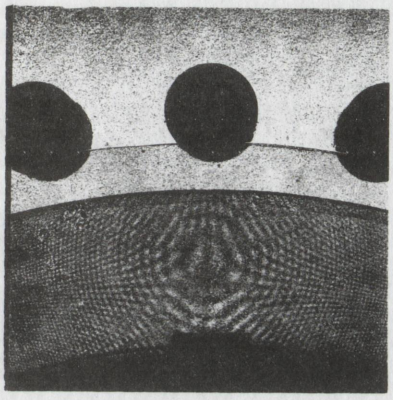

Figure 5.19

Moiré Pattern for Beam
Four-Inch Inside Radius
200 Line/inch Master Grid
Model 1, Run No. 105

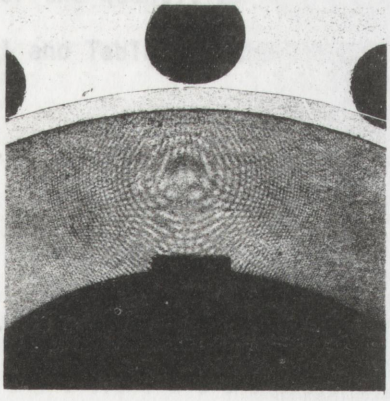

Figure 5.20

Moiré Pattern for Beam
Two-Inch Inside Radius
200 Line/inch Master Grid
Model 1, Run No. 106

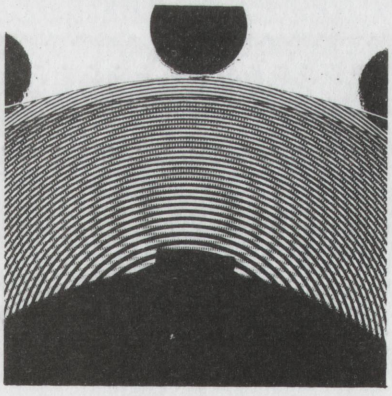

Figure 5.21

Moiré Pattern for Beam
Two-Inch Inside Radius
Fresnel Figure Master Grid
Model 2, Run No. 107

junction with the Fresnel figure master grid. Thus only one principal value of Green's deformation tensor was found for the test involving Model 2.[3]

5.4.3 Data and Results

Fringe dimensions were measured directly through the Plexiglas base of the straining frame using a standard transparent scale with a least count of 0.020 inch. To minimize the effects of parallax and to help determine the centerlines of the fringes, a small sighting tube equipped with a cross-hair was used. The tube was designed to keep the observer's line of sight perpendicular to the surface of the Plexiglas base. Table 5.7 presents the initial conditions and data obtained from the bending tests. The nomenclature and symbols used in the table correspond to those used in Sections 2.3, 3.5.1 and 3.5.2.

To compute the values for the components of Green's deformation tensor the quantities A_δ and C_δ had to be determined. From Sections 3.5.1 and Table 5.7 the applicable equations for Model 1 are

$$S = \frac{FM}{F + M} \quad , S < M$$

$$T = \frac{HN}{H + N} \quad , T < N$$

$$A_\delta = A_\delta(x_d) = \frac{x_d M}{S}$$

$$A_\delta = A_\delta(R_p) = \frac{R_p^2 - R_{p+q}^2}{2qS}$$

$$C_\delta = \frac{\arctan\left(\frac{y}{x}\right)}{T\left(\frac{y}{N} - p\right)} \quad . \qquad (5.4)$$

[3]See Section 5.5 for an example of the use of a radial-lined grid.

Table 5.7

Initial Conditions[+] and Moiré Data for the Block Bending Experiment

Run No.	Model No.	r_1, inch	r_2, inch	x_d, inch	R_{p-3}, inch	R_{p-8}, inch	x	y	p	c
104	1	5.97	7.01	6.67	0.400	0.702	6.675	0.290	2	-
105	1	4.00	5.03	4.60	0.335	0.585	4.750	0.370	5	-
106	1	1.975	3.03	2.63	0.245	0.440	2.675	0.340	6	-
107	2	1.975	3.07	2.37	0.540	0.950	--	--	-	1.5

[+]For tests involving Model 1, the master pitch was M = N = m = n = 0.005 inch. The initial fringe pitches were F = 0.70 inch, S < M, and H = 2.00 inch, T < N. The height of the beam for both models was $2X_0$ = 1.015 inches. The value of A_m for the Fresnel figure master grid used with Model 2 was 0.0756 in^2. The initial specimen pitch for Model 2 was 0.0375 inch.

Similarly from Section 3.5.2 for Model 2

$$A_\delta = A_\delta(x_d) = \frac{x_d A_m}{2S(x_d - c)}$$

$$A_\delta = A_\delta(R_p) = \frac{A_m(R^2_{p+q} - R^2_p)}{2S(R^2_{p+q} - R^2_p - qA_m)} \quad . \tag{5.5}$$

Another method for computing A_δ is given by Equation (2.36) as

$$A_\delta = A_\delta(r_i) = \frac{r_2^2 - r_1^2}{4X_0} \quad . \tag{2.36}$$

The various values of A_δ and C_δ were computed using the input from Table 5.7 and are given in Table 5.8. From Section 2.3, the principal values of Green's deformation tensor are

$$C_1 = \frac{A_\delta^2}{r^2}$$

$$C_2 = C_\delta^2 r^2 \quad . \tag{2.41}$$

Table 5.9 presents the principal values calculated at the radial positions r_1 and r_2.

Table 5.8

Specimen Grid Parameters for the Block Bending Experiment

Run No.	Model No.	r_1, inch	r_2, inch	$A_\delta(x_d)$, inch	$A_\delta(R_p)$, inch	$A_\delta(r_i)$, inch	C_δ, rad./inch
104	1	5.97	7.01	6.72	6.71	6.68	0.156
105	1	4.00	5.03	4.63	4.65	4.58	0.227
106	1	1.975	3.03	2.65	2.69	2.60	0.410
107	2	1.975	3.07	2.74	2.65	2.72	--

Table 5.9

Principal Values of Green's Deformation Tensor from the Block Bending Experiment

Run No.	Model No.	Value at r_1		Value at r_2	
		C_1	C_2	C_1	C_2
	Values of C_1 Computed Using $A_s(x_d)$				
104	1	1.266	0.869	0.918	1.199
105	1	1.340	0.825	0.846	1.309
106	1	1.802	0.656	0.765	1.542
107	2	1.920	--	0.796	--
	Values of C_1 Computed Using $A_s(R_p)$				
104	1	1.263	0.869	0.917	1.199
105	1	1.350	0.825	0.855	1.309
106	1	1.857	0.656	0.787	1.542
107	2	1.800	--	0.765	--
	Values of C_1 Computed Using $A_s(r_i)$				
104	1	1.250	0.869	0.906	1.199
105	1	1.311	0.825	0.829	1.309
106	1	1.732	0.656	0.736	1.542
107	2	1.897	--	0.784	--

5.5 Experiments on Bending of an Initially Curved Cuboid

5.5.1 Equipment and Experimental Setup

No straining frame was used in this experiment since the Hysol model itself was used to provide the forces required to bend the initially curved cuboid. Figures 5.22 and 5.23 show the model before and after deformation. No restraint in the direction of the thickness was used during the test.

In the figures, the upper half of the specimen grid was printed using a negative of a Fresnel figure, Edmund Moiré Pattern No. 70,719(6). The lower half of the grid was printed with a radial-line grid, Edmund Moiré Pattern No. 70,719(4).

The transmitted light technique was used, and data were recorded using the Linhof Technika camera previously described in the block bending experiment.

5.5.2 Procedure

A 3.53 inch diameter disc was cut from a 3/8 inch thick sheet of Hysol CP-4485. After the specimen grids were printed, a 1.51 inch diameter hole was drilled through the center of the disc and a 60 degree circular ring sector was machined out and discarded. The undeformed specimen was then checked against the master grids to assure that there was no discernible initial deformation. The master grids used for the experiment were a Fresnel figure, Edmund Moiré Pattern No. 70,719(6), and a radial-line grid, Edmund Moiré Pattern No. 70,719(4).

The specimen was then deformed by bonding the two free radial planes together using ordinary contact cement. The overall dimensions were recorded and photographs of the moiré patterns were taken as shown in Figures 5.24 and 5.25. The master grids were held in intimate con-

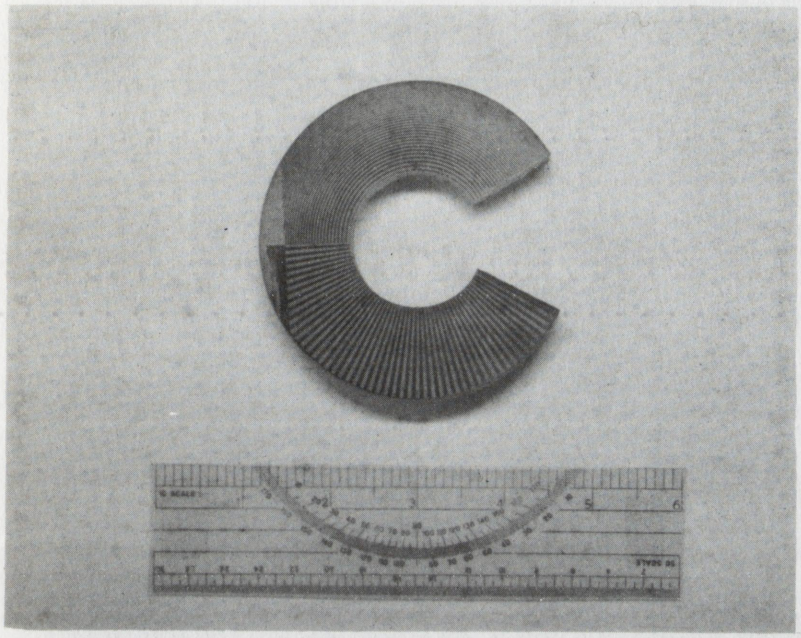

Figure 5.22
Initially Curved Cuboid Before Deformation

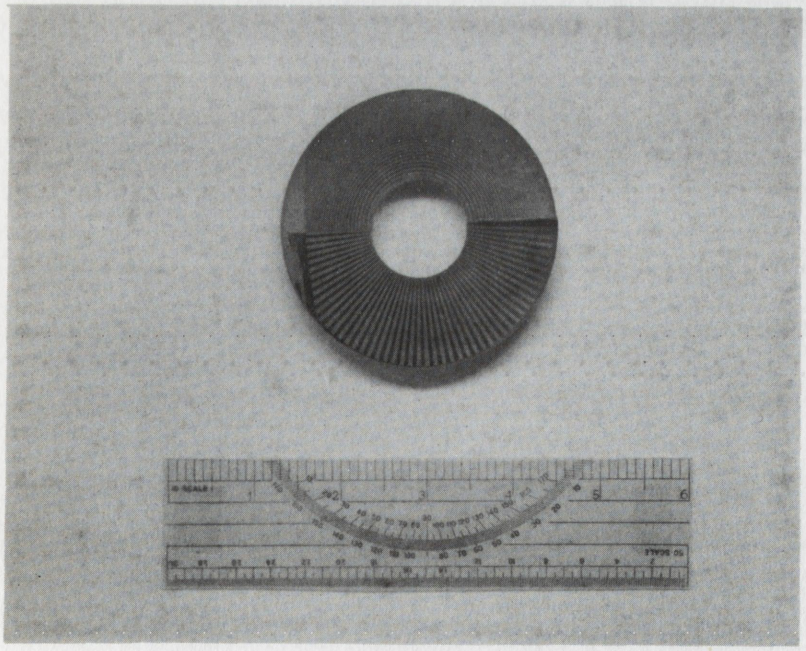

Figure 5.23
Initially Curved Cuboid After Deformation

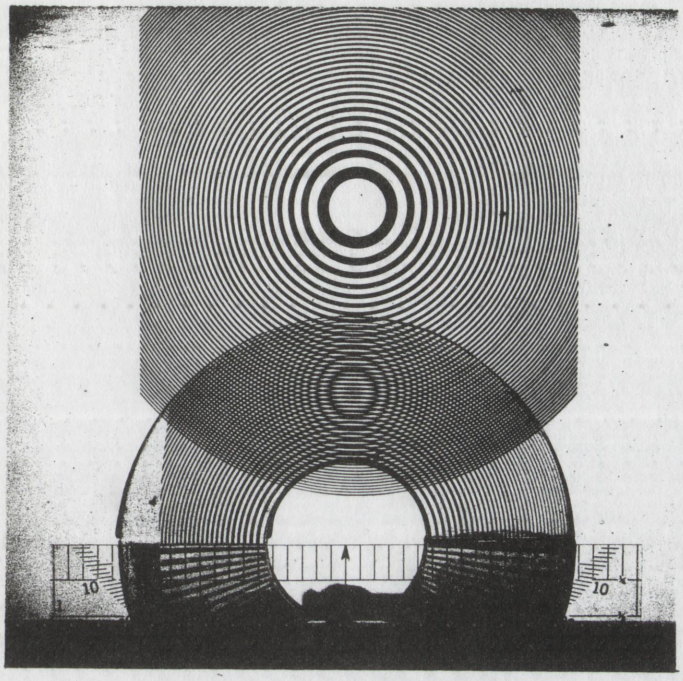

Figure 5.24

Moiré Pattern for Bending of Initially Curved Cuboid
with Fresnel Figure Master Grid, Run No. 113

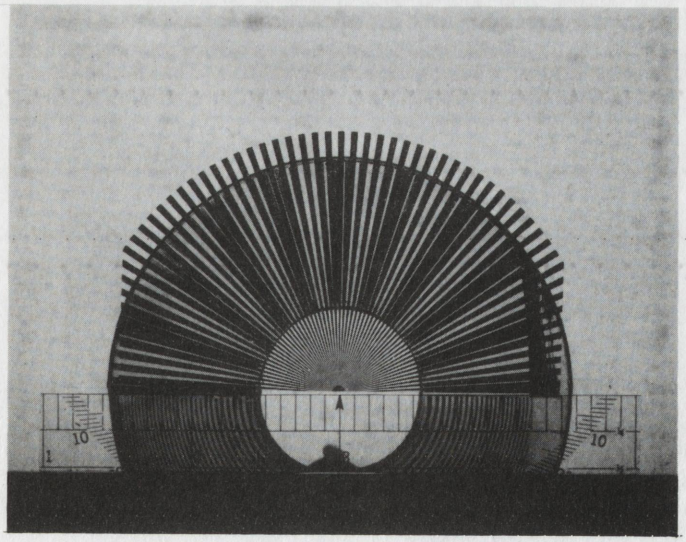

Figure 5.25

Moiré Pattern for Bending of Initially Curved Cuboid
with Radial-Line Master Grid, Run No. 114

tact with the specimen by coating it with heavy mineral oil and carefully applying each master so that no air bubbles were trapped in the interface.

5.5.3 Data and Results

Fringe dimensions were read from the photographs using the Gerber scale previously described in the simple shear experiment. Angular measurements were made with a protractor having a least count of 1/2 degree. Overall dimensions and moiré data are presented in Tables 5.10 and 5.11. The nomenclature and symbols used in the tables correspond with those in Sections 2.4 and 3.5.4.

To compute the values for the components of Cauchy's deformation tensor, the quantities A_δ, B_δ and C_δ had to be determined. From Section 3.5.4 and Tables 5.10 and 5.11, the applicable equations are

$$A_\delta = A_\delta(x_d) = \frac{-x_d}{x_d - c}$$

$$A_\delta = A_\delta(R_p) = \frac{-R^2_{p+q} + R^2_p}{R^2_{p+q} - R^2_p - qA_m}$$

$$K = \frac{R_1^2}{A_m}$$

$$J = \frac{(r_1 - c)^2}{A_m}$$

$$P = J + K$$

$$B_\delta = B_\delta(R_p) = R^2_p(A_\delta + 1) + A_\delta\left(\frac{c^2}{A_\delta + 1} - A_m P\right)$$

$$C_\delta = C_\delta(\Delta\phi) = \frac{\Delta\phi}{\Delta\phi - \Delta\Theta} \quad . \tag{5.6}$$

Table 5.10

Overall Dimensions of Initially Curved Cuboid

R_1, inch	R_2, inch	Θ_0, degree	r_1, inch	r_2, inch	θ_0, degree
0.755	1.765	150	0.55	1.565	180

Table 5.11

Moiré Data for Initially Curved Cuboid Experiment[+]

Run No.	x_d, inch	c inch	R_{p+3}, inch	R_{p+8}, inch	R_p,* inch	$\Delta\phi$, degree
113	1.04	2.25	0.31	0.520	0.488	--
114	--	0	--	--	--	18.25

[+]For the Fresnel figure master grid $A_M = 0.0756$ in^2; $B_M = 0$. For the radial master grid, $\Delta\Theta = 3$ degrees. The initial specimen grid values were identical to the master grid.

*R_p is the radius of the fringe intersecting the inside radius of the cuboid at the point $x = r_1$, $y = 0$. In this particular case the fringe was dark, thus it is a half-order fringe.

The values of A_δ, B_δ, and C_δ may also be found from Equations (2.46). That is

$$A_\delta = A_\delta(r_i) = \frac{r_2^2 - r_1^2}{R_2^2 - R_1^2}$$

$$B_\delta = B_\delta(r_i) = \frac{R_2^2 r_1^2 - R_1^2 r_2^2}{R_2^2 - R_1^2}$$

$$C_\delta = C_\delta(\theta_0) = \frac{\theta_0}{\Theta_0} \quad . \tag{2.46}$$

The values of the parameters noted in the equations above are presented in Table 5.12. The principal values of Cauchy's deformation tensor at the inside and outside radii were found using Equations (2.47) and are presented in Table 5.13.

Table 5.12

Specimen Grid Parameters for the Initially Curved Cuboid Experiment

Run No.	$A_\delta(x_d)$	$A_\delta(R_p)$	$A_\delta(r_i)$	$B_\delta(R_p)$	$B_\delta(r_i)$	$C_\delta(\Delta\phi)$	$C_\delta(\theta_0)$
113	0.860	0.857	0.843	-0.176	-0.178	--	--
114	--	--	--	--	--	1.195	1.200

Table 5.13

Principal Values of Cauchy's Deformation Tensor
from the Initially Curved Cuboid Experiment

Values of c_1 and c_2 computed using $A_\delta(x_d)$, $B_\delta(R_p)$ and $C_\delta(\Delta\phi)$

Values at r_1		Values at r_2	
c_1	c_2	c_1	c_2
0.735	1.540	1.085	1.042

Values of c_1 and c_2 computed using $A_\delta(R_p)$, $B_\delta(R_p)$ and $C_\delta(\Delta\phi)$

Values at r_1		Values at r_2	
c_1	c_2	c_1	c_2
0.738	1.545	1.089	1.047

Values of c_1 and c_2 computed using $A_\delta(r_i)$, $B_\delta(r_i)$ and $C_\delta(\Theta_0)$

Values at r_1		Values at r_2	
c_1	c_2	c_1	c_2
0.747	1.572	1.106	1.060

5.6 Experiment on Extension of a Plane Tapered Tensile Specimen

5.6.1 Equipment and Experimental Setup

A plane tapered tensile specimen was machined from a 0.215-inch thick piece of Hysol CP-4485 as shown in Figure 5.26. The overall length of the specimen was 6.84 inches. The width tapered from 3.34 inches at the large end down to 2.07 inches at the narrow end, resulting in an included angle of taper of 10.64 degrees. The moiré and registration grids were printed before machining the specimen, using the same master and negative used for the simple shear specimen. Each major registration grid division on the specimen was 0.997 inches.

The specimen was deformed by placing it in the straining frame shown in Figure 5.27. A standard transparent scale was located next to the model for reference purposes. The grips of the straining frame overlapped the specimen by 3/4 inch at each end.

The transmitted light technique was used and data were recorded using the Linhof Technika camera previously described in the cuboid bending experiment.

The master grating used was a film transparency of a 200 line-per-inch Photolastic, Inc. VPM=16-200 parallel-lined glass master.

5.6.2 Procedure

The master grating transparency was checked against the glass master to assure that the pitch was the same. The specimen was coated with heavy mineral oil to provide intimate contact with the master grating, and the initial uniform fringe spacings were observed and recorded for the unloaded specimen. After securing the sample in the straining frame, the distance between the grips was extended 1/2 inch. The resulting moiré patterns are shown in Figures 5.28 and 5.29.

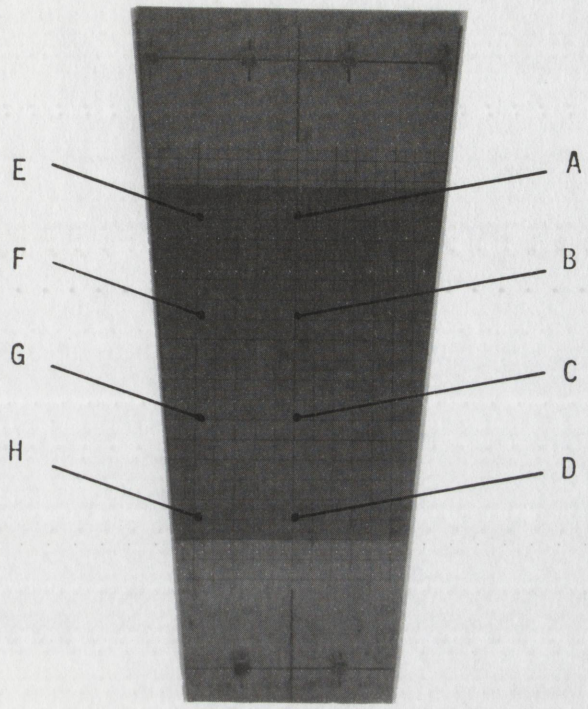

Figure 5.26
Plane Tapered Tensile Specimen

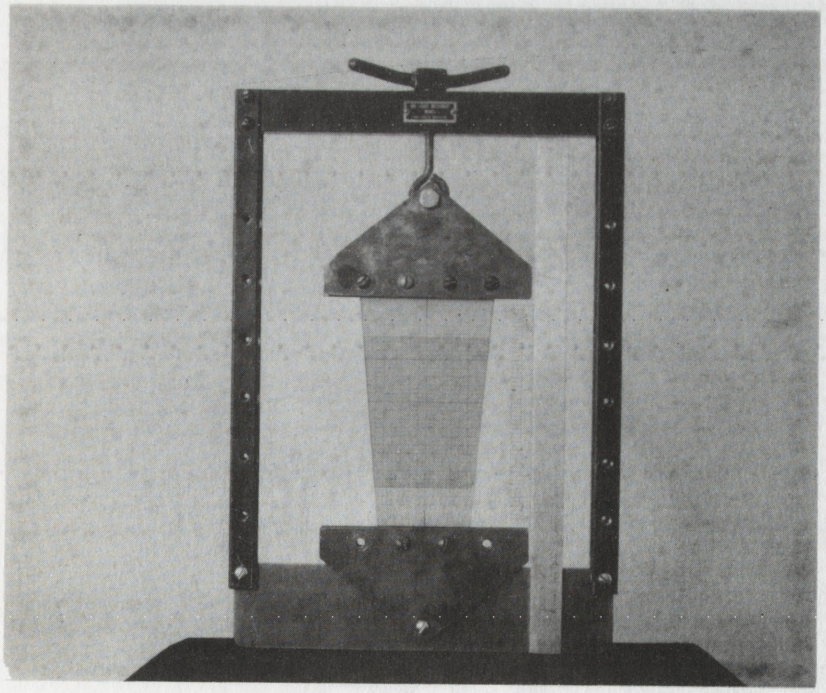

Figure 5.27
Straining Frame and Plane Tapered Tensile Specimen

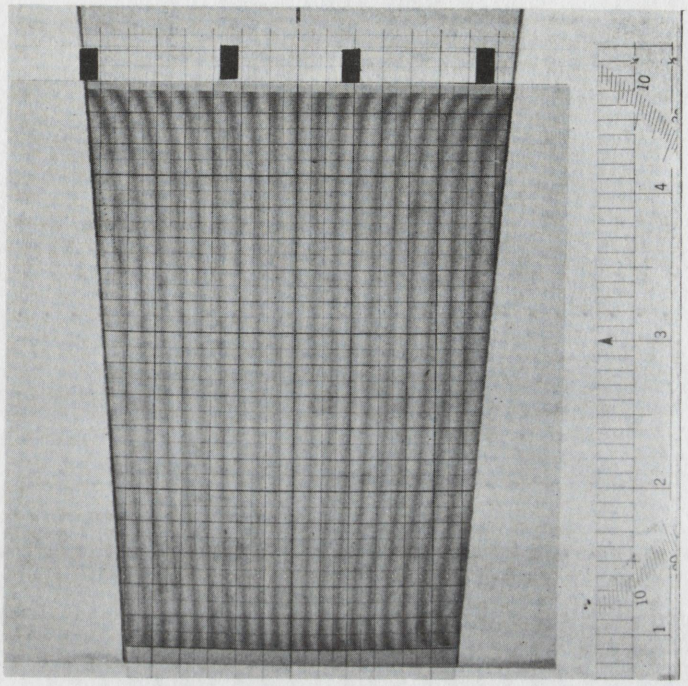

Figure 5.28

Moiré Pattern for Extension of Plane Tapered Specimen
Vertical Master Grating, Run No. 111

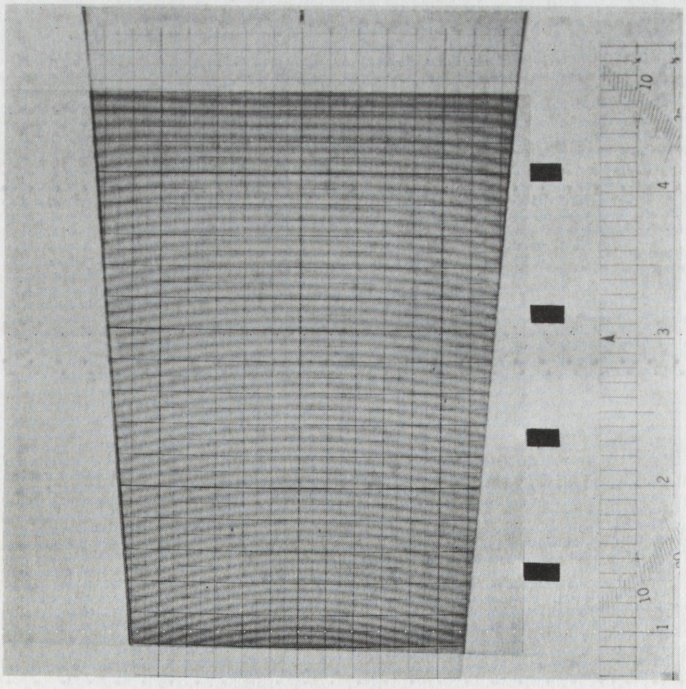

Figure 5.29

Moiré Pattern for Extension of Plane Tapered Specimen
Horizontal Master Grating, Run No. 112

5.6.3 Data and Results

Fringe dimensions were read from the photographs using the Gerber scale and Edmund optical comparator previously described in the simple shear experiment. All dimensions were referenced to the scales in the photographs. Fringe angles were determined by measuring the angle of a straightedge laid tangent to fringes, and also by using a mirror oriented perpendicular to the fringes. The mirror was aligned so that the fringe and its reflection formed an apparently smooth curve with no discontinuity of slope at the reflecting surface. All angular measurements were referenced to the center line of the specimen. The least count of the protractor used for the angular measurements was one degree.

Eight points on the specimen were selected for data reduction. These are denoted by the letters A through H and are located as shown in Figure 5.26. The initial conditions and moiré data are presented in Table 5.14. The nomenclature corresponds to that used in the development of the moiré equations in Section 3.2. To compute the values of the components of Green's deformation tensor, the quantities s/S, t/T, γ and ω had to be determined. From Section 3.2 and Table 5.14 the applicable equations are:

$$\frac{s}{S} = \frac{f[F + M]}{F[f^2 + M^2 + 2fM\cos\phi]^{\frac{1}{2}}}$$

$$\tan\gamma = \frac{M\sin\phi}{f + M\cos\phi}$$

$$\frac{t}{T} = \frac{h[H + N]}{H[h^2 + N^2 - 2hN\cos\psi]^{\frac{1}{2}}}$$

$$\tan\omega = \frac{M\sin\psi}{h - N\cos\psi} \quad . \tag{5.7}$$

Table 5.14

Initial Conditions[+] and Moire Data for the Plane Tapered Specimen Experiment

Position	ϕ, degree	ψ, degree	f, inch s<m	h, inch t>n
A	0	0	0.1428	0.0810
B	0	0	0.1318	0.0755
C	0	0	0.1240	0.0710
D	0	0	0.1086	0.0600
E	-4.8	-1.0	0.1428	0.0847
F	-3.2	-8.0	0.1339	0.0790
G	-3.8	-13.0	0.1240	0.0745
H	-5.0	-18.0	0.1150	0.0645

[+]During all runs the master pitch was constant, thus M = N = m = n = 0.005 inch. The masters were aligned so that $\Theta = \theta = 0$, $\Upsilon = \upsilon = 0$. The initial fringe pitches were F = 1.4 inch, S < M, and H = 1.1 inch, T < N. Initial fringe angles were zero.

Table 5.15 presents the values of the specimen grid parameters described by Equations (5.7). The components and principal values of Green's deformation tensor were computed using Equations (3.47), and are presented in Table 5.16 and Figures 5.30 and 5.31. It should be noted that there is sufficient moiré data in Tables 5.14 and 5.15 to calculate Cauchy's deformation tensor if desired.

Table 5.15

Specimen Grid Parameters for the
Plane Tapered Specimen Experiment

Position	γ, degrees	ω, degrees	$\frac{s}{S}$	$\frac{t}{T}$
A	0	0	0.96962	1.07064
B	0	0	0.96689	1.07579
C	0	0	0.96467	1.08065
D	0	0	0.95940	1.09587
E	-0.162	-0.063	0.96975	1.06757
F	-0.115	-0.557	0.96751	1.07200
G	-0.146	-0.925	0.96475	1.07466
H	-0.208	-1.483	0.96192	1.08423

Table 5.16

Values of the Components of Green's Deformation Tensor
from the Plane Tapered Specimen Experiment

Position	C_{XX}	C_{XY}	C_{YY}	C_1	C_2	C_{12}	B_1, degrees
A	0.94016	0	1.14627	1.14627	0.94016	0.10305	90
B	0.93488	0	1.15733	1.15733	0.93488	0.11123	90
C	0.93059	0	1.16781	1.16781	0.93059	0.11861	90
D	0.92045	0	1.20094	1.20094	0.92045	0.14024	90
E	0.94042	-0.00179	1.13971	1.13973	0.94041	0.09966	-89.48
F	0.93614	0.00800	1.15000	1.15100	0.93585	0.10670	87.88
G	0.93091	0.01410	1.15509	1.15597	0.93003	0.11297	86.42
H	0.92575	0.02322	1.17614	1.17829	0.92361	0.12734	84.73

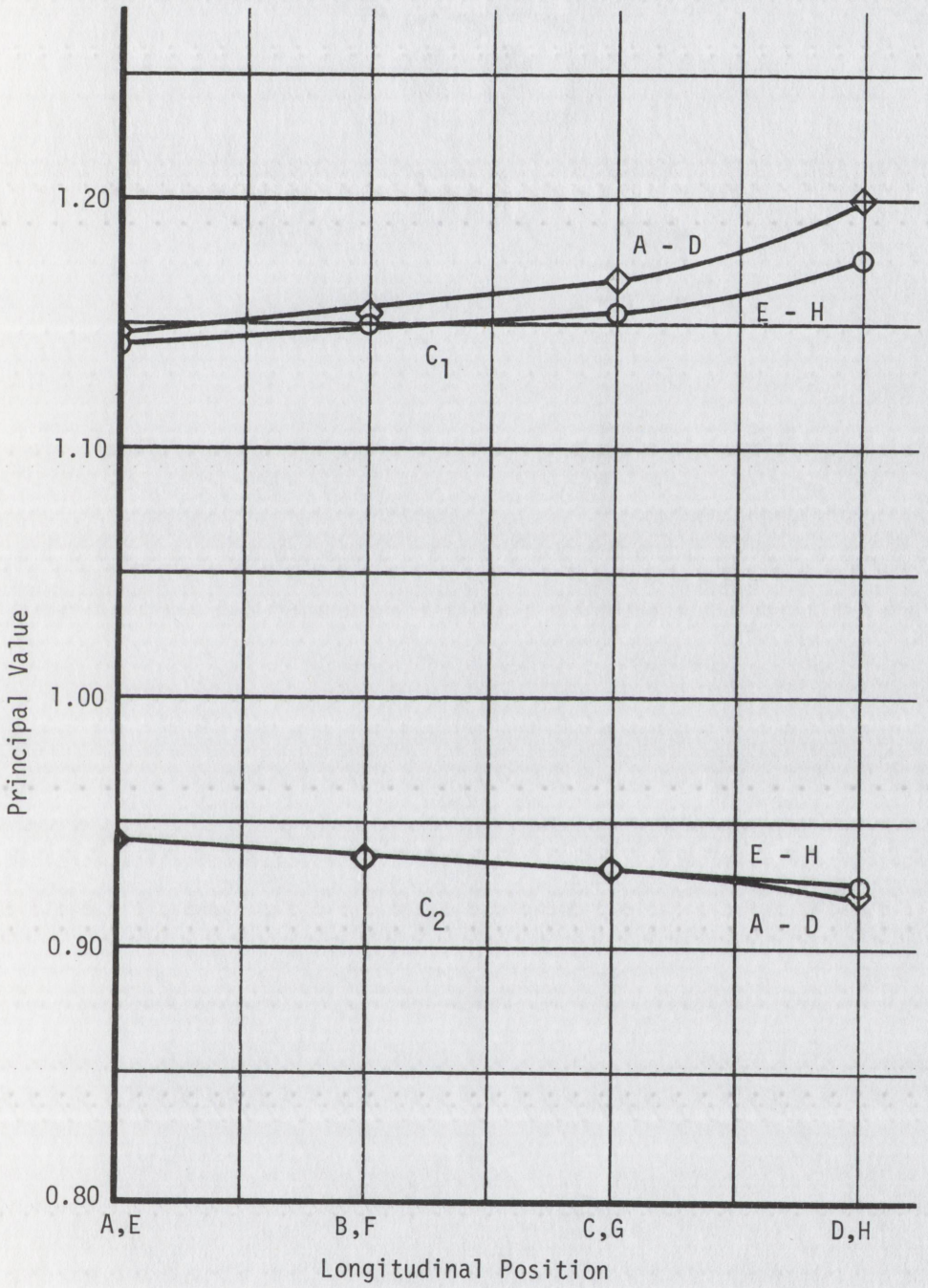

Figure 5.30

Principal Values of Green's Deformation Tensor
for the Plane Tapered Tensile Specimen

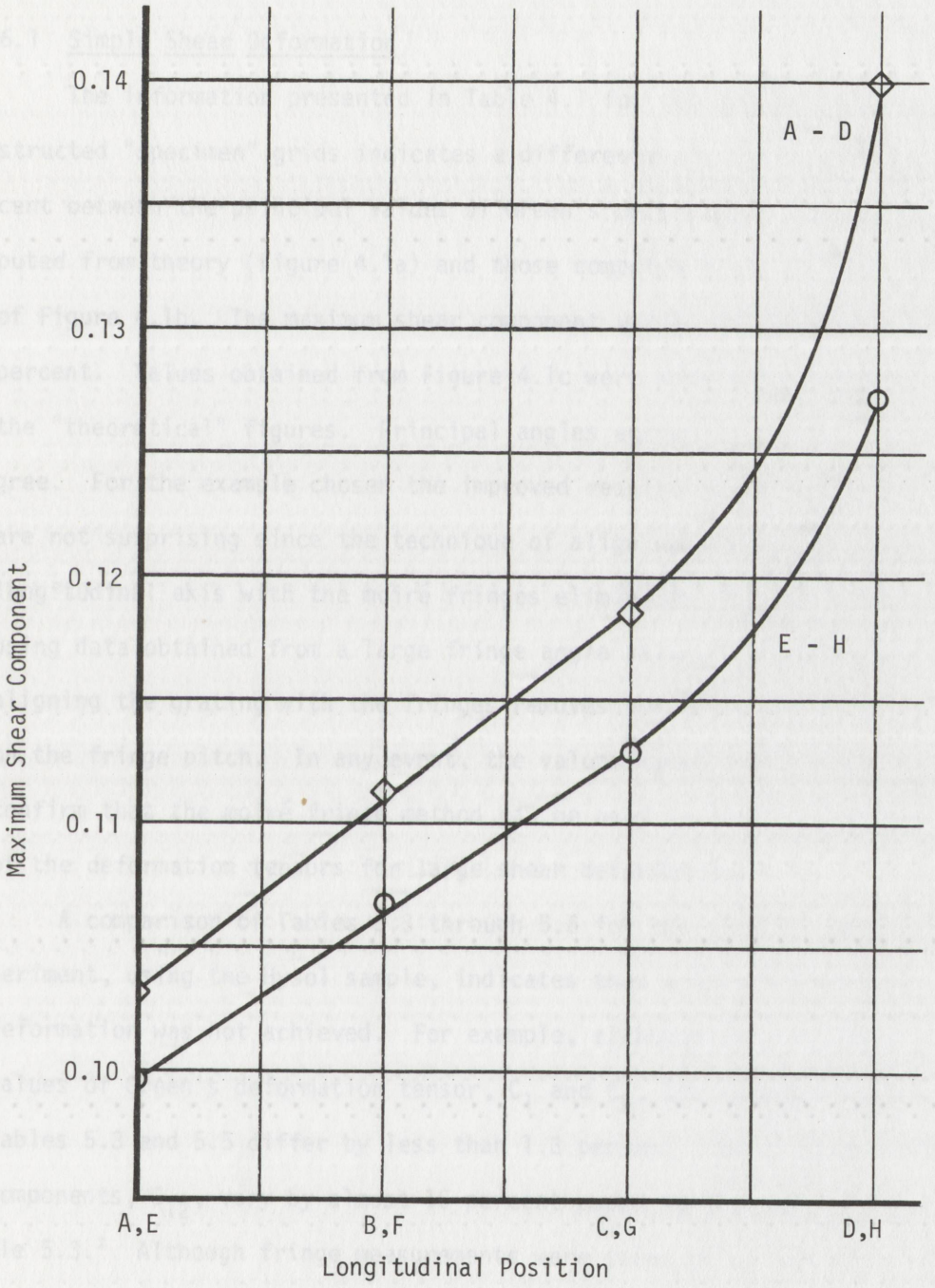

Figure 5.31

Maximum Shear Component of Green's Deformation Tensor
for the Plane Tapered Tensile Specimen

6. DISCUSSION OF RESULTS

6.1 Simple Shear Deformation

The information presented in Table 4.1 for the geometrically constructed "specimen" grids indicates a difference of less than 0.8 percent between the principal values of Green's deformation tensor computed from theory (Figure 4.1a) and those computed from the moiré data of Figure 4.1b. The maximum shear component varies by less than 1.5 percent. Values obtained from Figure 4.1c were within 0.2 percent of the "theoretical" figures. Principal angles agreed to within 0.3 degree. For the example chosen the improved results from Figure 4.1c are not surprising since the technique of aligning the master grating longitudinal axis with the moiré fringes eliminates the necessity of using data obtained from a large fringe angle value.[1] Furthermore, aligning the grating with the fringes removes the effect of rotation on the fringe pitch. In any event, the values agree well enough to confirm that the moiré fringe method can be used to find the components of the deformation tensors for large shear deformations.

A comparison of Tables 5.3 through 5.6 for the simple shear experiment, using the Hysol sample, indicates that a true simple shear deformation was not achieved. For example, although the principal values of Green's deformation tensor, C_1 and C_2, for Increment 3 in Tables 5.3 and 5.5 differ by less than 1.3 percent, the maximum shear components, C_{12}, vary by almost 15 percent based on the value in Table 5.3.[2] Although fringe measurements were taken using the previously

---

[1] At high fringe angles, the ratio ϕ/γ becomes quite small, thus affecting the precision of the measurement of γ.

[2] Furthermore, the fringes in Figures 5.9 through 5.14 show some small amount of curvature indicating a departure from a truly homogeneous deformation .

noted technique of aligning the master grid longitudinal axis with the fringe angle, these data were not used in any of the computations for two reasons. First, the least count of the angular scale on the master grating mounting mechanism of the Photolastic, Inc. Moiré Bench was 1 degree. It was felt that this was not precise enough compared to the maximum shear of approximately 4 degrees. Secondly, the values of the moiré fringe angles obtained with the master grating oriented vertically and horizontally were not excessively high, and thus provided no real data reduction problems.

Based on the discussion above, it is felt that the data given in Tables 5.3 and 5.4 reflect the actual state of strain in the specimen; whereas the data in Tables 5.5 and 5.6 are in error due to the assumption that $Q = \tan(\gamma - \omega)$ which implies that a simple shear deformation was achieved.

6.2 Bending of a Block

Tables 4.2 and 4.3 for the geometrically constructed "specimen" grids indicate a maximum variation of less than 4 percent among the values of C_1, and less than 2 percent for the values of C_2. In Table 4.2 the value of C_{12} varies by about 5-1/2 percent based on the "theoretical" or constructed value. Considering the coarseness of the grids used, this is probably not an excessive variation. The fringe patterns of Figures 4.2 and 4.3 qualitatively confirm the moiré analyses which predict the Fresnel figure fringe geometries.

The results of the actual block bending experiments presented in Table 5.9 indicate that the maximum variation in the values of C_1 computed by three different methods is about 8 percent. The values of C_2 were all obtained from identical measurements and thus provide no basis

for a comparison. The differences between the various values of C_1 indicate that a pure bending deformation was probably not attained. This can also be qualitatively inferred from the photographs presented in Figures 5.18 through 5.21 in which the fringes show slight deviations from perfect circles. This is particularly true of Run No. 107. Figure 5.21, in which relatively coarse specimen and master grids were used. It should also be noted that the equations predicting the moiré response were based on an isochoric deformation. With the materials and test fixtures used, there is no guarantee that this condition was attained. Nevertheless, the experiments show substantial agreement with theoretically predicted results.

6.3 Bending of an Initially Curved Cuboid

For this experiment, the principal values of Cauchy's deformation tensor given in Table 5.13 differ by less than 2-1/4 percent, despite the fact that the thickness of the specimen was not controlled or restrained during the experiment. The theoretical moiré pattern predictions were based on the assumption of uniform thickness after deformation. Since relatively coarse grids were used in the experiment, the error caused by this secondary effect may well be less than the data reduction error.

6.4 Plane Tapered Tensile Specimen

The results of this experiment, given in Table 5.16, and Figures 5.30 and 5.31, can only be qualitatively examined since no theoretical analysis is known to exist. A first order approximation would suggest that the principal values and maximum shear component should vary approximately linearly with longitudinal position on the specimen. The plotted data substantiate this except near the narrow end of the spec-

imen where the curves deviate markedly from a straight line. This is probably due in part to end effects since there was evidence of slippage in the grips as can be seen by an examination of the registration grid in Figure 5.29.

7. CONCLUSIONS

In general, it is concluded that the moiré fringe method provides a convenient, versatile and precise experimental technique to determine the components of Green's and Cauchy's deformation tensors for large two-dimensional deformations. The lagrangian or eulerian strain tensors may be determined from the deformation tensors, or directly from the moiré measurements. The components of any of the tensors mentioned may be determined from the same set of moiré data without additional computations to account for the use of material or spatial coordinates.

Specifically, for homogeneous deformations the required moiré fringes are produced by the interaction of two specimen grids consisting of initially straight equispaced parallel lines, with similar, but not necessarily identical, master gratings. The initial pitches and angular orientations of the specimen and master grids are arbitrary, and may be selected at the convenience of the experimenter. During the course of an experiment the master grating pitch and orientation may be changed at will. The only essential restraint on the selection of master grating and initial specimen grid parameters is that they must be chosen to produce a reasonable moiré response consistent with the objectives of the experiment. The data which must be obtained from the experiment are the master grating and moiré fringe pitches and angular orientations for each of two sets of specimen grid lines. In addition the direction of rotation of the moiré fringes with respect to master grating rotation should be recorded if the relative sizes of the master and specimen grid pitches are unknown.

It is further concluded that the method of indicial representation of geometric figures may be used to predict the exact moiré fringe response for specific large nonhomogeneous deformations. Geometrical pa-

rameters of the fringes may then be used to determine the deformation tensors. Deformations investigated are bending of a block and an initially curved cuboid. The method of approach is demonstrated using a variety of specimen and master grids including parallel lines, radial lines, Fresnel figures and concentric circles.

In summary, the research described in this report extends and generalizes the moiré fringe method for measuring large two-dimensional deformation by: 1) unambiguously relating the moiré data directly to fundamental tensor strain measures; 2) permitting the experimenter to choose specimen and master grids best suited to a particular experiment; and 3) applying the method of indicial representation of geometric figures to predict the exact response of moiré fringes to specific large nonhomogeneous deformations.

8. LIST OF REFERENCES

1. Bromely, R. H., "Two-Dimensional Strain Measurement by Moiré." Proceedings of the Physical Society, (London), Section B, vol. 69, part 3, March, 1956.

2. Duffey, H. J. and Mesmer, G. K., "Finite Rotation and Strain Measurement Using the Moiré Technique," Experimental Mechanics, vol. 7, no. 12, December 1967, pp. 537-540.

3. Durelli, A. J., and Parks, V. J., "Moiré Fringes as Parametric Curves," Experimental Mechanics, vol. 7, no. 3, March 1967, pp. 97-104.

4. Durelli, A. J., Parks, V. J., and Feng, H., "Experimental Methods of Large Strain Analysis," International Journal of Non-Linear Mechanics, vol. 2, 1967, pp. 387-404.

5. Durelli, A. J., Phillips, E. A., and Tsao, C. H., Introduction to the Theoretical and Experimental Analysis of Stress and Strain, McGraw-Hill Book Co., New York, 1958.

6. Durelli, A. J., Sciammarella, C. A., and Parks, V. J., "Interpretation of Moiré Patterns," Proceedings of the American Society of Civil Engineers, vol. 89, no. EM 2, April 1963.

7. Eringen, A. C., Nonlinear Theory of Continuous Media, McGraw-Hill Book Co., New York, 1962.

8. Holister, G. S., and Luxmoore, A. R., "Production of High-density Moiré Grids," Experimental Mechanics, vol. 8, no. 5, May 1968, pp. 210-216.

9. Meyer, M. L., "Interpretation of Surface-Strain Measurements in Terms of Finite Homogeneous Strains," Experimental Mechanics, vol. 7, no. 12, December 1967, pp. 294-301.

10. Morse, S., Durelli, A. J., Sciammarella, C. A., "Geometry of Moiré Fringes in Strain Analysis," Proceedings of the American Society of Civil Engineers, vol. 86, no. EM 4, August 1960.

11. Oster, G., Wasserman, M., and Zwerling, C., "Theoretical Interpretation of Moiré Patterns," Journal of the Optical Society of America, vol. 54, no. 2, Feb. 1964, pp. 169-175.

12. Parks, V. J., and Durelli, A. J., "On the Definitions of Strain and Their Use in Large-Strain Analysis," Experimental Mechanics, vol. 7, no. 6, June 1967, pp. 279-280.

13. Post, D., "The Moiré Grid-Analyzer Method of Strain Analysis," Experimental Mechanics, vol. 5, no. 11, November 1965, pp. 368-377.

8. LIST OF REFERENCES

1. Bromely, R. H., "Two-Dimensional Strain Measurement by Moiré." Proceedings of the Physical Society, (London), Section B, vol. 69, part 3, March, 1956.

2. Duffey, H. J. and Mesmer, G. K., "Finite Rotation and Strain Measurement Using the Moiré Technique," Experimental Mechanics, vol. 7, no. 12, December 1967, pp. 537-540.

3. Durelli, A. J., and Parks, V. J., "Moiré Fringes as Parametric Curves," Experimental Mechanics, vol. 7, no. 3, March 1967, pp. 97-104.

4. Durelli, A. J., Parks, V. J., and Feng, H., "Experimental Methods of Large Strain Analysis," International Journal of Non-Linear Mechanics, vol. 2, 1967, pp. 387-404.

5. Durelli, A. J., Phillips, E. A., and Tsao, C. H., Introduction to the Theoretical and Experimental Analysis of Stress and Strain, McGraw-Hill Book Co., New York, 1958.

6. Durelli, A. J., Sciammarella, C. A., and Parks, V. J., "Interpretation of Moiré Patterns," Proceedings of the American Society of Civil Engineers, vol. 89, no. EM 2, April 1963.

7. Eringen, A. C., Nonlinear Theory of Continuous Media, McGraw-Hill Book Co., New York, 1962.

8. Holister, G. S., and Luxmoore, A. R., "Production of High-density Moiré Grids," Experimental Mechanics, vol. 8, no. 5, May 1968, pp. 210-216.

9. Meyer, M. L., "Interpretation of Surface-Strain Measurements in Terms of Finite Homogeneous Strains," Experimental Mechanics, vol. 7, no. 12, December 1967, pp. 294-301.

10. Morse, S., Durelli, A. J., Sciammarella, C. A., "Geometry of Moiré Fringes in Strain Analysis," Proceedings of the American Society of Civil Engineers, vol. 86, no. EM 4, August 1960.

11. Oster, G., Wasserman, M., and Zwerling, C., "Theoretical Interpretation of Moiré Patterns," Journal of the Optical Society of America, vol. 54, no. 2, Feb. 1964, pp. 169-175.

12. Parks, V. J., and Durelli, A. J., "On the Definitions of Strain and Their Use in Large-Strain Analysis," Experimental Mechanics, vol. 7, no. 6, June 1967, pp. 279-280.

13. Post, D., "The Moiré Grid-Analyzer Method of Strain Analysis," Experimental Mechanics, vol. 5, no. 11, November 1965, pp. 368-377.

9. CURRICULUM VITAE

Biographical Information on Mr. Lowell P. Martin

1) Born in Chicago, Illinois, January 12, 1932.

2) Received B.S.M.E. degree from Purdue University, 1954.

3) Served in United States Air Force from 1954 to 1956. Attained rank of First Lieutenant.

4) Received M.S. degree from the University of New Mexico, 1958.

5) Served as head of the Structural Analysis Group in the Systems Analysis Department; head of the Filament Winding Section of the Applied Research and Development Department; and head of the Experimental Mechanics Section of the Applied Research and Development Department at the Albuquerque Division of ACF Industries, Inc., 1957 to 1967.

6) Served in the position of Senior Engineer at the Albuquerque Division of EG&G, Inc., 1967.